EVALUATION OF EDTA AND GLDA CORROSION ON S13CR-110 METAL ALLOY AT HIGH TEMPERATURE AND HIGH PRESSURE WITH AND WITHOUT SALT

A Thesis

by

TARANG LAL

Submitted to the Office of Graduate and Professional Studies of
Texas A&M University
in partial fulfillment of the requirements for the degree of

MASTER OF SCIENCE

Chair of Committee,	Hisham A. Nasr-El-Din
Committee Members,	Jerome Schubert
	Mahmoud El-Halwagi
Head of Department,	Daniel A. Hill

August 2016

Major Subject: Petroleum Engineering

ABSTRACT

As the petroleum industry has moved to deeper formation at high temperatures (>200°F) in more corrosive environments, both stimulation fluids and well tubing metallurgies have changed. Traditional well stimulation fluids such as HCl have been replaced by chelating agents such as ethylene diamine tetra-acetic acid (EDTA). In offshore environments, where environmental regulations are stricter, biodegradable and environmentally friendly chelating agents such as glutamic acid N,N-diacetic acid (GLDA) are preferred over EDTA. Well tubing designs have progressed from low carbon steel alloys such as L-80 and P-110 to corrosion resistant alloys (CRA's) such as S13Cr-110 to account for acidic and sour environments. There is a need to understand the corrosion of CRA alloys such as S13Cr-110 with chelating agents (EDTA and GLDA) as they interact with the metal during stimulation work (approximately 6 hr).

In this work, the corrosion rate of 20 wt% EDTA and 20 wt% GLDA on S13Cr-110 is analyzed at high temperature (300°F and 350°F) and high pressure (>1000 psi) for 6 hr. In addition, the effect of a 5 wt% brine (NaCl) solution investigated. All pH values were held to 4 with the exception of EDTA in the presence of salt (pH = 9). This was due to the low solubility of EDTA in acidic solutions with high ionic strength.

The results show that corrosion rate increases with temperature, GLDA is more corrosive than EDTA under the same conditions, and that EDTA at pH 9 is more corrosive than EDTA at pH 4. All corrosion rates calculated are <0.02 lb/ft^2, the current acceptable corrosion rate per industry standards for well stimulation. The results are explained using the mononuclear and binuclear chelation theory and understanding the differences in conditional stability constants for the two fluids. A reaction mechanism is proposed that is consistent with the results obtained.

ACKNOWLEDGEMENTS

I would like to thank my committee chair, Dr. Nasr-El-Din, and my committee members, Dr. Schubert, and Dr. El-Halwagi, for their guidance and support throughout the course of this research.

Thanks also go to my friends and colleagues and the department faculty and staff at Texas A&M University. Special thanks to Gia Alexander for her help in editing my thesis and Clarence Ng, Rixing Zhang, and Zimo Wang for their help in conducting the experiments and analyzing the data.

Finally, thanks to my mother, father, sister, and Jazmine for their encouragement and support.

TABLE OF CONTENTS

Page

LIST OF FIGURES

Page

LIST OF TABLES

Page

NOMENCLATURE

ACS	American Chemical Society
APCA	Amino poly-carboxylic acids
ASDA	Aspartic acid N,N-diacetic acid
CO_2	Carbon dioxide
CRA	Corrosion resistant alloy
DI	Deionized
DTPA	Diethylene triamine penta-acetic acid
EDTA	Ethylene diamine tetra-acetic acid
EDG	Ethanol di-glycinic acid
GLDA	Glutamic acid N,N-diacetic acid
H_2S	Hydrogen sulfide
HCl	Hydrochloric acid
HEDTA	Hydroxyethyl ethylene diamine tri-acetic acid
HSE	Health, safety and environmental
HT	High temperature (350°F)
ICP-OES	Inductively coupled plasma- optical emission spectroscopy
ID	Inner diameter
LT	Low temperature (300°F)
MAWP	Maximum allowable working pressure
MGDA	Methyl glycine diacetic acid
mpy	Mills per year

MSG	Monosodium glutamate
S	Salt (5 wt% NaCl)
SOP	Standard operating procedure
wt%	Weight percent

1. INTRODUCTION

1.1 Literature Review

1.1.1 Background

The annual cost of corrosion is $2.2 trillion worldwide (Hayes 2013). Within the upstream petroleum industry, Koch et al. (2001) estimates the annual cost of corrosion at $1.4 billion. Some of the most common areas of corrosion are associated with the sub-surface piping (tubing for producers and injectors), surface piping (gathering lines, transfer pipelines), and equipment (tanks, vessels, etc.). Within the sub-surfacing piping, there can be significant corrosion when wells are stimulated with acid to increase productivity.

1.1.2 Corrosion in Piping During Well Stimulation

The corrosion cell consists of the anode, cathode, a metallic path, and a fluid (Wikipedia 2016a). In the context of corrosion within a pipe wall, the cathode is the corrosive element (acid) and the anode is the electron donor (pipe). The fluid is the stimulation fluid and there is direct contact between the acid and the pipe.

If there is corrosion on the pipe, it can be categorized as general corrosion, localized/pitting corrosion, and/or crevice corrosion. General corrosion occurs when there is a uniform corrosion of the pipe. Localized or pitting corrosion occurs when certain locations within the pipe corrode preferentially. This can be due to changes in the solution chemistry, especially the pH. Often times, buffering a solution can mitigate the affect.

1.1.3 Well Stimulation: HCl

Hydrochloric acid (HCl) is the most commonly used acid in well stimulation because of its low cost and high reactivity (Finšgar and Jackson 2014). However, as the industry has moved to deeper formations, the reservoir temperatures and pressures have risen. The increase in temperature (>200°F) with deeper formations has reduced the well stimulation effectiveness (Buijse et al. 2004) and intensified the corrosion issues with HCl and the inner pipe wall. According to Finšgar and Jackson (2014), HCl can have extremely high corrosion rates (>0.11 lb/ft^2) with the pipe metal at elevated temperatures due to its high reactivity. A typical industry standard is to maintain a corrosion rate of <0.05 lb/ft^2 (Al-Mutairi et al. 2005; Kalfayan 2008). Corrosion inhibitors, which are used to protect the pipe surface from acid attack, often have thermal degradation concerns at these high temperatures. This makes controlling HCl reactivity at high temperatures difficult and costly (Wang et al. 2009). There are also safety concerns with HCl, as it can react with the formation and form calcium chlorine brine that can cause skin injuries (Singh and Dey 1993).

1.1.4 Well Stimulation: Alternatives to HCl

The petroleum industry has investigated reducing the reaction rate of HCl at high temperatures by increasing the viscosity with polymers and viscoelastic surfactants. Alternative weak acids such as organic acids have been considered to provide a lower reaction rate. According to Buijse et al. (2004), the organic acids provide deeper penetration into the formation, but are more expensive per unit volume. Additionally, there

are limitations on the concentrations that can be used for both acetic acid (13 wt%) and formic acid (9 wt%) due to the limited solubility of their reaction products (LePage et al. 2009). To overcome these concerns, chelating agents have been proposed as a primary stimulation fluid instead of acids.

1.1.5 Well Stimulation: Chelating Agents

According to Dwyer and Mellor (1964), chelating agents were originally discovered in 1920 and their name comes from the Greek term, chēlē, meaning lobster claw. A chelating agent forms a chelate ring, which results in multiple attachments to the metal. The ring is an octahedral structure, which was originally theorized by Werner, in 1893.

In 1996, Fredd and Fogler pioneered the application of chelating agents as a stimulation fluid as a substitute for HCl. They studied two chelating agents within the amino poly-carboxylic acids (APCA) family; ethylene diamine tetra-acetic acid (EDTA) and diethylene triamine penta-acetic acid (DTPA) (Fredd and Fogler 1997). In 2001, Frenier introduced hydroxyethyl ethylene diamine tri-acetic acid (HEDTA) as an alternative to EDTA and DTPA due to its improved environmental profile. Frenier then demonstrated its use in the field (Frenier 2003; 2004).

As new health, safety and environmental (HSE) regulations have been introduced, there has been an environmental challenge in using EDTA, HEDTA, and other chelating agents, especially in offshore environments (Oviedo et al. 2003) because they are not readily biodegradable (LePage et al. 2009). To overcome this challenge, a newer set of

greener chelating agents, such as glutamic acid N,N-diacetic acid (GLDA), aspartic acid N,N-diacetic acid (ASDA), methyl glycine tetra-acetic acid (MGDA), and ethanol di-glycinic acid (EDG) that have been developed.

GLDA is readily biodegradable as it is derived from monosodium glutamate (MSG), a commonly used food enhancer (LePage et al. 2009). In literature, GLDA has been the most prevalent of the more environmentally friendly chelating agents. It has effective kinetics with calcite (Mahmoud et al. 2011; Rabie et al. 2011) and dolomite (Adenuga et al. 2013) at high temperatures (>250°F), is thermally stable up to 350°F (Sokhanvarian et al. 2012), and is environmentally friendly, meeting the HSE regulations (LePage et al. 2009; Braun et al. 2012).

De Wolf et al. (2012) has shown that GLDA has a lower corrosion rate that various organic acids (acetic acid, HEDTA, and formic acid) with 13Cr alloys at 300°F over a 6 hour period. A six hour duration was selected as it is a good estimate of typical soak times during acid stimulations (Kalfayan 2008). In De Wolf et al. (2014), data is provided comparing the corrosion rate (over a 6 hour period) between GLDA and other environmentally friendly chelating agents (ASDA, EDG, and MGDA) with 13Cr alloys at 300°F. Among the four chelating agents evaluated, GLDA has the lowest corrosion rate on 13Cr pipe (De Wolf et al. 2014).

Furthermore, GLDA is shown to be stable in seawater at a wide range of pH values, making it effective as a stimulation fluid for water injectors (Mahmoud et al. 2015). GLDA has also been shown to be successful in field applications in carbonate (Nasr-El-Din et al. 2013) and sandstone reservoirs (Nasr-El-Din et al. 2014).

In this work, the focus will be on EDTA and GLDA. Their structures are shown in **Fig. 1** and **Fig. 2**. GLDA has one nitrogen and 4 carboxylic groups while EDTA has 2 nitrogen atoms and 4 carboxylic groups. These functional groups are important in forming metal chelate complexes, as will be later discussed.

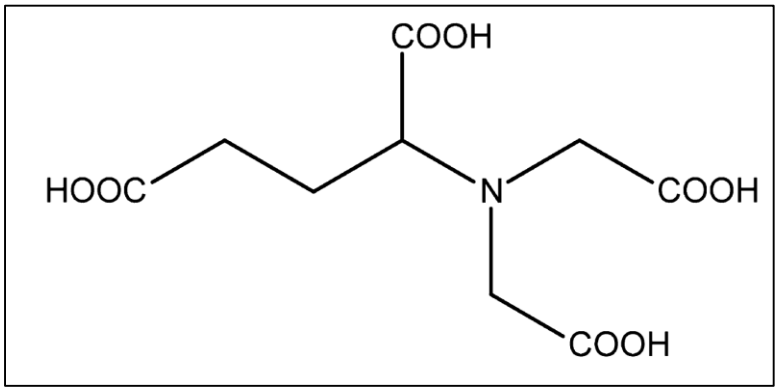

Fig. 1 – Chemical structure of GLDA.

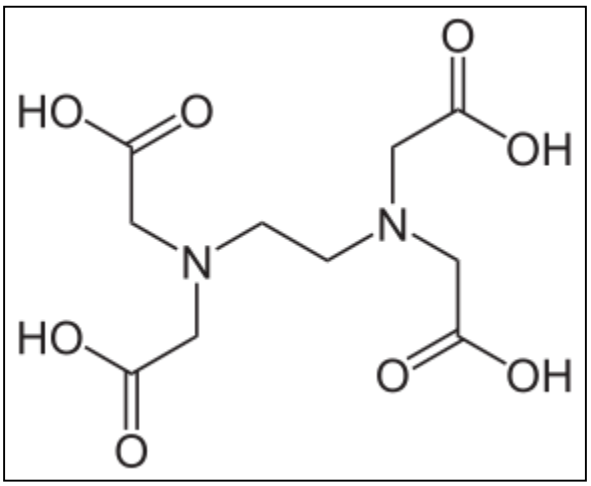

Fig. 2 – Chemical structure of EDTA.

1.1.6 Well Tubing: Low Alloy Carbon Steel

Similar to the progression for well stimulation fluids as reservoir temperatures and environmental concerns have increased, there has been a progression in metal alloys used for tubing in the petroleum industry.

The typical tubing material used in production and injection wells is low alloy carbon steel. Examples include N-80, J-55, K-55, and P-110 (see **Table 1**). These alloys (N-80, J-55, K-55) are relatively low cost, are easy to manufacture, and provide adequate strength for use in shallow formations. P-110 has a higher tensile and yield strength, making it more suitable for deeper applications. **Table 2** provides the mechanical properties for each of these alloys. The only elemental limitation when manufacturing these metals is the maximum allowable phosphorus (P) and sulfur (S) concentration, measured in weight percent (wt%). Therefore, these carbon steel alloys have similar elemental composition. However, they have different mechanical properties (tensile and yield strength). Carbon steel alloys are susceptible to corrosion and therefore, additives are included with the acidizing fluid to reduce metal corrosion.

	Low Alloy Carbon Steels							
	N-80		K-55		J-55		P-110	
All in wt%	Min	Max	Min	Max	Min	Max	Min	Max
P		0.03		0.03		0.03		0.03
S		0.03		0.03		0.03		0.03
Fe	Balance		Balance		Balance		Balance	

Table 1 – Elemental composition of selected low alloy carbon steels.

	Low Alloy Carbon Steels							
	N-80		K-55		J-55		P-110	
	Min	Max	Min	Max	Min	Max	Min	Max
Tensile Strength (kpsi)	100		95		75		125	
Yield Strength (kpsi)	80	111	55	80	55	80	110	140

Table 2 – Mechanical properties of selected low alloy carbon steels.

If the formation contains H_2S, it is considered sour, and if it contains CO_2, it is considered acidic. Either of these situations (or both) drastically increases the corrosion rate in the carbon steel alloys mentioned in Table 1 and Table 2. H_2S can interact with the iron in the pipe and lead to corrosion and the formation of iron sulfide, especially at low pH (Walker et al. 1991). Carbon dioxide can also lead to corrosion of the iron in pipe and form other inorganic scales. Therefore, there is a need for alternative metal alloys that are resistant to corrosion.

1.1.7 Well Tubing: Corrosion Resistant Alloys (CRA's)

When producing oil and gas in corrosive environments, CRA's can be used as an alternative to low carbon steel alloys. These alloys form a passive layer, which is a protective oxide layer that significantly reduces the ability of a fluid to cause corrosion (Lopez 2004). There are multiple ways to categorize these alloys, but in this document, CRA's are broken down into two groups; low alloy steels, which offer some corrosion

resistance, and high alloy steels, which offer greater corrosion resistance. **Table 3** shows the elemental composition of selected low alloy carbon steels that exhibit some corrosion resistant properties (L-80, C-90, and T-95). **Table 4** shows the mechanical properties of those same alloys.

	Low Alloy Steels					
	L-80		C-90		T-95	
All in wt%	Min	Max	Min	Max	Min	Max
C		0.43		0.35		0.35
Mn		1.9		1.2		1.2
Mo			0.25	0.85	0.25	0.85
Cr				1.5	0.4	1.5
Ni		0.25		0.99		0.99
Cu		0.35				
P		0.03		0.02		0.02
S		0.03		0.01		0.01
Si		0.45				
Fe	Balance		Balance		Balance	

Table 3 – Elemental composition of selected low alloy steels.

	Low Alloy Steels					
	L-80		C-90		T-95	
	Min	Max	Min	Max	Min	Max
Tensile Strength (kpsi)	95		100		105	
Yield Strength (kpsi)	80	95	90	105	95	110

Table 4 – Mechanical properties of selected low alloy steels.

The low alloy steels have more specifications in their composition when compared to the low alloy carbon steels. The mechanical strengths of both alloy types are similar.

Within the high alloy steels, there are ferritic, austenitic, martensitic, duplex, and precipitation alloys (American Welding Society 2016). Ferritic steels have <0.1 wt% carbon (C), they are magnetic, cannot be hardened, and have limits on welding. Therefore, they are not commonly used in the petroleum industry. Their crystal structure is body-centered cubic.

Austenitic steels are the most common high alloy steel. They are easier to form and weld, and have a face centered cubic structure. A concern with austenitic steels is their high potential for stress corrosion cracking (SCC) (ArcelorMittal 2010). Chromium (Cr) and nickel (Ni) blends such as 304 and 316 can help in providing some resistance to SCC. **Table 5** shows the elemental composition of these alloys and **Table 6** shows their mechanical properties.

	Austenitic Steels			
	304-SS		316-SS	
All in wt%	Min	Max	Min	Max
C		0.08		0.08
Mn		2		2
Mo			2	3
Cr	18	20	16	18
Ni		10.5		14
Cu				
P		0.045		0.045
S		0.03		0.03
Si		1		1
Fe	Balance		Balance	

Table 5 – Elemental composition of selected austenitic steels.

	Austenitic Steels			
	304-SS		316-SS	
	Min	Max	Min	Max
Tensile Strength (kpsi)	75		75	
Yield Strength (kpsi)	30		30	

Table 6 – Mechanical properties of selected austenitic steels.

Martensitic steels can have up to 1 wt% C and have higher strength than austenitic steels (Table 6). Martensitic steel corrosion resistance can be improved by hardening through quenching and tempering processes. The final polishing can also impact corrosion resistance (AZO Materials 2014). These alloys have a passive layer than can be improved by bright annealing and/or chemical treatment (Lopez 2004). A common example of a martensitic metal is 410, which is often referred to as 13Cr. **Table 7** shows the elemental

composition of the three types of 13Cr steels and **Table 8** shows their mechanical properties. The prefix S in front of 13Cr denotes a super chrome. Super chrome 13 has a similar weight percent of Cr, but has additional elements such as titanium (Ti), vanadium (V), and aluminum (Al). The suffix at the end of the 13Cr represents the minimum yield strength in kpsi. The 13Cr-80 alloy has a lower yield strength than either S13Cr-95 or S13Cr-110 alloys.

	Martensitic Steels: 13-Cr					
	13Cr-80		S13Cr-95		S13Cr-110	
All in wt%	Min	Max	Min	Max	Min	Max
C	0.15	0.22		0.03		0.03
Mn	0.25	1		1		0.5
Mo			1.5	2.5	1.8	2.5
Cr	12	14	11.5	13.5	11.5	13.5
Ni		0.5		6	5	6.5
Cu		0.25				0.3
Ti				0.5		0.5
P		0.02		0.02		0.02
S		0.01		0.005		0.005
Si		1		0.5		0.5
V				0.5		0.5
Al						0.1
Fe	Balance		Balance		Balance	

Table 7 – Elemental composition of selected martensitic steels.

	Martensitic Steels: 13-Cr					
	13Cr-80		S13Cr-95		S13Cr-110	
	Min	Max	Min	Max	Min	Max
Tensile Strength (kpsi)	95		105		115	
Yield Strength (kpsi)	80	95	95	120	110	125

Table 8 – Mechanical properties of selected martensitic steels.

Some of the concerns associated with martensitic 13 chrome steels are that they fail due to hydrogen embrittlement and/or chloride stress corrosion cracking. Studies done by Turnbull and Griffiths (2003) and Boellinghaus et al. (1999) have shown hydrogen embrittlement is a function of hydrogen uptake, the concentration of hydrogen in the lattice structure, including both reversible and irreversible, and that the diffusivity of hydrogen is a function of the material, the environment, and temperature. Some of the factors that impact hydrogen embrittlement is the composition of the material and the heat-treatment procedure used (Ueda et al. 1996). In the event that the passive layer of these alloys have been broken down, chloride stress cracking can occur (Felton and Schofield 1998). If the level of carbon or nitrogen is high, it can lead to chrome depletion (Masamura et al. 1998).

Duplex steels are a combination of austenitic and ferritic steels, have medium strength (in between austenitic and martensitic), and high corrosion resistance. They are not commonly used in tubing material, but are used in surface facilities. **Table 9** shows the two most common grades of duplex steel and **Table 10** shows its mechanical properties.

	Duplex Steel			
	2205		2304	
All in wt%	Min	Max	Min	Max
C		0.03		0.03
Mn		2		2.5
Mo	2.5	3.5		
Cr	21	23	21.5	24.5
Ni	4.5	6.5	0.03	3.5
Cu			0.05	2
Ti				
P		0.03		0.04
S		0.02		0.03
Si		1		1
V				
N	0.08	0.2	0.05	2
Fe	Balance		Balance	

Table 9 – Elemental composition of selected duplex steels.

	Duplex Steel			
	2205		2304	
	Min	Max	Min	Max
Tensile Strength (kpsi)	90		87	
Yield Strength (kpsi)	65		58	

Table 10 – Mechanical properties of selected duplex steels.

The fifth type of high alloy steels are precipitation steels. These are not common in the petroleum industry, but are known for their extremely high strength (American Welding Society 2016).

1.1.8 Effect of Elements in Metal Composition

In the section above, multiple alloys were presented and their elemental compositions were provided (Table 3, Table 5, Table 7, and Table 9). It is important to understand the effect each of these elements have in reducing the corrosion rate between the fluid and the metal surface:

- Effect of carbon (C): having a lower concentration of carbon makes it easier to weld the material (lower hardness level in heat affected zone) and improves the resistance of general corrosion and pitting (lower carbide formation). In chrome alloys, carbide can form as $Cr_{23}C_6$ and it can cause chrome depletion (Turnbull and Griffiths 2003; Masamura et al. 1998). If CO_2 and H_2S are present, low carbon levels can also mitigate the sulfide stress cracking in these alloys (Ueda et al. 1996).
- Effect of nitrogen (N): according to the work of Masamura et al. (1998), high levels of nitrogen can have detrimental effects on chrome alloys. Similar to C, an unwanted byproduct (Cr_2N) can be formed, thereby limiting the effectiveness of the chrome oxide layer. The effective chrome is the total chrome minus 10 times the sum of the carbon and nitrogen content in the alloy (all wt%).
- Effect of chrome (Cr): according to the work of Bondietti et al. (1993), chrome forms an oxide layer that is much more resistant to corrosion than an iron oxide layer. It is able to interfere with the surface sites of binuclear surfaces (chelating agents), and has a low water exchange rate, making it harder to be removed into the bulk fluid phase. It is typically 1-2 mm thick (Cunat 2004).

- Effect of nickel (Ni): according to the work of Felton and Scholfield (1998), nickel in higher concentrations (4-5 wt%) increases corrosion resistance, but in low concentrations, can decrease corrosion resistance. Nickel is a stabilizing element; it improves the ability to weld alloys. In sulfuric environments, nickel improves the ductility and toughness of the metal alloy (Cunat 2004).
- Effect of molybdenum (Mo): molybdenum is often added in conjunction with nickel and it improves pitting resistance. Both nickel and molybdenum have shown to enhance the chrome oxide passive layer by a factor of 5 (Ueda et al. 1996). In sour environments, molybdenum can form MoS to prevent the breakdown of the chrome oxide layer, while enhancing the passive film in the inner-layer. Studies have also shown that molybdenum does not impact pH (Ueda et al. 1996).
- Effect of manganese (Mn): manganese is a strong oxidizing agent and acts as a deoxidizer in steel to prevent iron from bonding with sulfur (Cunat 2004).
- Effect of other elements (titanium (Ti), vanadium (V)): The Ti helps in grain refinement (El-Faramawy et al. 2012), and V helps improve tensile strength at higher temperatures (Pan et al. 2003).

The primary elements that determine the effectiveness of chrome alloys are Cr, Ni, Mo, and C. Hashizume and Inohara (2000) and Masamura et al. (1998) provide various arithmetic equations relating the concentration (wt%) of these elements to the effectiveness of the alloys. The main objectives are to reduce the carbon and nitrogen content while maximizing the chrome, nickel, and molybdenum content. In a cost effective manner.

1.1.9 Corrosion of Metal Alloys with Chelating Agents

While there is limited data on chelating agents and corrosion, there have been multiple studies done on the interaction of chelating agents and various cations. The most common chelating agent studied is EDTA and the most common cation studied is Fe(III). Therefore, the focus of this section will be primarily based on Fe-EDTA complexes. Since the focus of this work is on S13Cr-110 and EDTA/GLDA, these interactions can help explain the results later in the document.

In order to corrode a metal surface with a chelating agent, there must first be an interaction at the surface resulting in the formation of a chelated complex. This process has been described by multiple authors (Mercier et al. 2008; Nowack and Sigg 1997; Stumm 1997; Bondietti et al. 1993). Details on chrome alloy corrosion are provided by Turnbull and Griffiths (2003), Boellinghaus et al. (1999), Masamura et al. (1998), Felton and Schofield (1998), and Ueda et al. (1996). The next step is to form the chelated complex and to determine its conditional stability and structure. For the purpose of EDTA and GLDA, the primary chelating agents of interest, Begum et al. (2012a; 2012b) provides the information on stability constants. The work of all these authors is further elaborated in the "Discussion" section.

1.2 Objectives

The focus of this work is understand the corrosion behavior of S13Cr-110 in a solution of 20 wt% EDTA and 20 wt% GLDA. The reason for this study is to better understand the interaction of CRA's with chelating agents, as the industry moves to deeper

reservoirs at higher temperatures. To the knowledge of this author, there is no previous study that has compared the corrosion of these two chelating agents with the aforementioned alloy. The objectives of this work are to:

1. Design:
    a. Acquire the equipment to conduct corrosion testing. At the start of this project, the equipment needed was not available.
    b. Develop procedures to safely operate the equipment.
2. Proof of concept with L-80 coupon:
    a. Demonstrate the use of the equipment for corrosion testing.
    b. Build a workflow for corrosion testing by analyzing corrosion coupons using the weight loss method, inductively coupled plasma-optical emission spectroscopy (ICP-OES), and 3D optical profiler.
3. Compare the corrosion of S13Cr-110 with EDTA and GLDA at 300°F and 350°F for a 6 hour duration in a non-brine and brine solution while maintaining at least 1000 psi with N_2 gas.
4. Provide preliminary results and recommendations.

2. MATERIALS, EQUIPMENT, AND METHODS

2.1 Materials and Equipment

There are five main components needed to conduct the testing and analyze the results. They are the reaction autoclave, the metal coupon samples, the fluids, the ICP-OES to analyze the fluids, and the 3D profiler to analyze the surface of the coupon. In addition, sodium chloride (NaCl) salt is used to form the brine composition and weigh balances are used to measure sample information.

The reaction autoclave is manufactured by Parr Instrument Company (Model 4523). It is a 1000 mL, bench top fixed head reactor, constructed out of alloy B-2. The cylinder dimensions are 4" ID by 5.4" depth. The alloy B-2 metal is a hastelloy compound that is corrosion resistant. It is composed of approximately 66 wt% Ni, 1 wt% Cr, 28 wt% Mo, and 1 wt% Mn, and other elements (balance) giving it excellent corrosion resistant properties (Parr Instruments 2015). It is manufactured by Haynes International (2015) and is described as having high resistance to uniform and localized corrosion. Furthermore, it has very high stress corrosion cracking resistance and is resistant to HCl and other strongly reducing chemicals.

The autoclave is rated for high pressures and temperatures (maximum working pressure of 1900 psi at 660°F). It is built with a magnetic drive with a 1/8 hp motor to give a maximum of 1700 rpm. The rotating shaft has pitched impellers for adequate mixing and has connection points for holding coupons. It has a 1000 watt heater and can reach a maximum temperature of 660°F. A thermowell is built into the reactor and a thermocouple is used to measure the temperature of the fluids. There are two inlets to the reactor; a

Teflon lined 300 mL liquid charging pipette to load the treating fluid into the main reactor and a flexible hose line supplying pressure to the reactor. The outlet of the reactor has a 600 mL scrubber system (2.5" ID by 8" depth) to neutralize any vapors. A filtered dip tube is used for sparging and there are two 1" round windows to view the gas and verify flow as it bubbles through the liquid. All tubing is ¼" Teflon lined stainless steel. The system is pressurized by an upstream N_2 tank. A control system is utilized to regulate the temperature and speed of mixing. The pressure is maintained manually by a regulator. A rupture disk is installed in the reactor, set at 2000 psi, to ensure safe operation. In addition, the inlet to the reactor has a double block system while the outlet is controlled by a single block needle valve. The system is operated at 115 V. An image of the complete Parr reactor system is shown in **Fig. 3**.

The coupons used for testing are manufactured by Alabama Specialty Products, Metal Samples. Each coupon is ordered to be 1" wide, 2.3" long, and 1/16" thick. Two 0.15" holes are cut 3/16" from the edge of each side and centered. A 600 grit finish is used and the samples are then stenciled for identification. The holes in the coupon are used to mount them onto the Parr reactor, as shown in **Fig. 4**. Special non-metallic screws and washers are used to isolate the metal coupon from the impeller to minimize galvanic corrosion. The elemental composition of the S13Cr-110 coupons are provided in **Table 11** and the mechanical properties are provided in **Table 12**.

All in wt%	S13Cr-110
C	0.01
Mn	0.41
Si	0.24
Cu	0.19
Ni	5.4
Cr	12
Mo	1.9
P	0.014
S	0.001
Ti	0.1
V	0.06
Al	0.03
Fe	Balance

Table 11 – Elemental composition of S13Cr-110 alloy used in experiments.

	S13Cr-110
Yield Strength (kpsi)	116.9
Tensile Strength (kpsi)	123.3

Table 12 – Mechanical properties of S13Cr-110 used in experiments.

In the proof of concept study, L-80 coupons were used. These were provided by CPCO Inc. and were cut from a 2" pipe. These coupons were used since they were readily available and could provide a base case for validating the procedures and equipment use.

Fig. 3 – Parr instrument reactor system assembled.

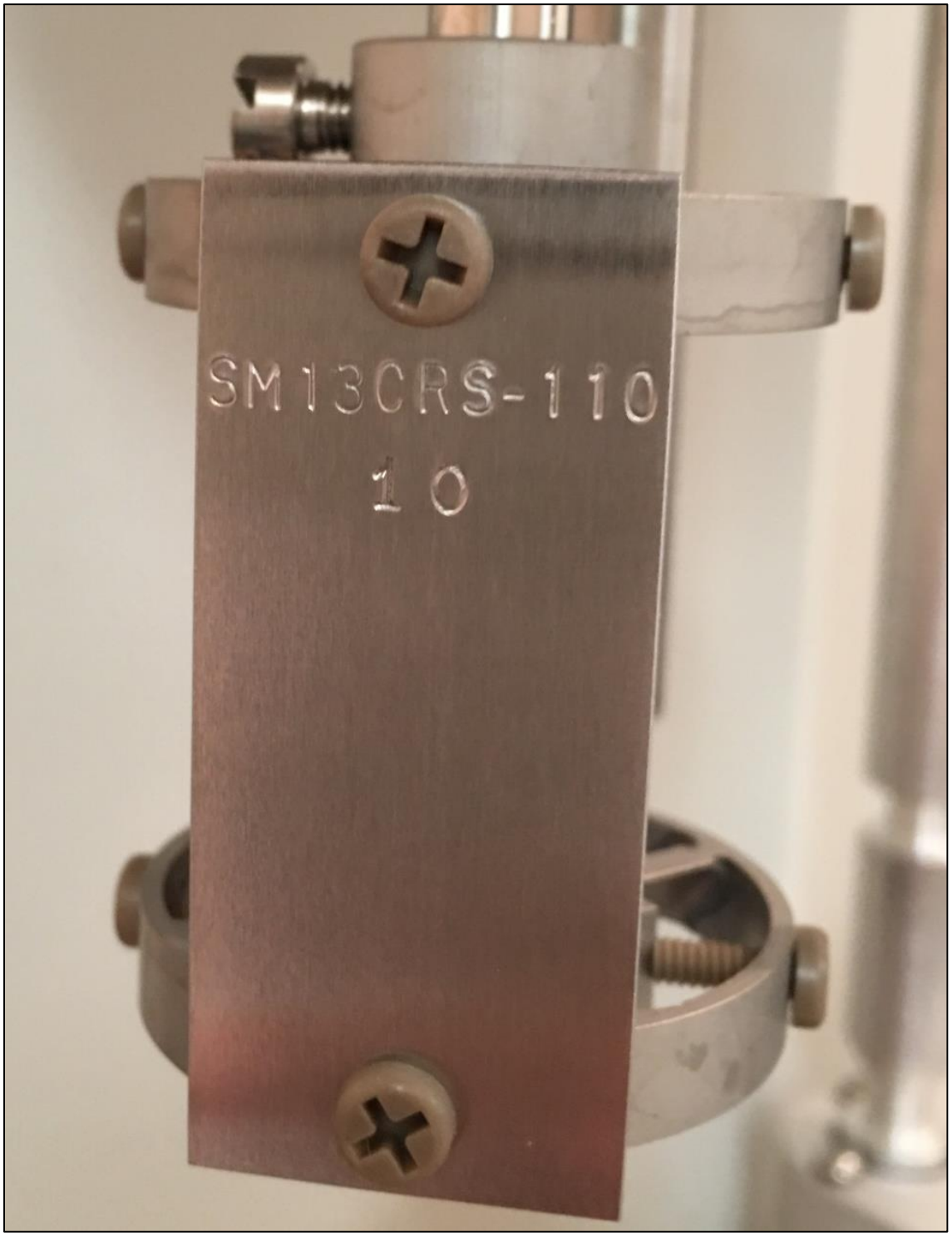

Fig. 4 – Parr reactor (coupon holder).

Two fluids were used to test the corrosion behavior on S13Cr-110; GLDA and EDTA. The GLDA was provided by Akzonobel Company (36.78 wt%, pH 4) and the EDTA was provided by BASF (40.1 wt%, pH 11.6). Salt (American Chemical Society (ACS) grade NaCl, supplied from Macron Chemicals) was used to form the brine solution. When testing with both chelating agents, they were diluted with DI water to a concentration of 20 wt% and the pH was held to 4. EDTA with NaCl was the exception due to its limited solubility in ionic solutions. Therefore, EDTA with salt (5 wt% NaCl) was tested at a pH of 9. Acid (ACS grade HCl provided by Macron Chemicals) was used reduce the EDTA pH as needed.

To analyze the sample, a weigh balance, ICP-OES, and 3D profiler were used. The ICP-OES is a type of mass spectrometry that can be used to determine the concentrations the spent fluid after the corrosion testing to validate what parts of the metal corroded. For the S13Cr-110 samples, the main elements of interest were Fe, Cr, Ni, Mo, and Mn. The machine was calibrated using standards for each cation of known concentrations (5ppm, 15 ppm, and 30 ppm). Samples were diluted so their values were in the 0-30 ppm range. Using Beer's law, which relates absorbance to concentration, the ICP-OES is capable of detecting ions at concentrations as low as one part per trillion (PerkinElmer 2010). The ICP-OES unit available is the Optima 7000 DV ICP-OES and the image is shown in **Fig. 5**. Once the concentrations were determined, they were multiplied by the dilution factor to determine the concentration of the cations in the solution.

Fig. 5 – Optima 7000 DV ICP-OES unit.

The surface of the coupon after corrosion testing was analyzed using a 3D profiler. It is a non-contact method of quantifying surface morphology. The equipment is shown in **Fig. 6**.

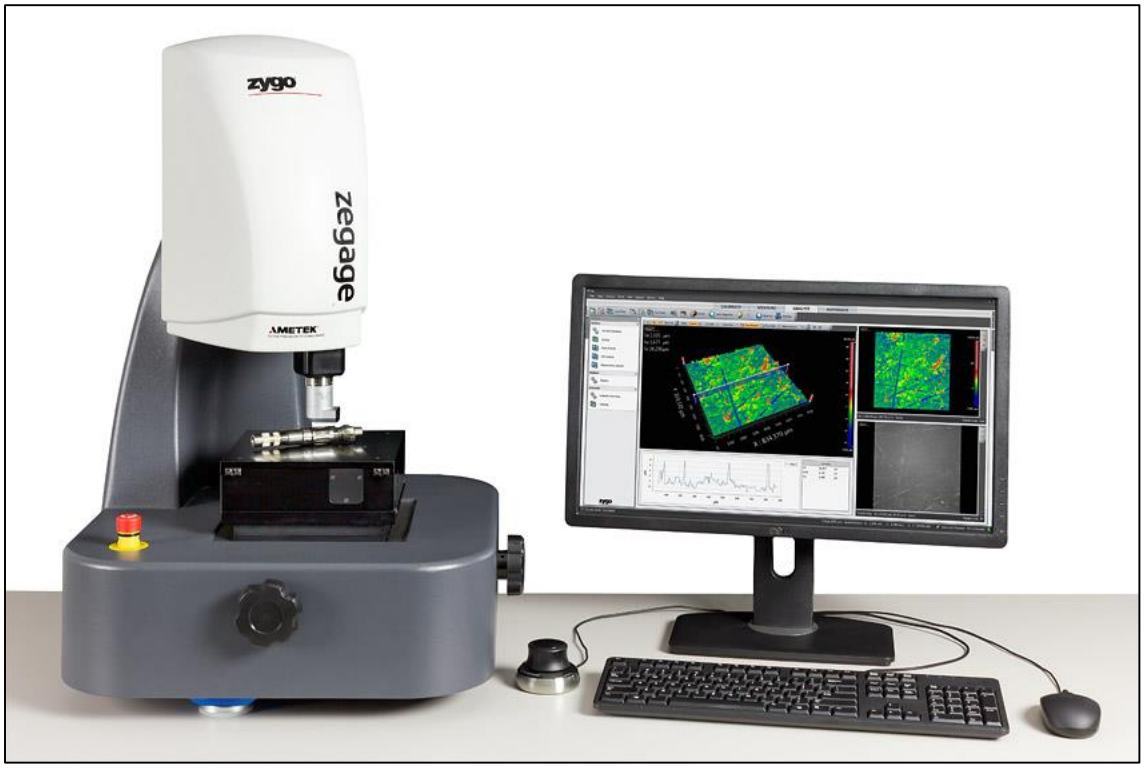

Fig. 6 – Zygo ZeGage.

The Zygo ZeGage has a vertical resolution of 0.1 nm and a reliability of >99.7% within 1 standard deviation (Zygo 2015). Therefore, it can provide a high level of detail in terms of surface topography and quantify the changes. The output provides certain surface roughness parameters such as S_{PV}, the difference between the maximum profile height and maximum valley depth. Another key parameter is the root mean square surface roughness, S_q. The current system requires the user to manually select a location on the surface and has a viewing window of 0.8 mm by 0.8 mm.

2.2 Methods

Each corrosion test conducted followed a set of detailed standard operating procedures (SOP's) to ensure safe and consistent operation. The first step was to ensure that the coupon was cleaned and dried using acetone. The coupon dimensions were measured using a caliper and the coupon weight was recorded.

After the coupon was ready for analysis, it was mounted to the reactor, as shown in Fig. 4, and 900g of fluid was prepared (GLDA or EDTA) and loaded to the reactor. Pictures were taken for documentation, and the scrubber vessel (Fig. 3) was filled with 400 mL of DI water and the system was assembled. Nitrogen gas was used to purge the system three times and remove any excess oxygen. Once the system had been purged, it was pressurized to the desired pressure (750-800 psi) and the heater was mounted. This min pressure was to ensure vapors stay in solution. Once the temperature to the reactor reached the desired set-point (300°F or 350°F), the pressure rose to >1000 psi and the 6 hour timer was started. The increase in pressure as a function of temperature was due to vaporization of some of the water in the fluid. Recordings of the temperature and pressure were taken periodically throughout the reaction duration. After 6 hours, the heater was removed and the system was cooled within 30 min to <85°F and the system was de-pressurized. Once the system was opened, images of the coupon and reactor fluid were documented. The coupon was cleaned using a non-metallic brush and acetone. After cleaning, the coupon weight was recorded. The coupon corrosion rate was determined by the weight loss method in accordance with NACE ASTM G31 (2012). A sample of the spent fluid was collected for ICP-OES analysis to determine the concentration (ppm) of

cations (Fe, Mn, Cr, Mo, and Ni) in the solution. The concentration was converted to a mass (mg) by multiplying by the fluid volume. The system was cleaned and dried using DI water, paper towels, and acetone to ensure that no unwanted fluids remained in the reactor.

In the proof of concept study, the coupon used was L-80 instead of S13Cr-110 due to the higher expected corrosion rate. The test duration was 4 hours instead of the standard 6 hours. Two coupons were used in this test to validate corrosion results. In S13Cr-110 tests, only 1 coupon was used. Furthermore, the ZeGage equipment was used both before and after the test to analyze the surface of the coupon and quantify the roughness. Since the operation of the equipment was manual, the average of multiple points was used to provide insight into the surface roughness.

When the S13Cr-110 coupons were used, their corrosion rate was so low that it was difficult to detect the change using the ZeGage. Therefore, it was determined not to use the ZeGage for the experimental work. The proof of concept data is shown to highlight the potential value of such an optical profiler for corrosion studies where either the fluid is more corrosive or the metal alloy is less corrosion resistant, such as L-80.

3. RESULTS

The purpose of this study is to design and acquire the Parr Reactor system, build SOP's to ensure safe operation, demonstrate the operation (proof of concept) of the reactor with a workflow for testing, and compare the corrosion of S13Cr-110 with EDTA and GLDA. The system has been acquired and SOP's have been built, so the remainder of this section will highlight the results of the corrosion tests. In the tests conducted, 300°F refers to low temperature (LT), 350°F refers to high temperature (HT), and tests with 5 wt% NaCl salt are labeled S. Solution pH was lowered by HCl as needed. The elemental composition of the S13Cr-110 coupons are provided in **Table 11** and the mechanical properties are provided in **Table 12**. Data for the L-80 coupons was not provided by the manufacturer but Table 3 and Table 4 can provide some guidelines on the elemental composition and mechanical properties.

3.1 Proof of Concept: L80 and GLDA

The proof of concept was conducting using 2 curved L-80 coupons, tested for 4 hours at 300°F at >1000 psi in 20 wt% GLDA solution of pH 4. The fluid/surface area ratio was 80 ml/in^2 and the results are summarized in **Table 13**. The corrosion rate was ~0.20 lb/ft^2 and an increase of greater than 100% was noted in the average surface roughness before and after the test. The coupons before and after testing are shown in **Fig. 7** and **Fig. 8**. The results of a selected ZeGage sample for coupon L-2 is shown in **Fig. 9** (before) and **Fig. 10** (after). The results of a selected ZeGage sample for coupon L-3 is shown in **Fig. 11** (before) and **Fig. 12** (after). ICP-OES results of the effluent sample are

shown in **Fig. 13** (Fe) and **Fig. 14** (Mn, Cr). Mo and Ni, the other 2 elements that were tested showed undetectable levels.

	Coupon L-2	Coupon L-3
Corrosion Rate (lb/ft^2)	0.21	0.20
Sq (μm) – Before (Avg)	5.1	5.8
Sq (μm) – After (Avg)	17.8	12.2

Table 13 – Results of L-80 test with 20 wt% GLDA (pH = 4). Each test was conducted for 4 hours at >1000 psi at 300°F.

Fig. 7 – Results of L-80 test with 20 wt% GLDA (pH = 4). Coupon before corrosion (left) and after corrosion (right). Test was conducted for 4 hours at >1000 psi at 300°F.

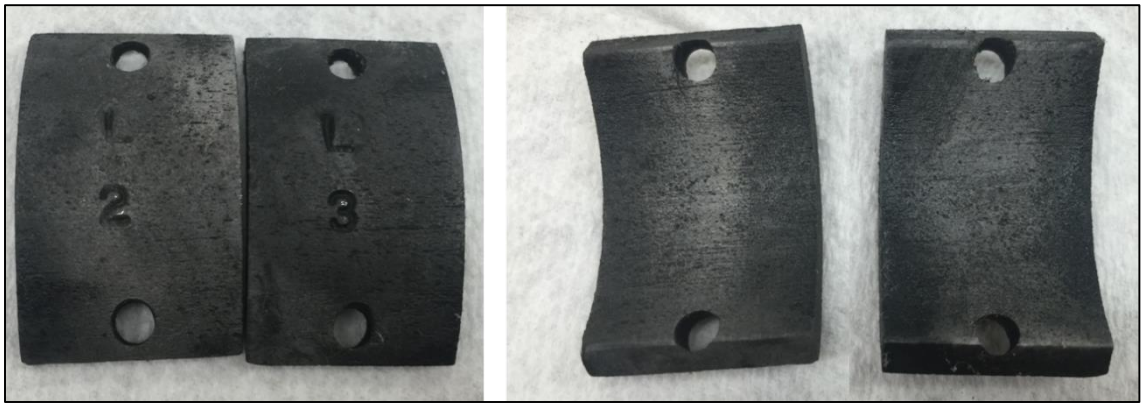

Fig. 8 – Results of L-80 test with 20 wt% GLDA (pH = 4). Coupon after corrosion outer side surface (left) and inner side surface (right). Test was conducted for 4 hours at >1000 psi at 300°F.

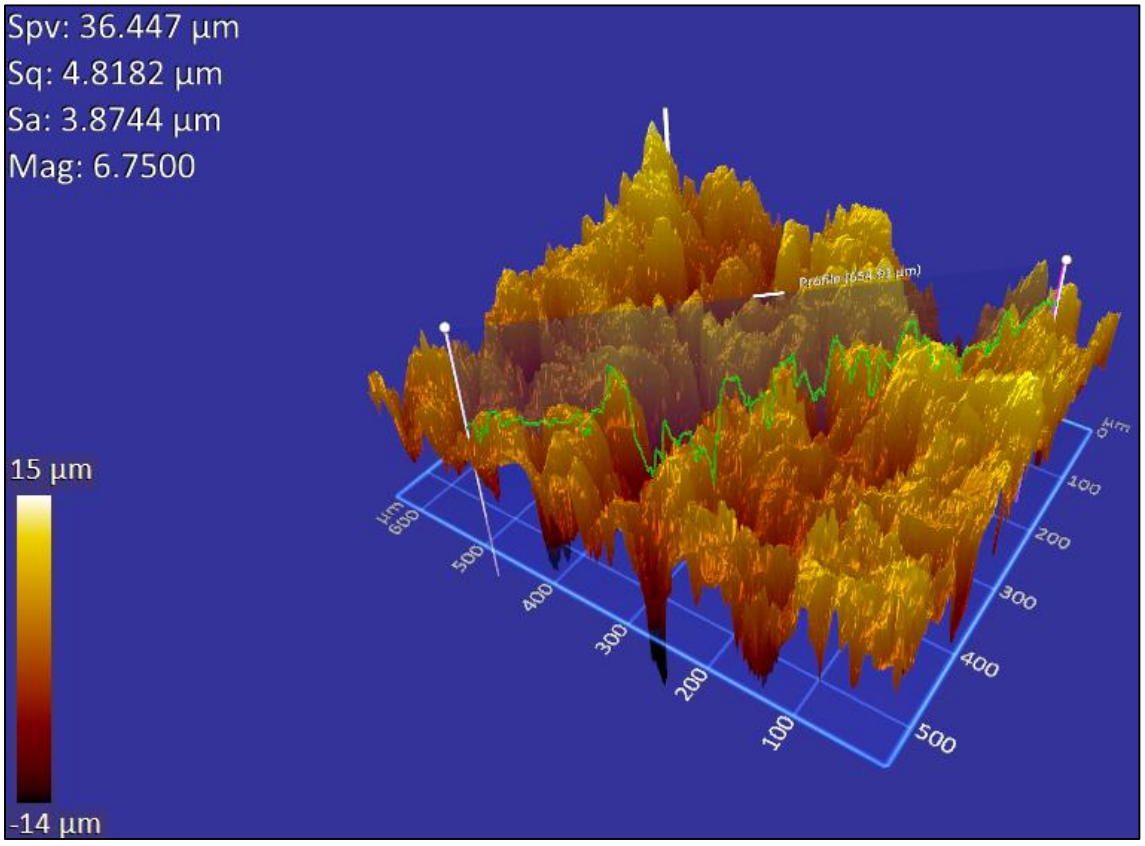

Fig. 9 – Results of L-80 test with 20 wt% GLDA (pH = 4). Selected ZeGage sample from coupon L-2 before corrosion test to show roughness parameters. Spv of 36.4 µm and Sq of 4.8 µm. Test was conducted for 4 hours at >1000 psi at 300°F.

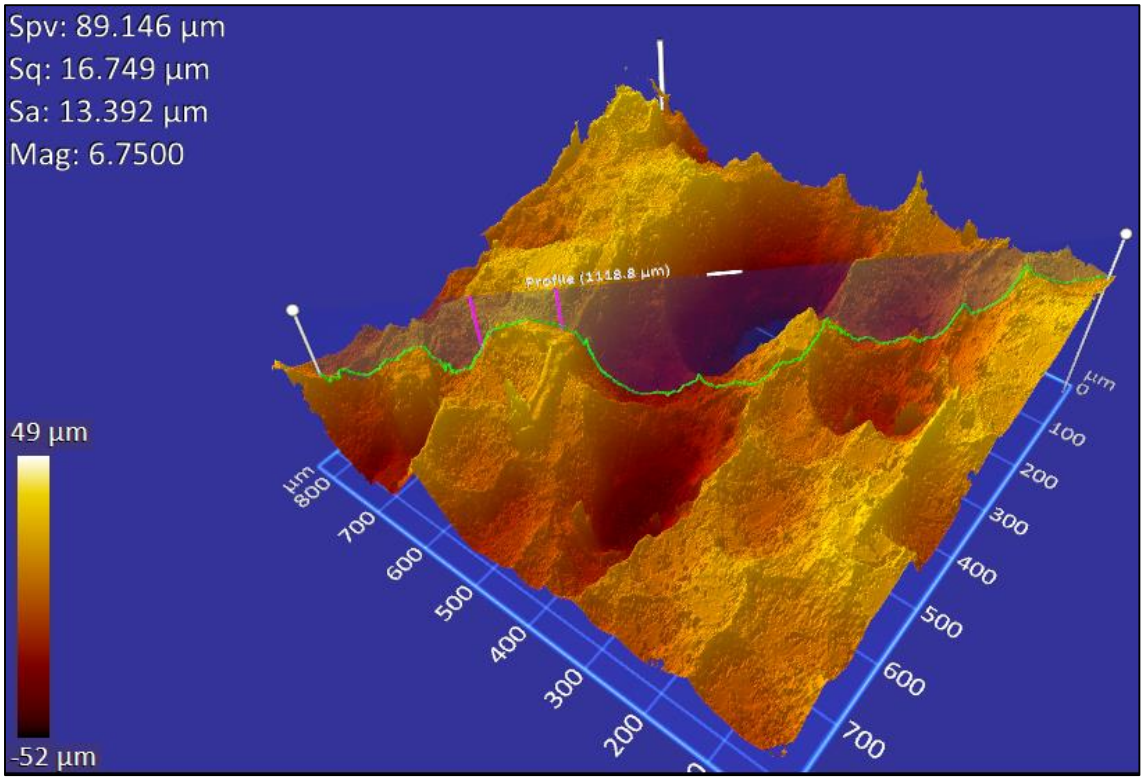

Fig. 10 – Results of L-80 test with 20 wt% GLDA (pH = 4). Selected ZeGage sample from coupon L-2 after corrosion test to show roughness parameters. Spv of 89.1 µm and Sq of 16.7 µm. Some evidence of pitting. Test was conducted for 4 hours at >1000 psi at 300°F.

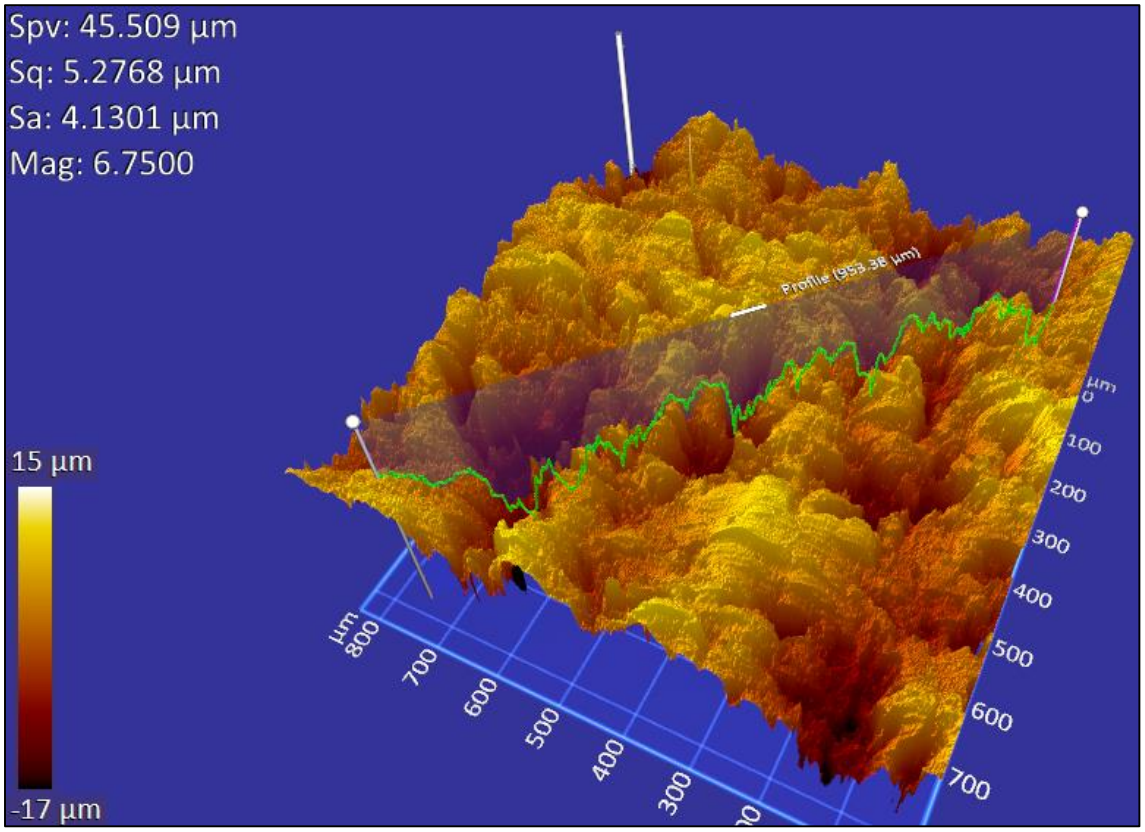

Fig. 11 – Results of L-80 test with 20 wt% GLDA (pH = 4). Selected ZeGage sample from coupon L-3 before corrosion test to show roughness parameters. Spv of 45.5 µm and Sq of 5.3 µm. Test was conducted for 4 hours at >1000 psi at 300°F.

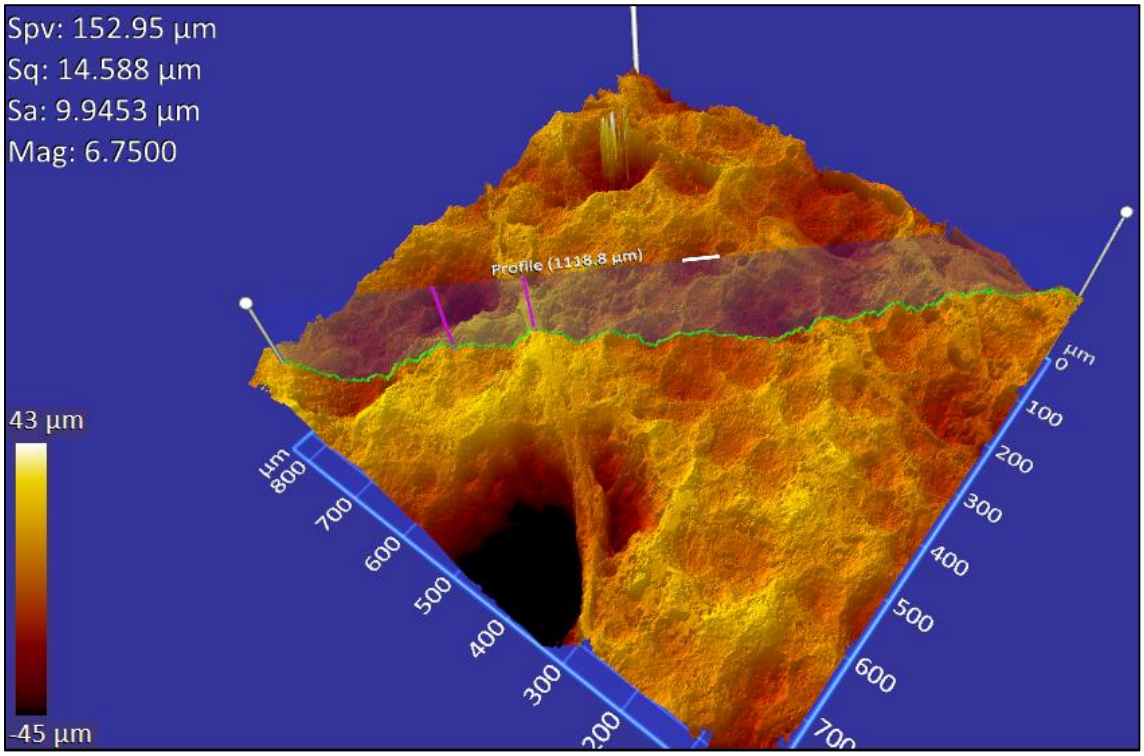

Fig. 12 – Results of L-80 test with 20 wt% GLDA (pH = 4). Selected ZeGage sample from coupon L-3 after corrosion test to show roughness parameters. Spv of 153.0 µm and Sq of 14.6 µm. Some evidence of pitting. Test was conducted for 4 hours at >1000 psi at 300°F.

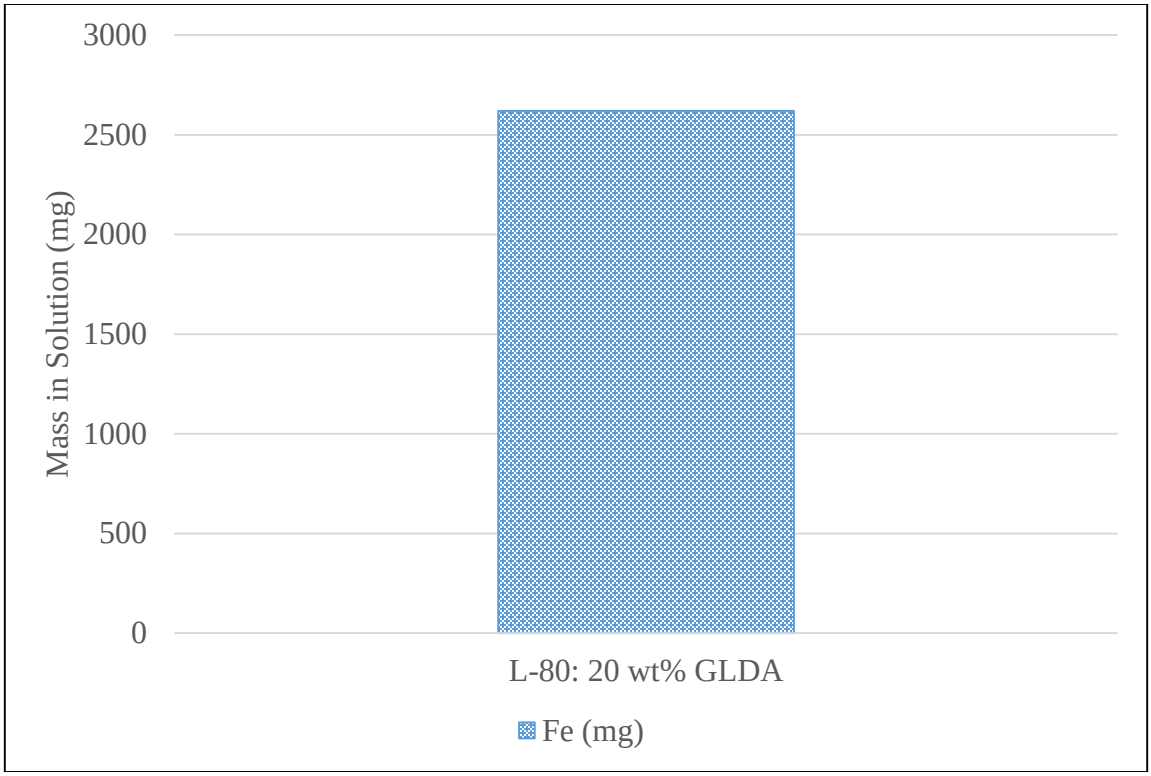

Fig. 13 – ICP-OES results for Fe for L-80 test with 20 wt% GLDA (pH = 4). Test was conducted for 4 hours at >1000 psi at 300°F.

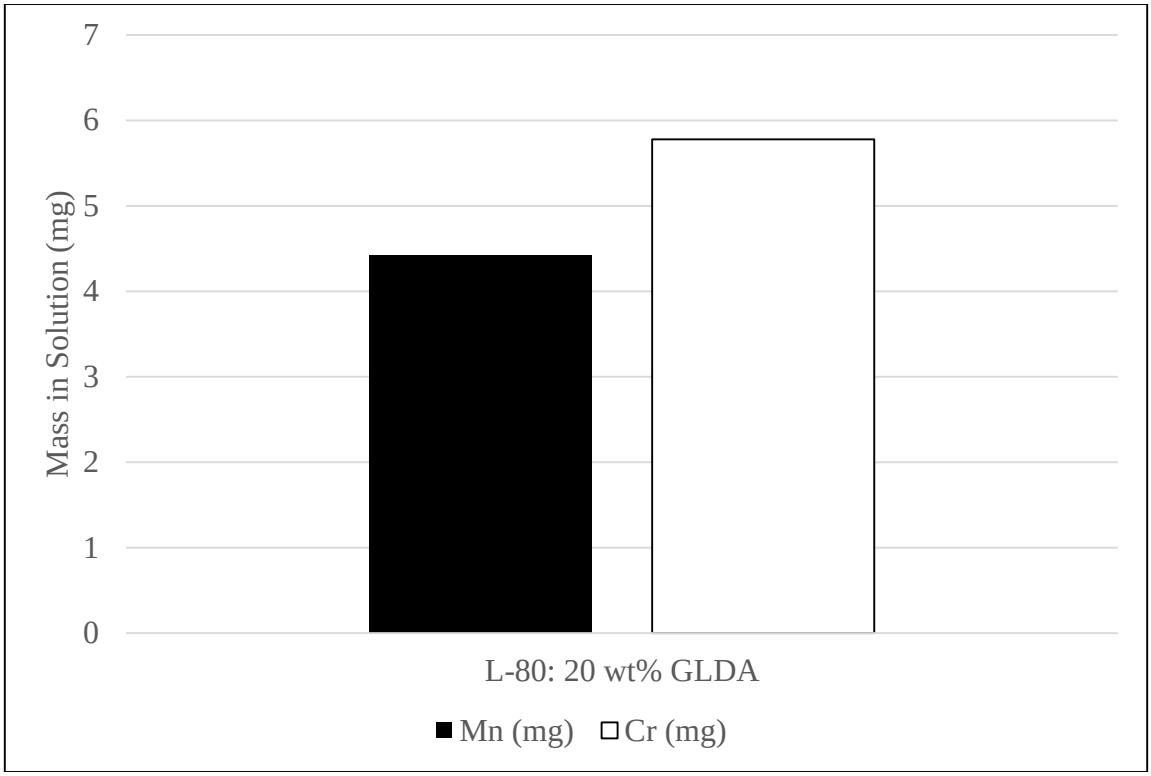

Fig. 14 – ICP-OES results for Mn and Cr for L-80 test with 20 wt% GLDA (pH = 4). Test was conducted for 4 hours at >1000 psi at 300°F.

3.2 Comparing EDTA and GLDA at 300°F (LT) with No Salt

The following shows the results between S13Cr-110 and the chelating agents (EDTA and GLDA) at 300°F (LT) for 6 hours at >1000 psi. The concentration of the chelating agent was maintained at 20 wt% and the balance fluid was DI water. The pH was maintained at 4. GLDA was already provided from the manufacturer at a pH of 4. For EDTA, HCl was used to bring the pH down from 11.6 to 4. The fluid/surface area ratio was 170 mL/in^2, which meets the NACE ASTM G31 (2012) requirement of at least 130 mL/in^2 and the corrosion rates were 1.14 x 10^{-4} lb/ft^2 (EDTA) and 2.51 x 10^{-4} lb/ft^2 (GLDA). The results are shown graphically in **Fig. 15**. Due to the low corrosion rate,

ZeGage analysis was not conducted on these tests. The coupons before and after testing are shown in **Fig. 16** (EDTA) and **Fig. 17 (**GLDA**)**. ICP-OES results of the effluent sample are shown in **Fig. 18** (Mn, Cr, Fe) and **Fig. 19** (Ni, Mo). The ICP-OES results were also summed together for the cations to give a mass loss by ICP-OES (**Fig. 20**). The fluid change is shown in **Fig. 21** (EDTA) and **Fig. 22** (GLDA).

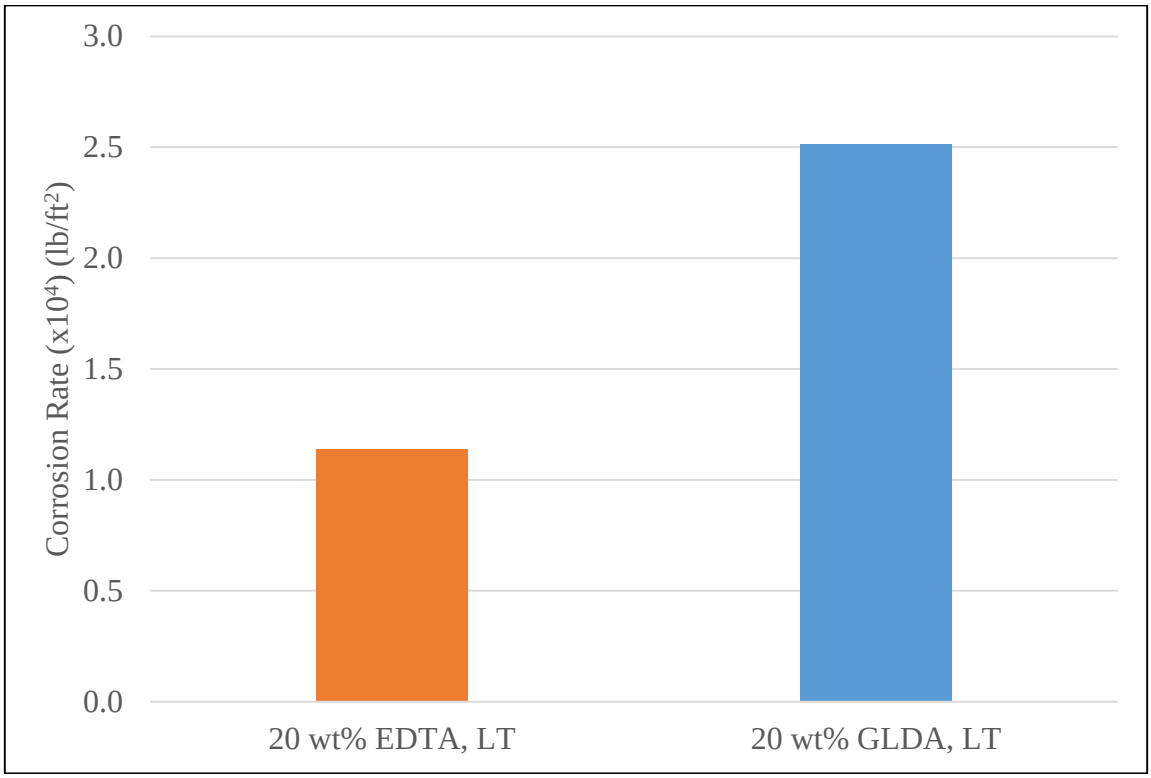

Fig. 15 – Corrosion rate results of S13Cr-110 with 20 wt% EDTA (pH = 4) and 20 wt% GLDA (pH = 4). Each test was conducted for 6 hours at >1000 psi at 300°F.

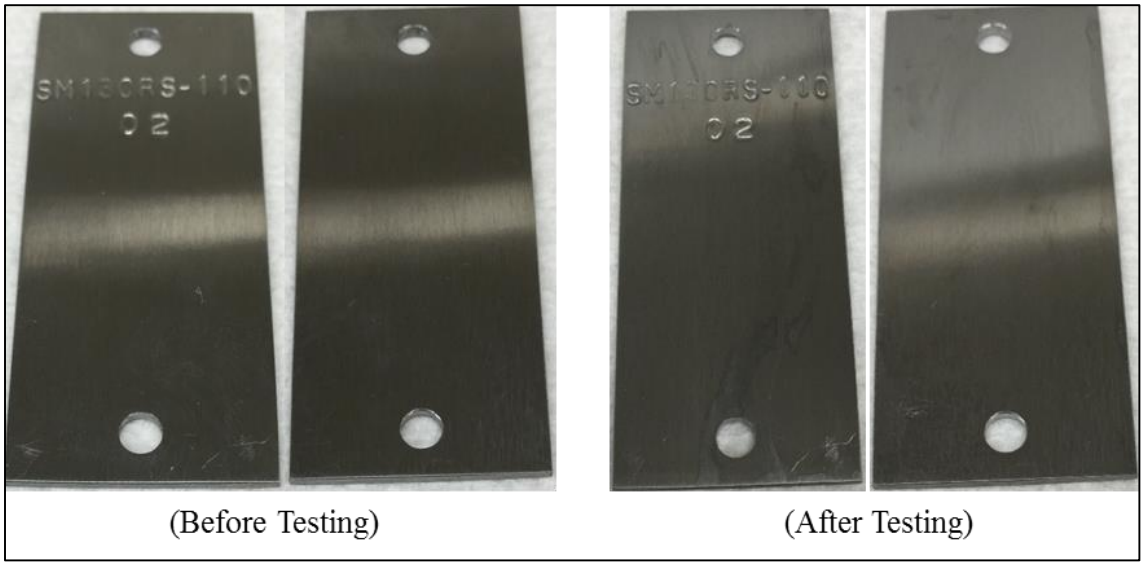

Fig. 16 – Results of S13Cr-110 test with 20 wt% EDTA (pH = 4). Coupon before testing (left) after testing (right). Test was conducted for 6 hours at >1000 psi at 300°F.

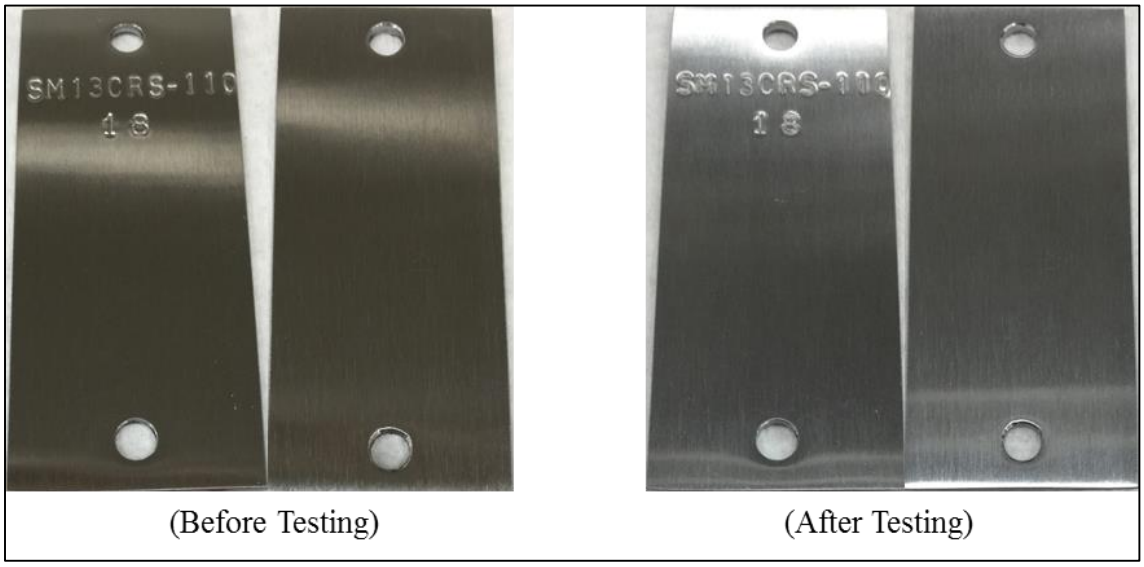

Fig. 17 – Results of S13Cr-110 test with 20 wt% GLDA (pH = 4). Coupon before testing (left) after testing (right). Test was conducted for 6 hours at >1000 psi at 300°F.

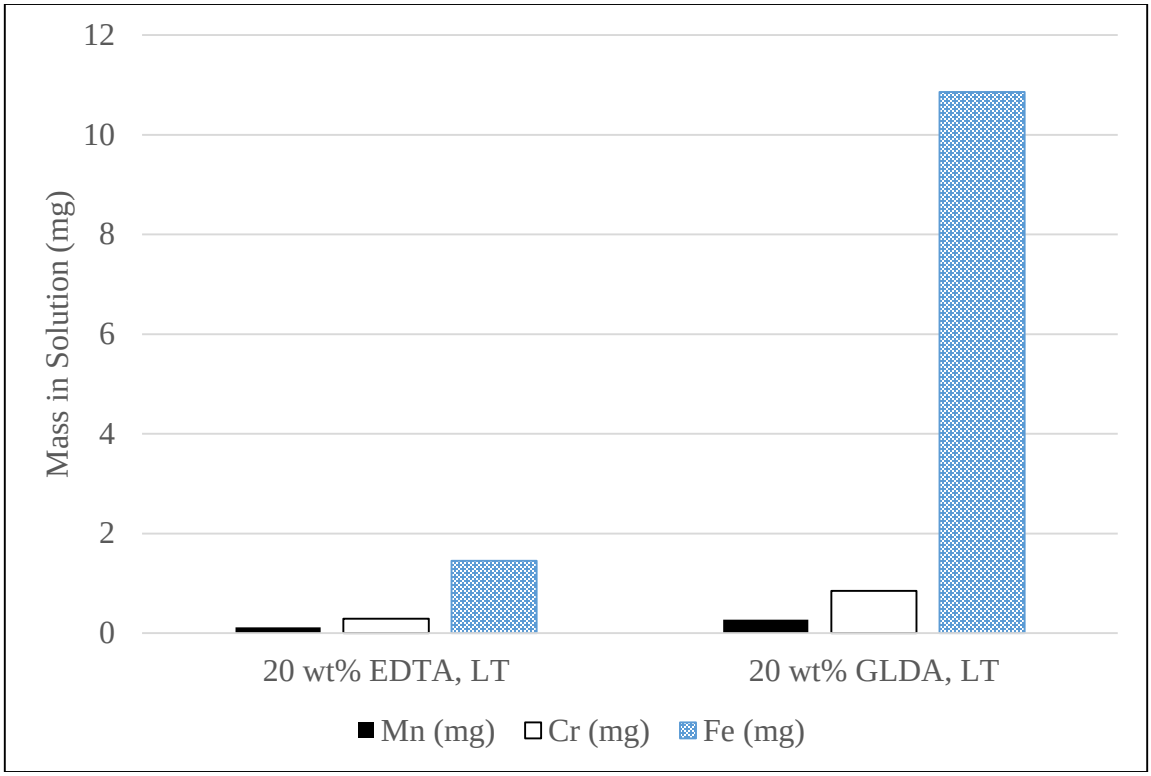

Fig. 18 – ICP-OES results for Mn, Cr, and Fe for S13Cr-110 test with 20 wt% EDTA (pH = 4) and 20 wt% GLDA (pH = 4). Each test was conducted for 6 hours at >1000 psi at 300°F.

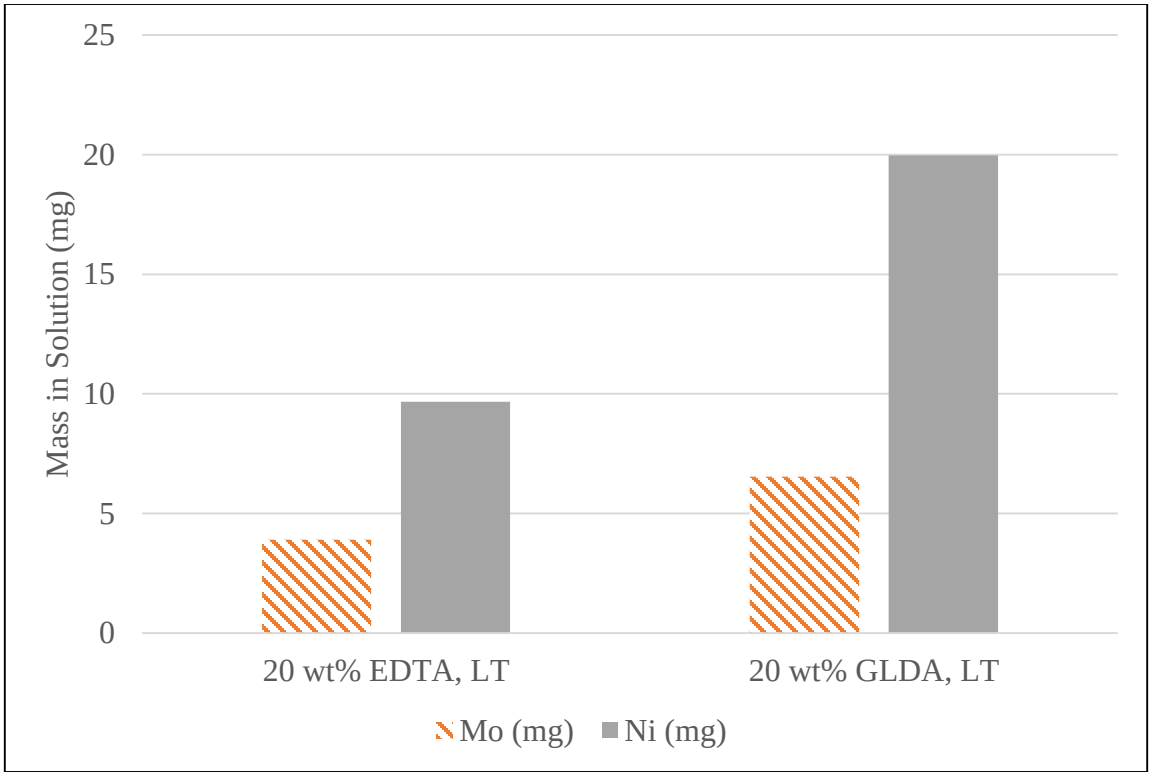

Fig. 19 – ICP-OES results for Mo and Ni for S13Cr-110 test with 20 wt% EDTA (pH = 4) and 20 wt% GLDA (pH = 4). Each test was conducted for 6 hours at >1000 psi at 300°F.

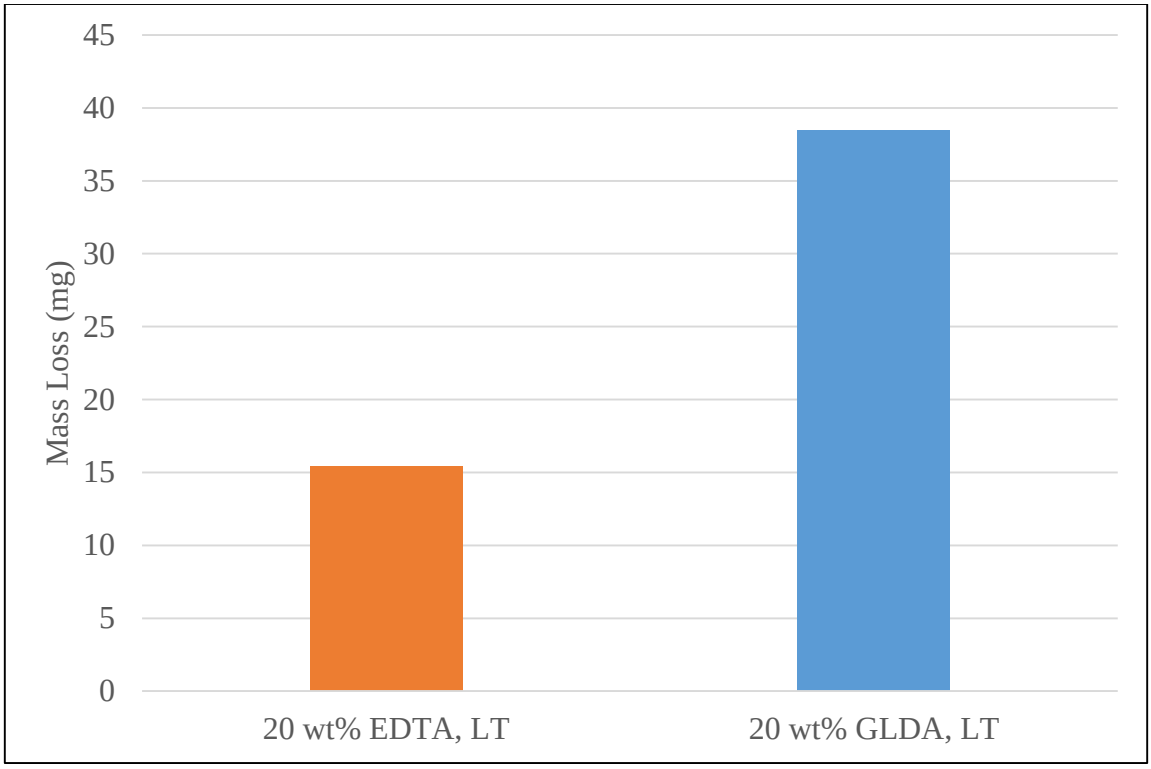

Fig. 20 – ICP-OES results for mass loss for S13Cr-110 test with 20 wt% EDTA (pH = 4) and 20 wt% GLDA (pH = 4). Each test was conducted for 6 hours at >1000 psi at 300°F.

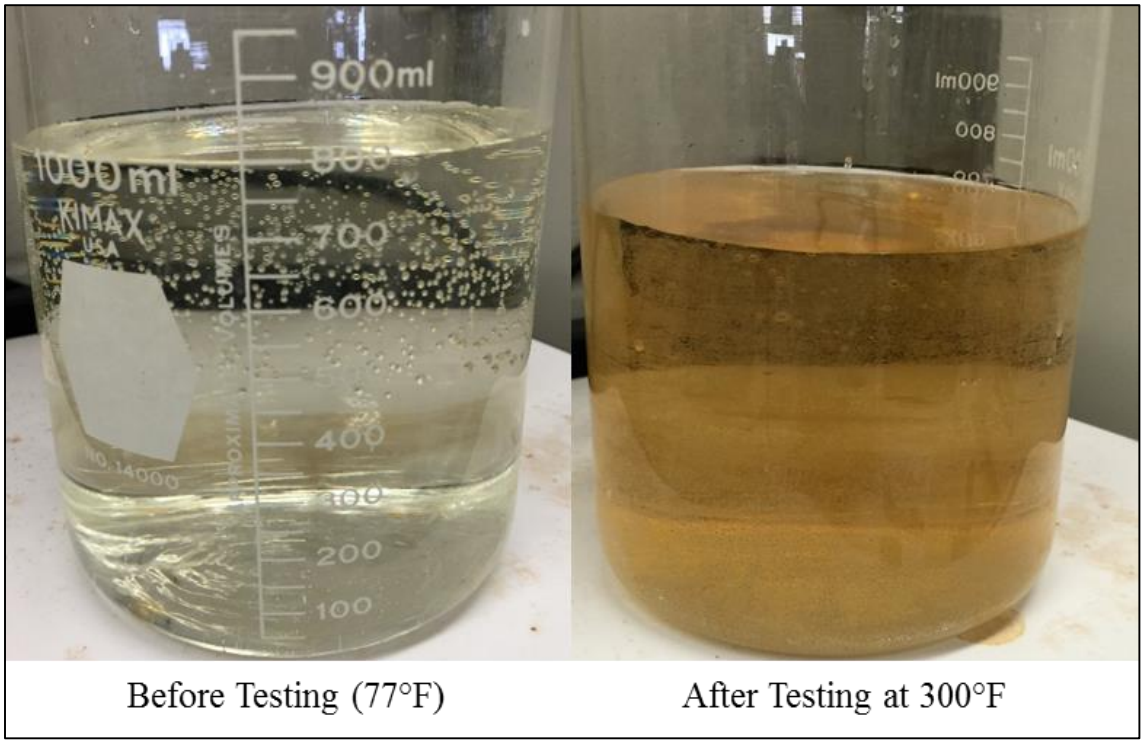

Fig. 21 – Fluid color change for S13Cr-110 test with 20 wt% EDTA (pH = 4). Test was conducted for 6 hours at >1000 psi at 300°F.

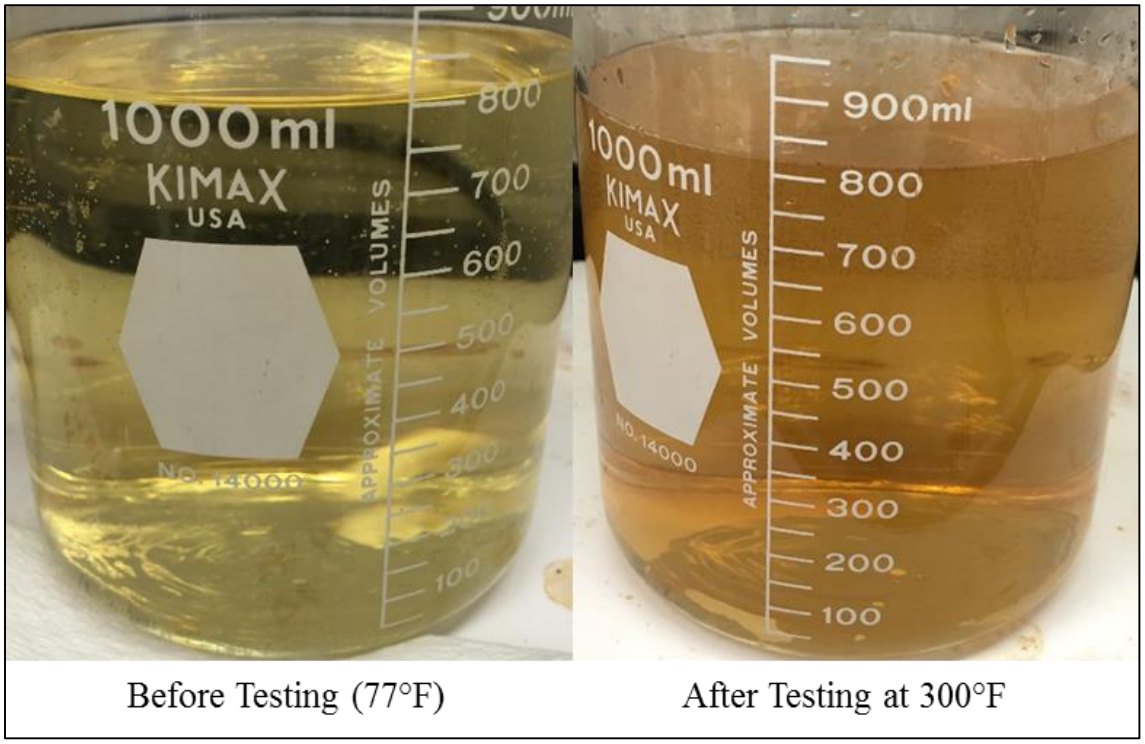

Fig. 22 – Fluid color change for S13Cr-110 test with 20 wt% GLDA (pH = 4). Test was conducted for 6 hours at >1000 psi at 300°F.

3.3 Comparing EDTA and GLDA at 350°F (HT) with No Salt

The following shows the results between S13Cr-110 and the chelating agents (EDTA and GLDA) at 350°F (HT) for 6 hours at >1000 psi. The concentration of the chelating agent was maintained at 20 wt% and the balance fluid was DI water. The pH was maintained at 4. GLDA was already provided from the manufacturer at a pH of 4. For EDTA, HCl was used to bring the pH down from 11.6 to 4. The fluid/surface area ratio was 170 mL/in^2, which meets the NACE ASTM G31 (2012) requirement of at least 130 mL/in^2, and the corrosion rates were 8.84 x 10^{-4} lb/ft^2 (EDTA) and 82.69 x 10^{-4} lb/ft^2 (GLDA). The results are shown graphically in **Fig. 23**. Due to the low corrosion rate,

ZeGage analysis was not conducted on these tests. The coupons before and after testing are shown in **Fig. 24** (EDTA) and **Fig. 25 (**GLDA**)**. ICP-OES results of the effluent sample are shown in **Fig. 26** (Mn, Cr, Fe) and **Fig. 27** (Ni, Mo). The ICP-OES results were also summed together for the cations to give a mass loss by ICP-OES (**Fig. 28**). The fluid change is shown in **Fig. 29** (EDTA) and **Fig. 30** (GLDA).

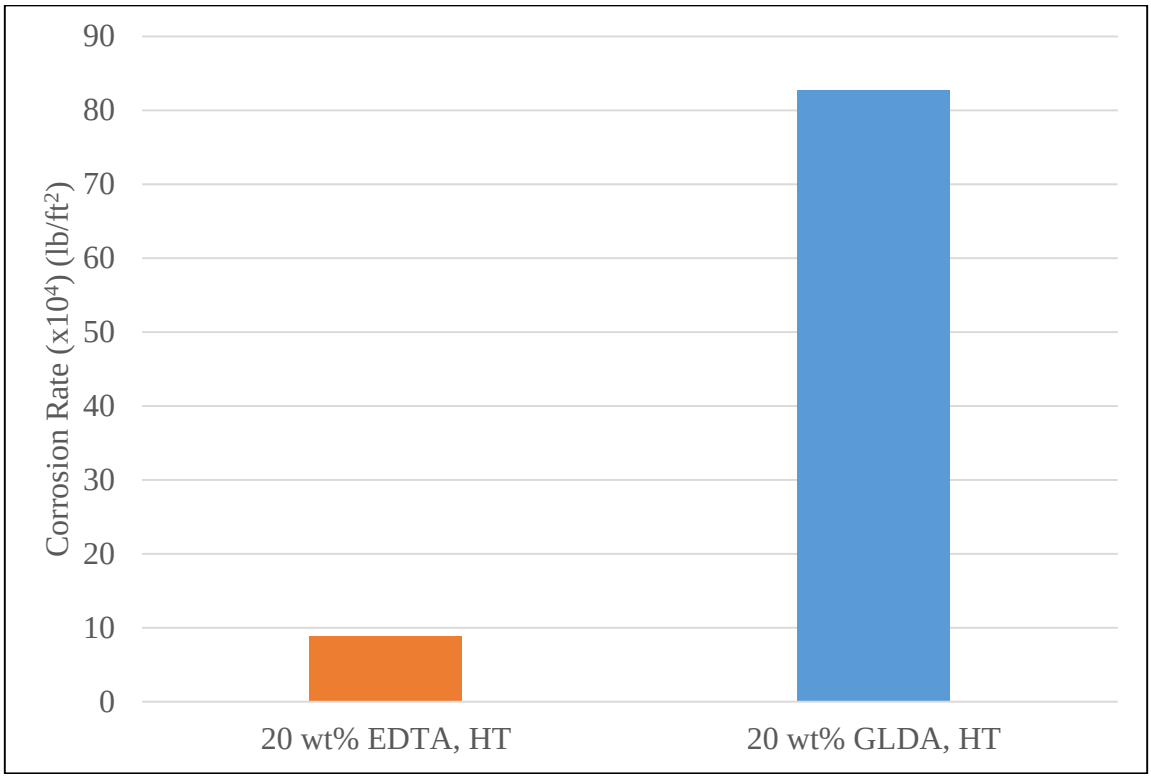

Fig. 23 – Corrosion Rate results of S13Cr-110 with 20 wt% EDTA (pH = 4) and 20 wt% GLDA (pH = 4). Each test was conducted for 6 hours at >1000 psi at 350°F.

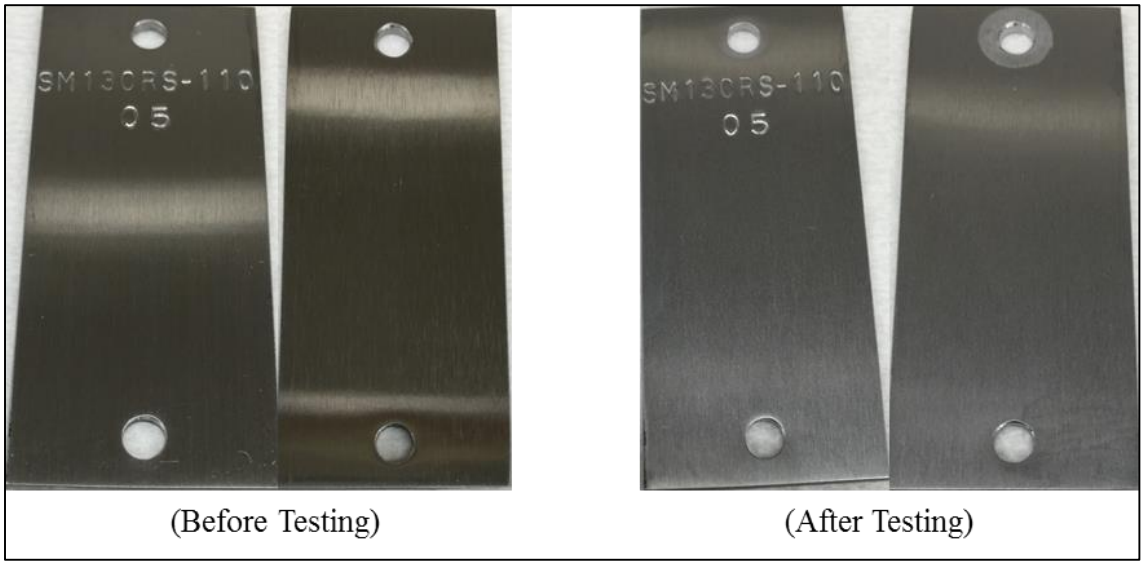

Fig. 24 – Results of S13Cr-110 test with 20 wt% EDTA (pH = 4). Coupon before testing (left) after testing (right). Test was conducted for 6 hours at >1000 psi at 350°F.

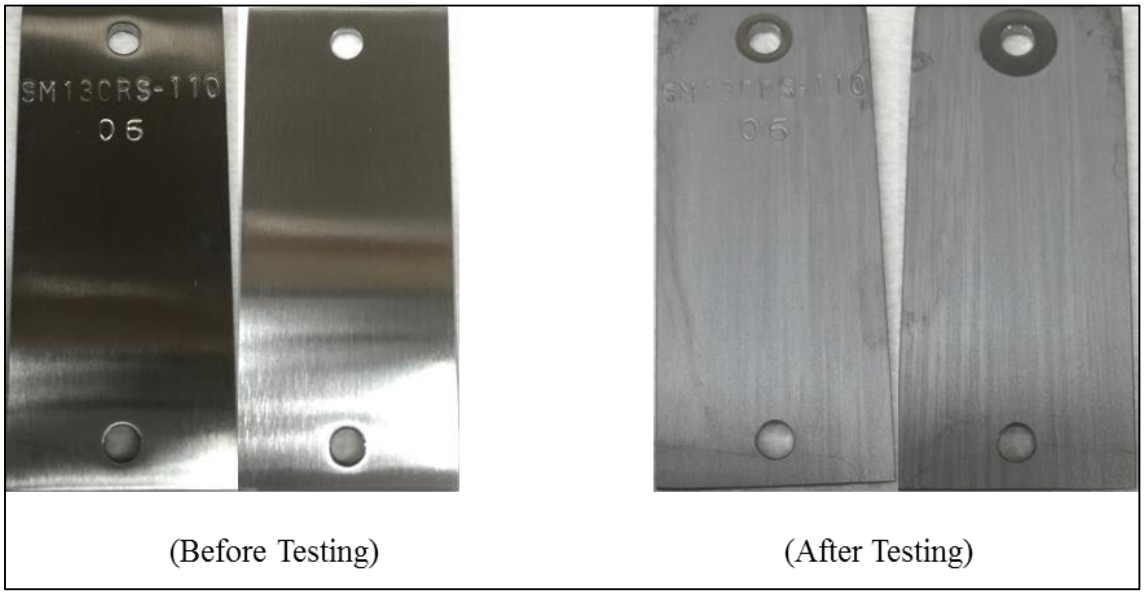

Fig. 25 – Results of S13Cr-110 test with 20 wt% GLDA (pH = 4). Coupon before testing (left) after testing (right). Test was conducted for 6 hours at >1000 psi at 350°F.

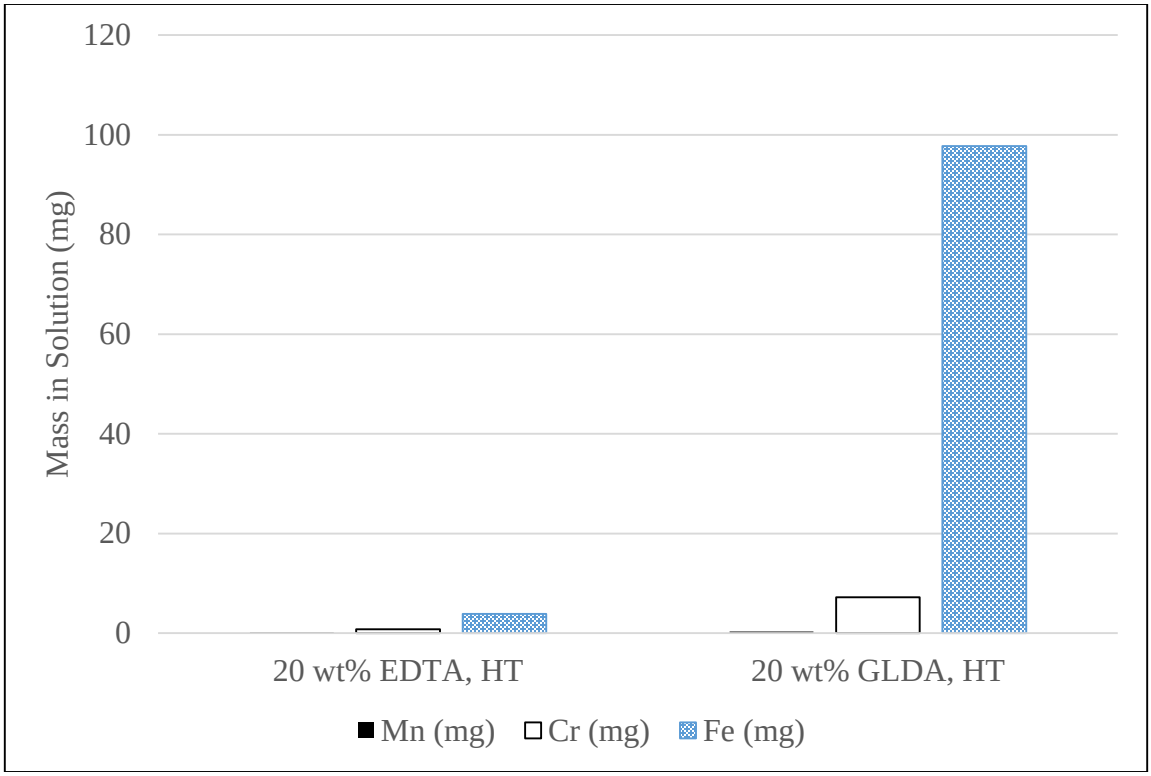

Fig. 26 – ICP-OES results for Mn, Cr, and Fe for S13Cr-110 test with 20 wt% EDTA (pH = 4) and 20 wt% GLDA (pH = 4). Each test was conducted for 6 hours at >1000 psi at 350°F.

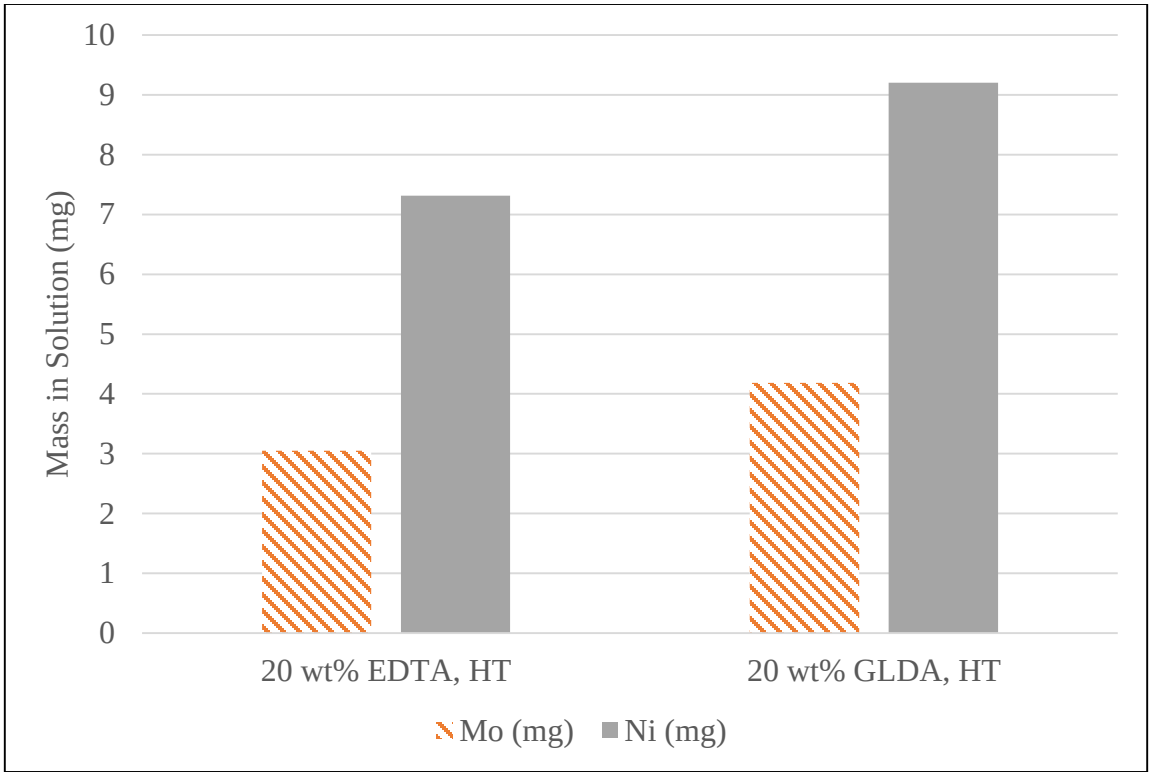

Fig. 27 – ICP-OES results for Mo and Ni for S13Cr-110 test with 20 wt% EDTA (pH = 4) and 20 wt% GLDA (pH = 4). Each test was conducted for 6 hours at >1000 psi at 350°F.

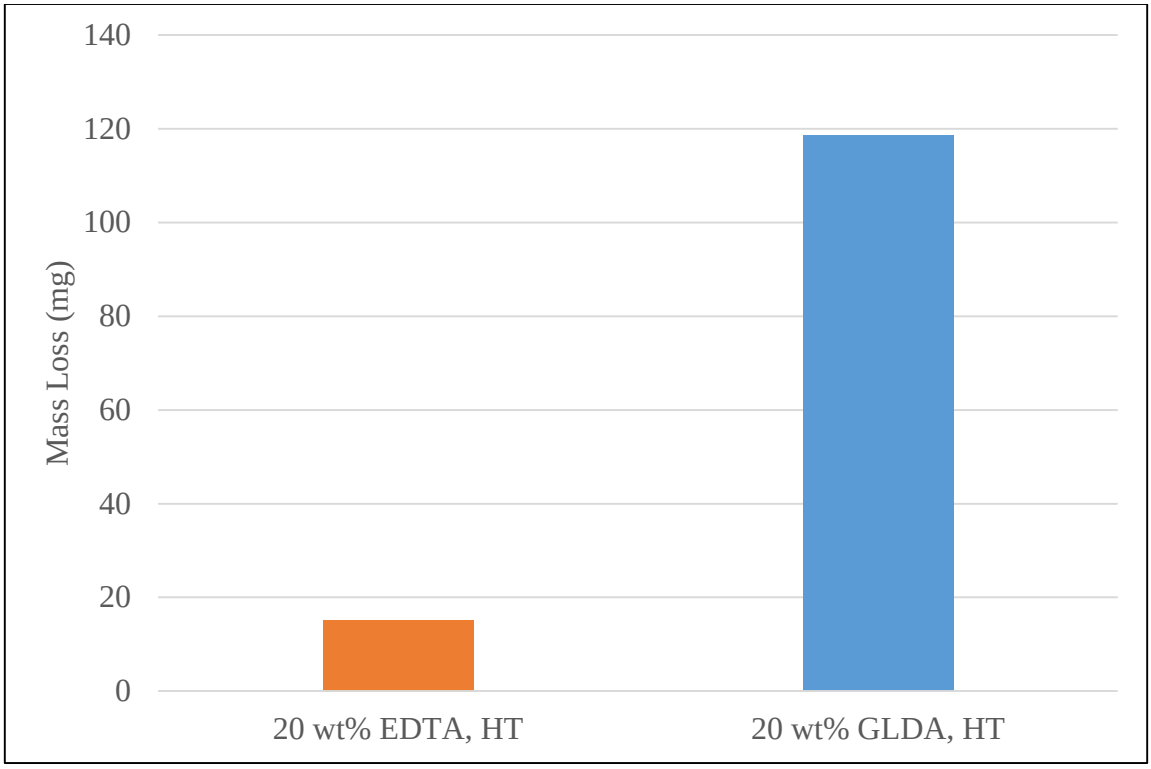

Fig. 28 – ICP-OES results for mass loss for S13Cr-110 test with 20 wt% EDTA (pH = 4) and 20 wt% GLDA (pH = 4). Each test was conducted for 6 hours at >1000 psi at 350°F.

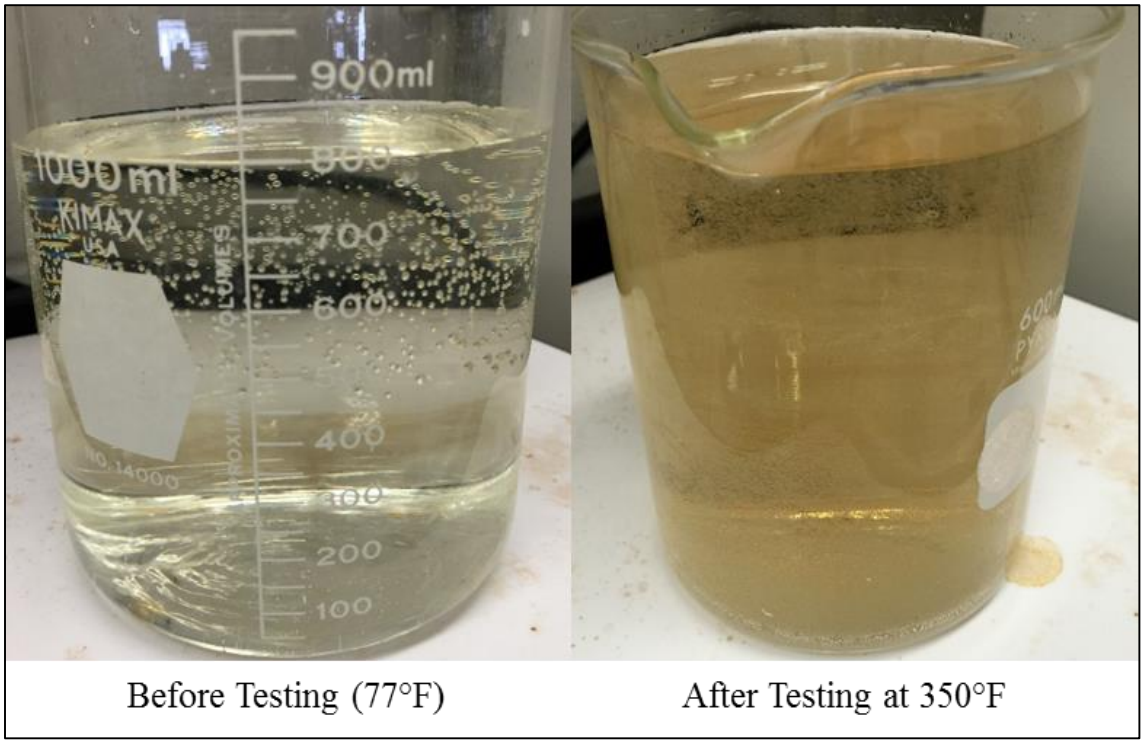

Fig. 29 – Fluid color change for S13Cr-110 test with 20 wt% EDTA (pH = 4). Test was conducted for 6 hours at >1000 psi at 350°F.

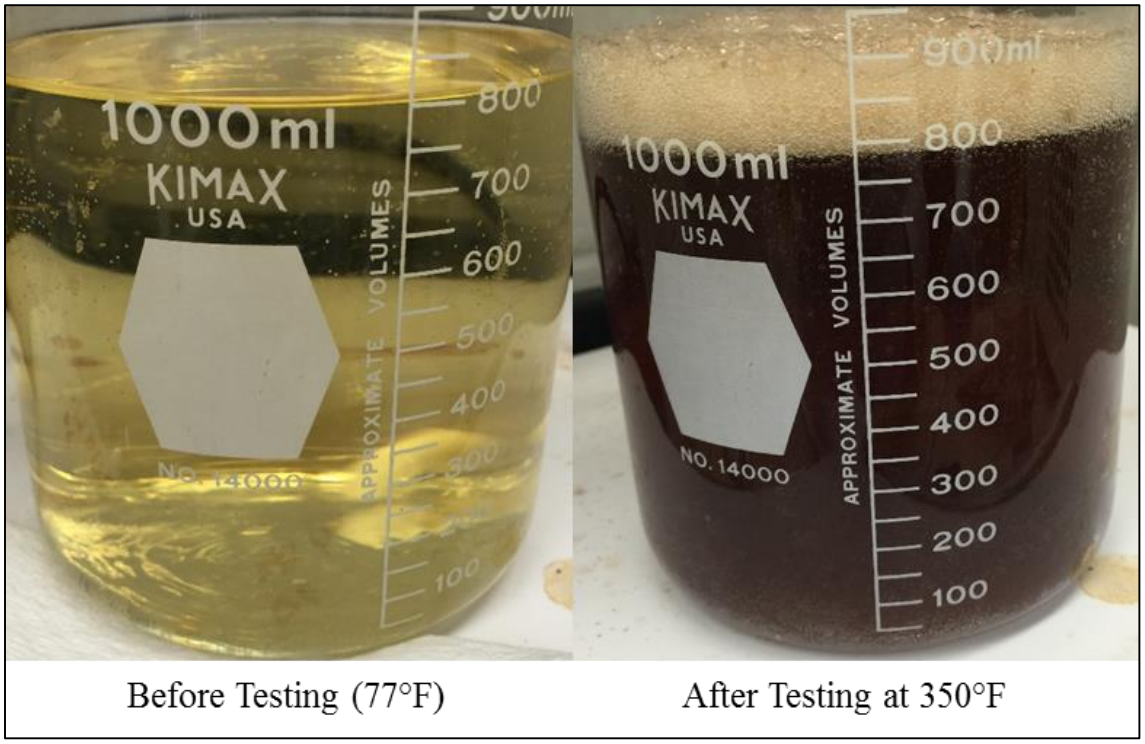

Fig. 30 – Fluid color change for S13Cr-110 test with 20 wt% GLDA (pH = 4). Test was conducted for 6 hours at >1000 psi at 350°F.

3.4 Comparing EDTA and GLDA at 300°F (LT) with Salt

The following shows the results between S13Cr-110 and the chelating agents (EDTA and GLDA) at 300°F (LT) for 6 hours at >1000 psi. The concentration of the chelating agent was maintained at 20 wt%, 5 wt% NaCl was added, and the balance fluid was DI water. The pH was maintained at 4 for GLDA. However, due to the low solubility of EDTA at low pH with NaCl, the pH tested was 9. HCl was used to bring the pH of EDTA from 11.6 to 9. The fluid/surface area ratio was 150 mL/in^2, which meets the NACE ASTM G31 (2012) requirement of at least 130 mL/in^2, and the corrosion rates were 3.34 x 10^{-4} lb/ft^2 (EDTA) and 2.33 x 10^{-4} lb/ft^2 (GLDA). The results are shown graphically in

Fig. 31. Due to the low corrosion rate, ZeGage analysis was not conducted on these tests. The coupons before and after testing are shown in **Fig. 32** (EDTA) and **Fig. 33 (**GLDA**)**. ICP-OES results of the effluent sample are shown in **Fig. 34** (Mn, Cr, Fe) and **Fig. 35** (Ni, Mo). The ICP-OES results were also summed together for the cations to give a mass loss by ICP-OES (**Fig. 36**). The fluid change is shown in **Fig. 37** (EDTA) and **Fig. 38** (GLDA).

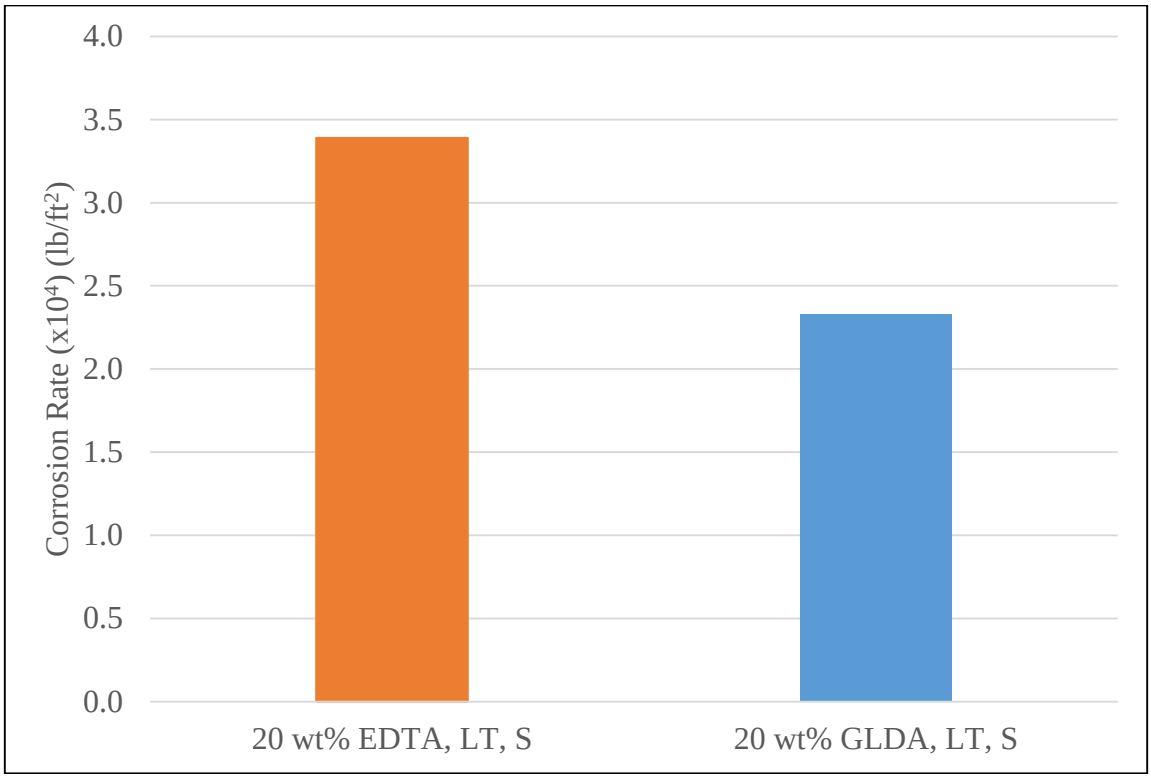

Fig. 31 – Corrosion Rate results of S13Cr-110 with 20 wt% EDTA (pH = 9) and 20 wt% GLDA (pH = 4). Each test was conducted for 6 hours at >1000 psi at 300°F with 5 wt% NaCl.

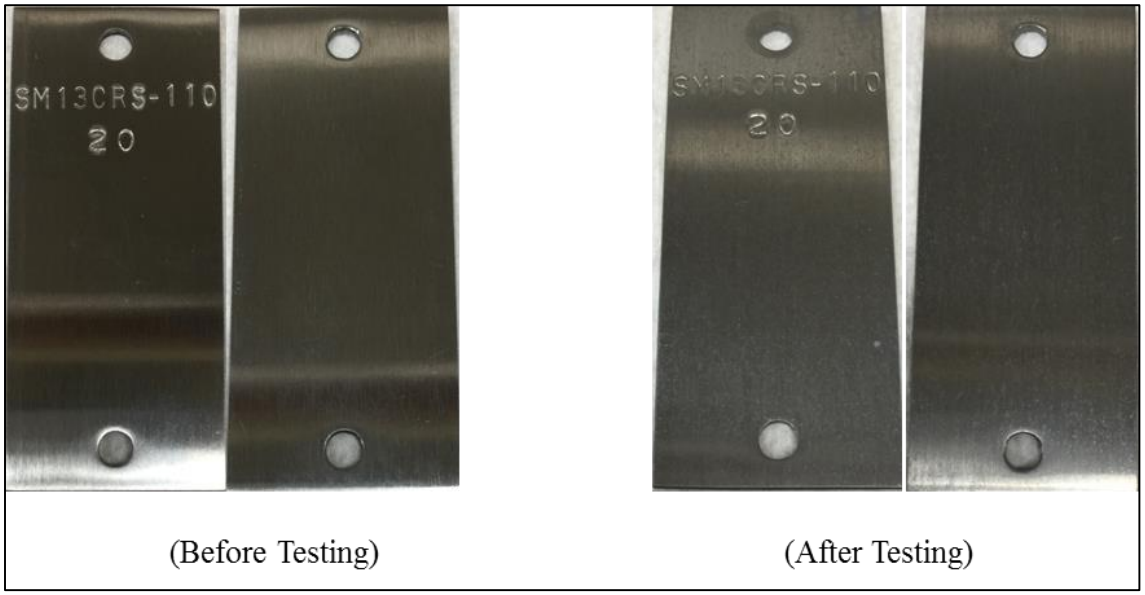

Fig. 32 – Results of S13Cr-110 test with 20 wt% EDTA (pH = 9). Coupon before testing (left) after testing (right). Test was conducted for 6 hours at >1000 psi at 300°F with 5 wt% NaCl.

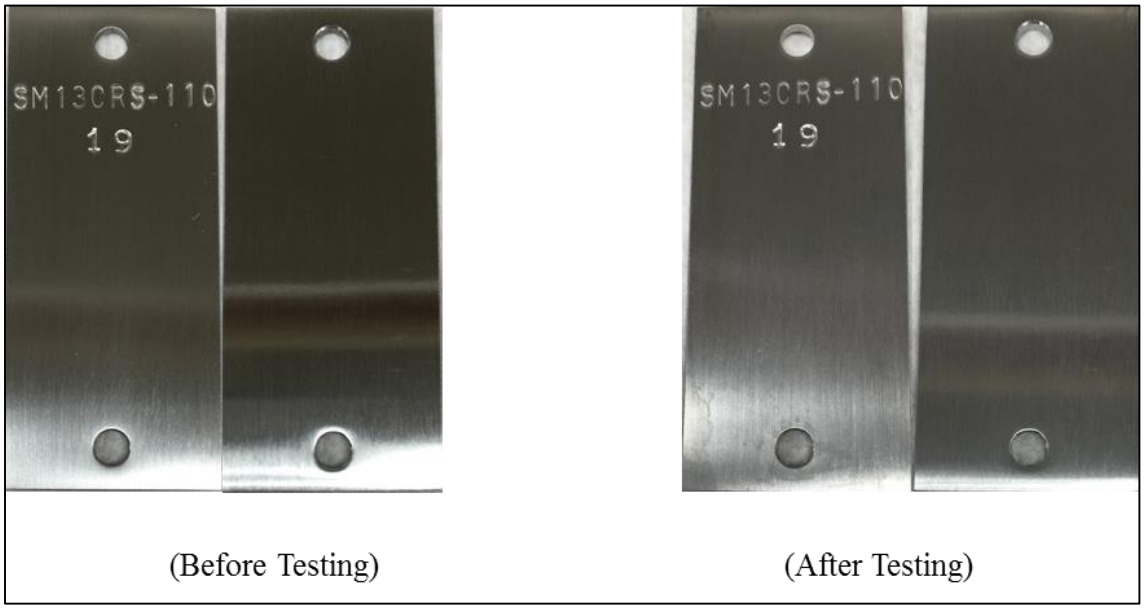

Fig. 33 – Results of S13Cr-110 test with 20 wt% GLDA (pH = 4). Coupon before testing (left) after testing (right). Test was conducted for 6 hours at >1000 psi at 300°F with 5 wt% NaCl.

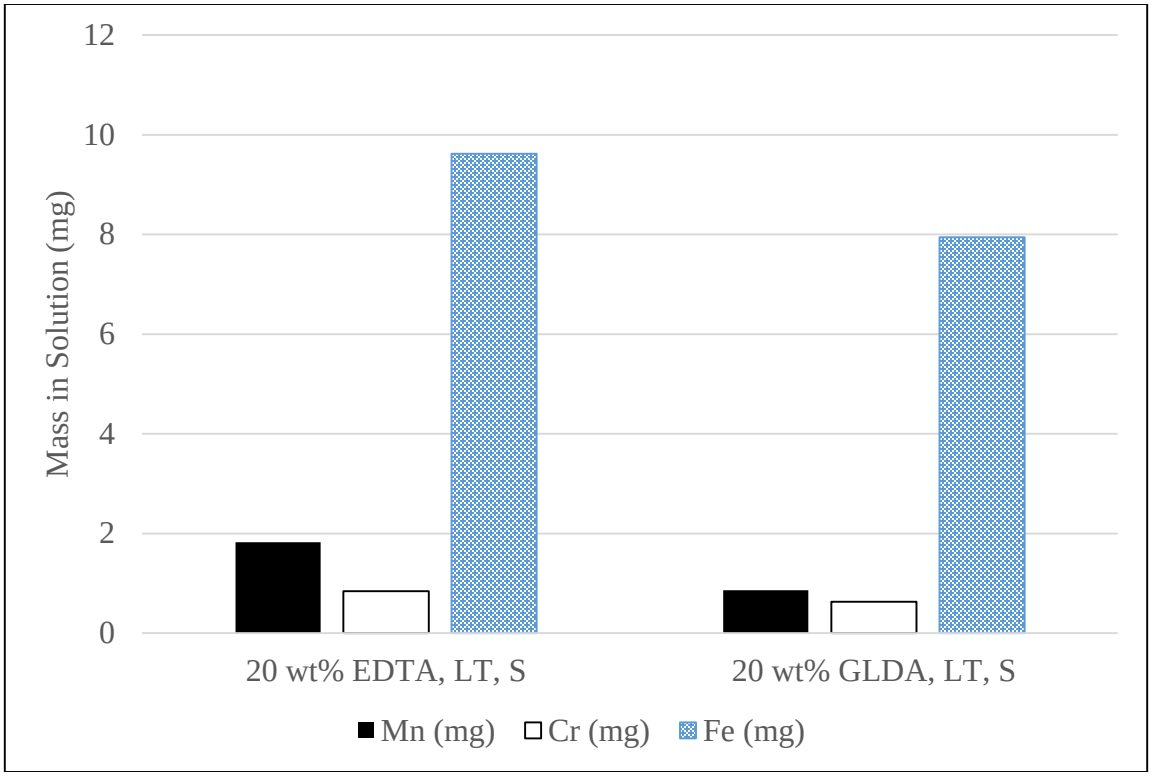

Fig. 34 – ICP-OES results for Mn, Cr, and Fe for S13Cr-110 test with 20 wt% EDTA (pH = 9) and 20 wt% GLDA (pH = 4). Each test was conducted for 6 hours at >1000 psi at 300°F with 5 wt% NaCl.

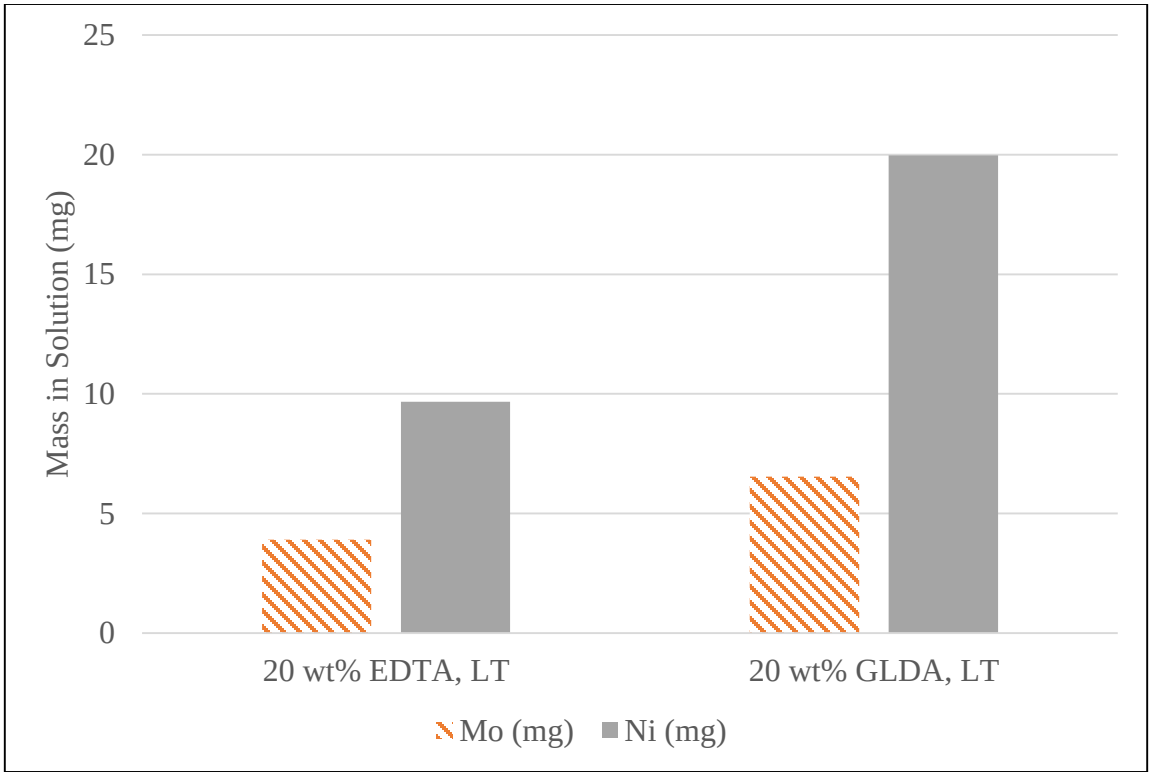

Fig. 35 – ICP-OES results for Mo and Ni for S13Cr-110 test with 20 wt% EDTA (pH = 9) and 20 wt% GLDA (pH = 4). Each test was conducted for 6 hours at >1000 psi at 300°F with 5 wt% NaCl.

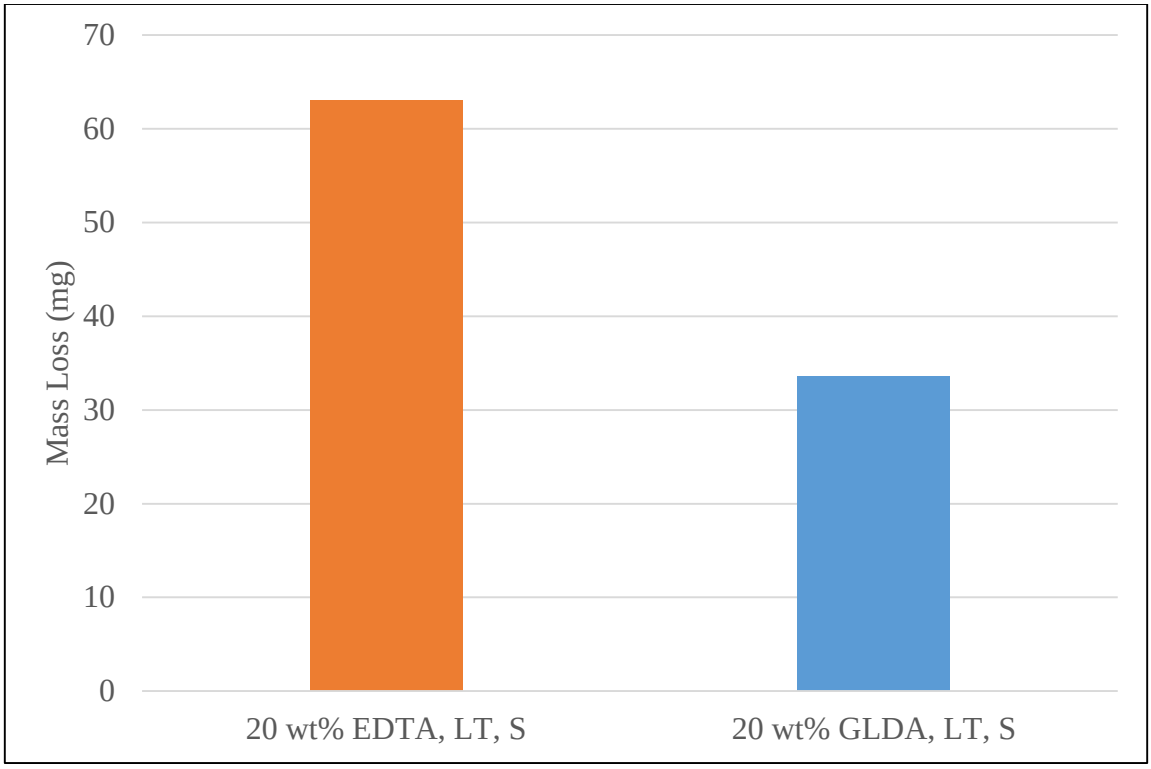

Fig. 36 – ICP-OES results for mass loss for S13Cr-110 test with 20 wt% EDTA (pH = 9) and 20 wt% GLDA (pH = 4). Each test was conducted for 6 hours at >1000 psi at 300°F with 5 wt% NaCl.

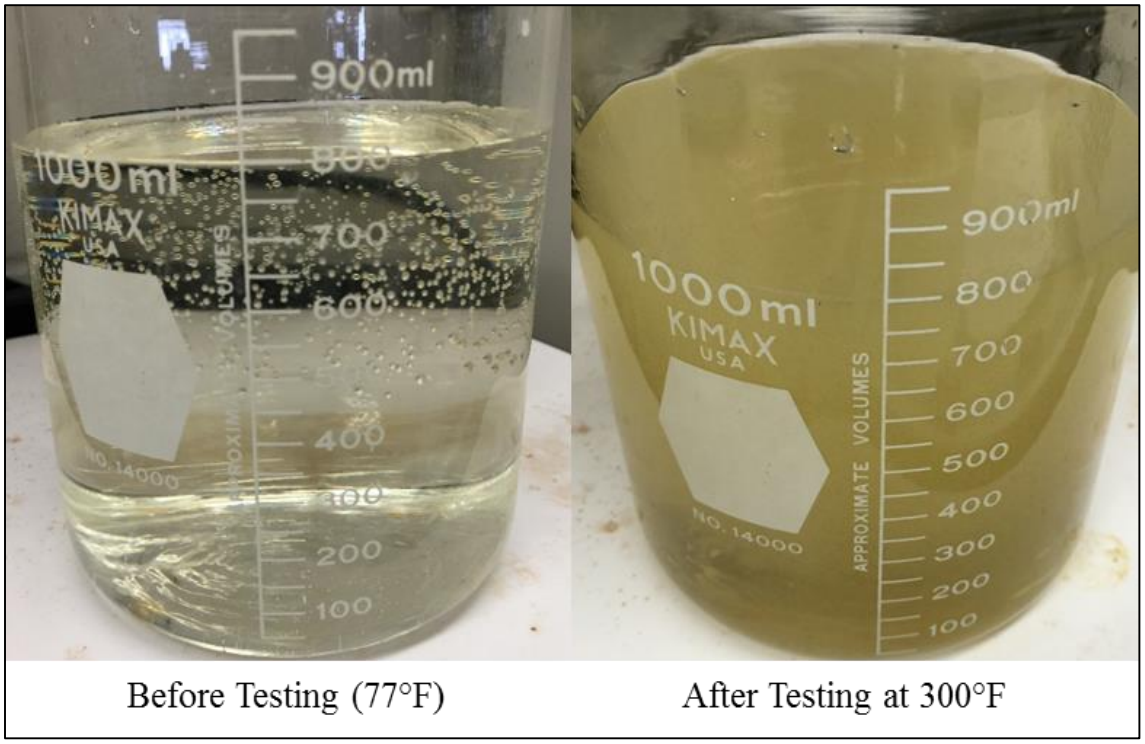

Fig. 37 – Fluid color change for S13Cr-110 test with 20 wt% EDTA (pH = 9). Test was conducted for 6 hours at >1000 psi at 300°F with 5 wt% NaCl.

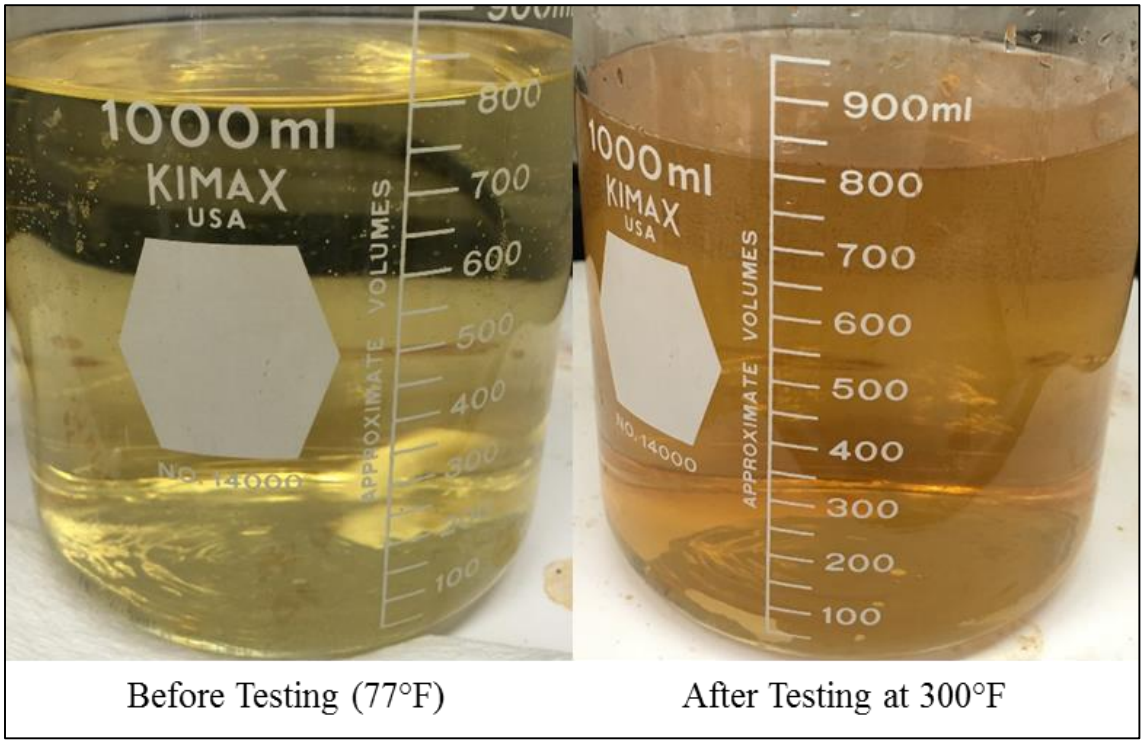

Fig. 38 – Fluid color change for S13Cr-110 test with 20 wt% GLDA (pH = 4). Test was conducted for 6 hours at >1000 psi at 300°F with 5 wt% NaCl.

3.5 Comparing EDTA and GLDA at 350°F (HT) with Salt

The following shows the results between S13Cr-110 and the chelating agents (EDTA and GLDA) at 350°F (LT) for 6 hours at >1000 psi. The concentration of the chelating agent was maintained at 20 wt%, 5 wt% NaCl was added, and the balance fluid was DI water. The pH was maintained at 4 for GLDA. However, due to the low solubility of EDTA at low pH with NaCl, the pH tested was 9. HCl was used to bring the pH of EDTA from 11.6 to 9. The fluid/surface area ratio was 150 mL/in^2, which meets the NACE ASTM G31 (2012) requirement of at least 130 mL/in^2, and the corrosion rates were 34.50 x 10^{-4} lb/ft^2 (EDTA) and 81.15 x 10^{-4} lb/ft^2 (GLDA). The results are shown graphically in

Fig. 39. Due to the low corrosion rate, ZeGage analysis was not conducted on these tests. The coupons before and after testing are shown in **Fig. 40** (EDTA) and **Fig. 41 (**GLDA**)**. ICP-OES results of the effluent sample are shown in **Fig. 42** (Mn, Cr, Fe) and **Fig. 43** (Ni, Mo). The ICP-OES results were also summed together for the cations to give a mass loss by ICP-OES (**Fig. 44**). The fluid change is shown in **Fig. 45** (EDTA) and **Fig. 46** (GLDA).

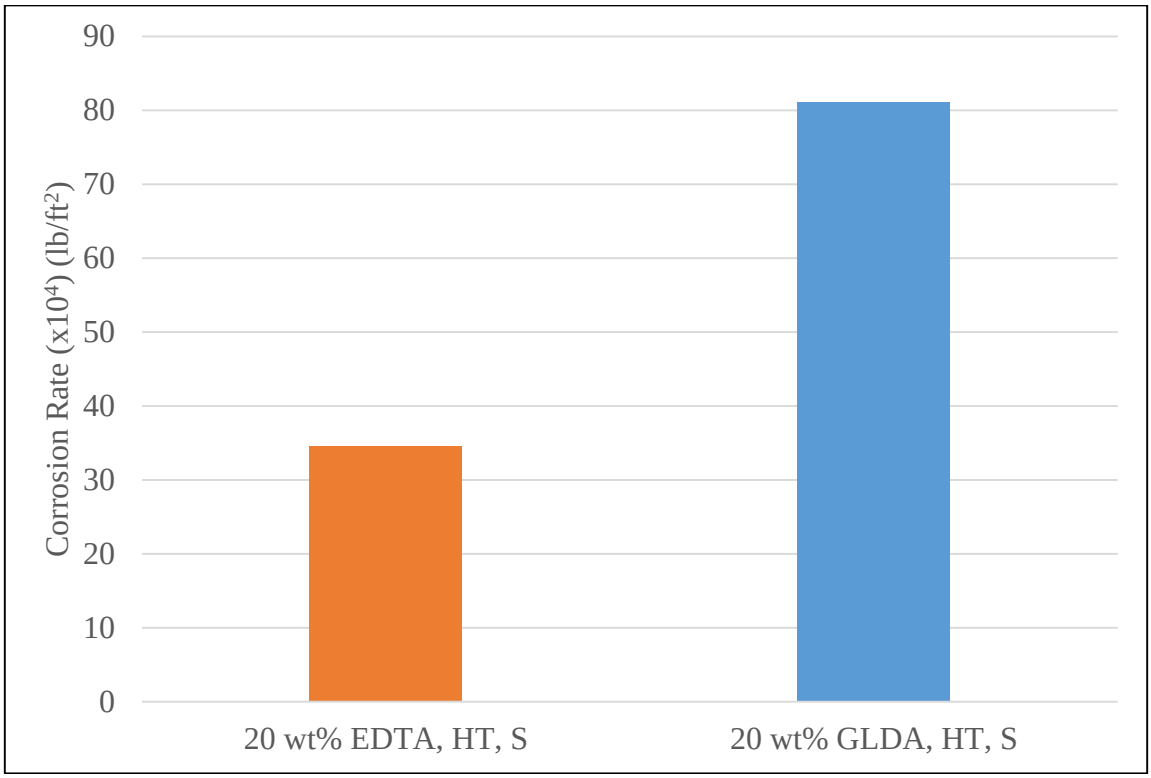

Fig. 39 – Corrosion Rate results of S13Cr-110 with 20 wt% EDTA (pH = 9) and 20 wt% GLDA (pH = 4). Each test was conducted for 6 hours at >1000 psi at 350°F with 5 wt% NaCl.

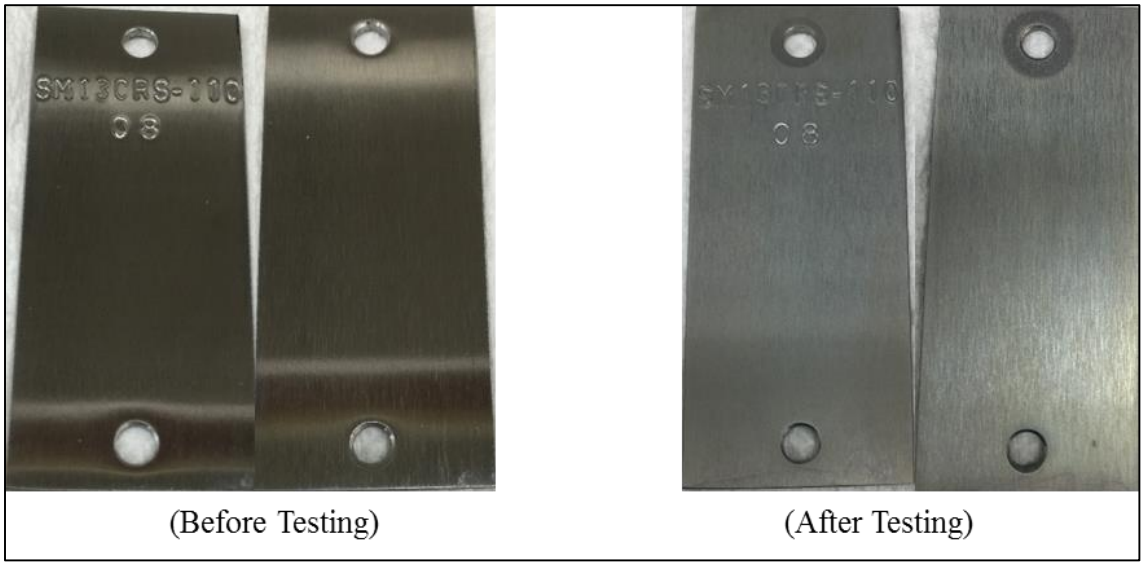

Fig. 40 – Results of S13Cr-110 test with 20 wt% EDTA (pH = 9). Coupon before testing (left) after testing (right). Test was conducted for 6 hours at >1000 psi at 350°F with 5 wt% NaCl.

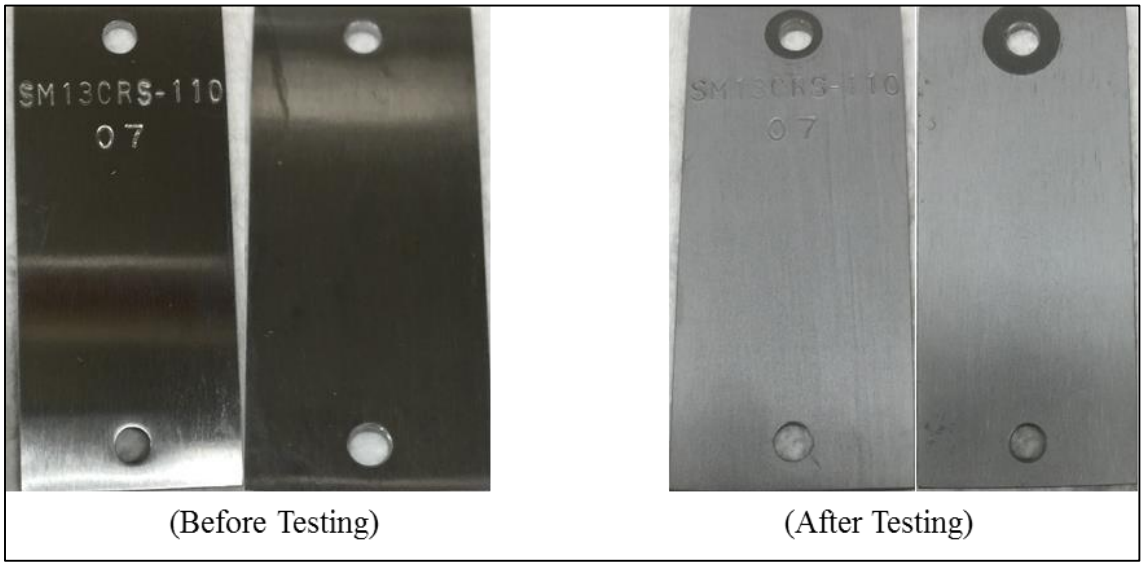

Fig. 41 – Results of S13Cr-110 test with 20 wt% GLDA (pH = 4). Coupon before testing (left) after testing (right). Test was conducted for 6 hours at >1000 psi at 350°F with 5 wt% NaCl.

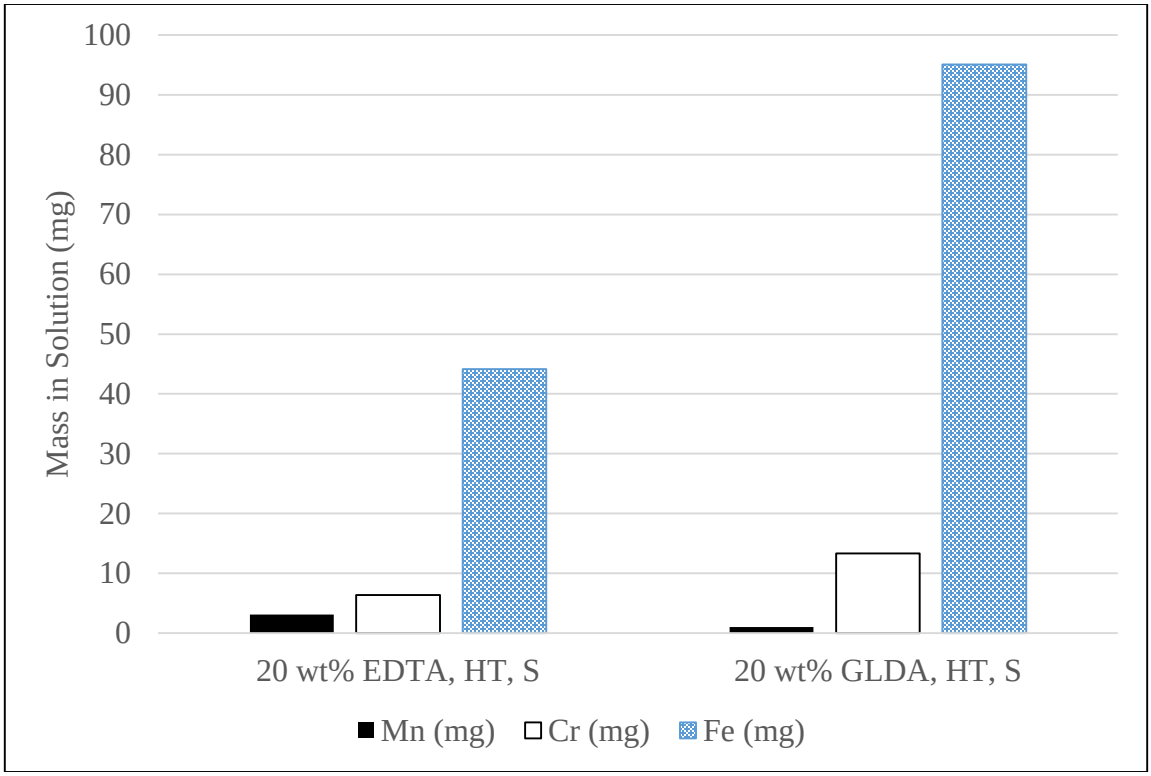

Fig. 42 – ICP-OES results for Mn, Cr, and Fe for S13Cr-110 test with 20 wt% EDTA (pH = 9) and 20 wt% GLDA (pH = 4). Each test was conducted for 6 hours at >1000 psi at 350°F with 5 wt% NaCl.

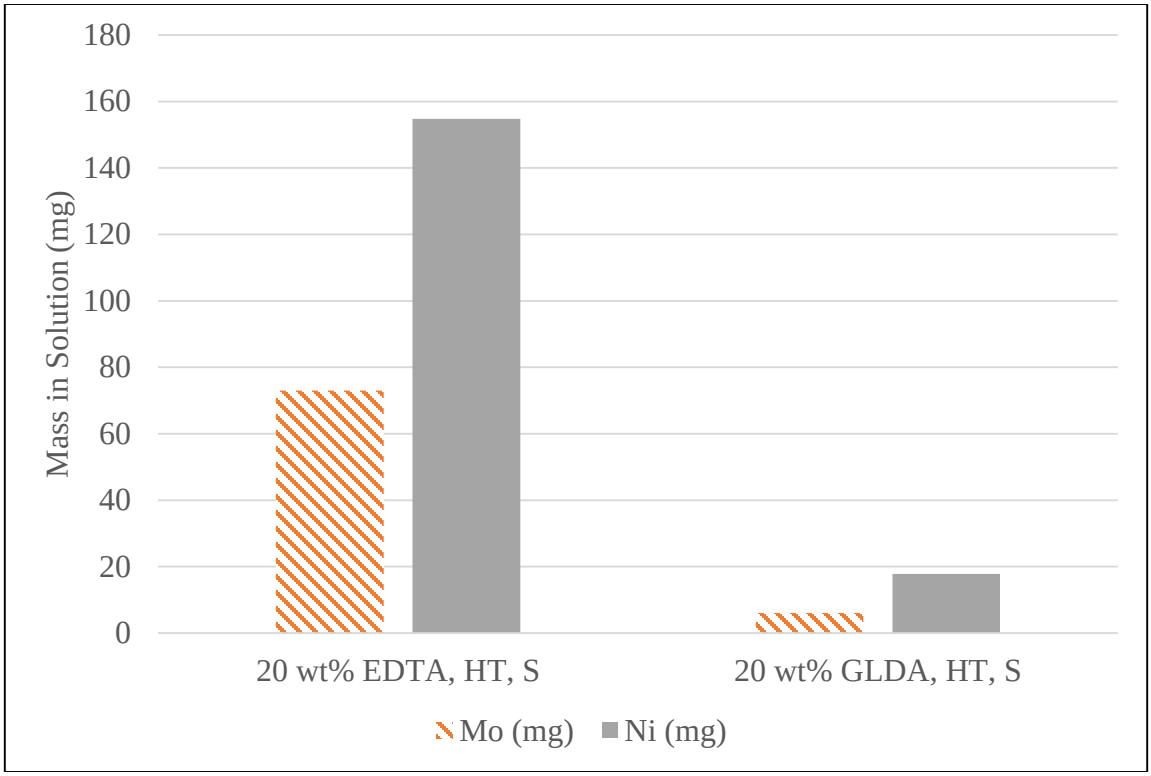

Fig. 43 – ICP-OES results for Mo and Ni for S13Cr-110 test with 20 wt% EDTA (pH = 9) and 20 wt% GLDA (pH = 4). Each test was conducted for 6 hours at >1000 psi at 350°F with 5 wt% NaCl.

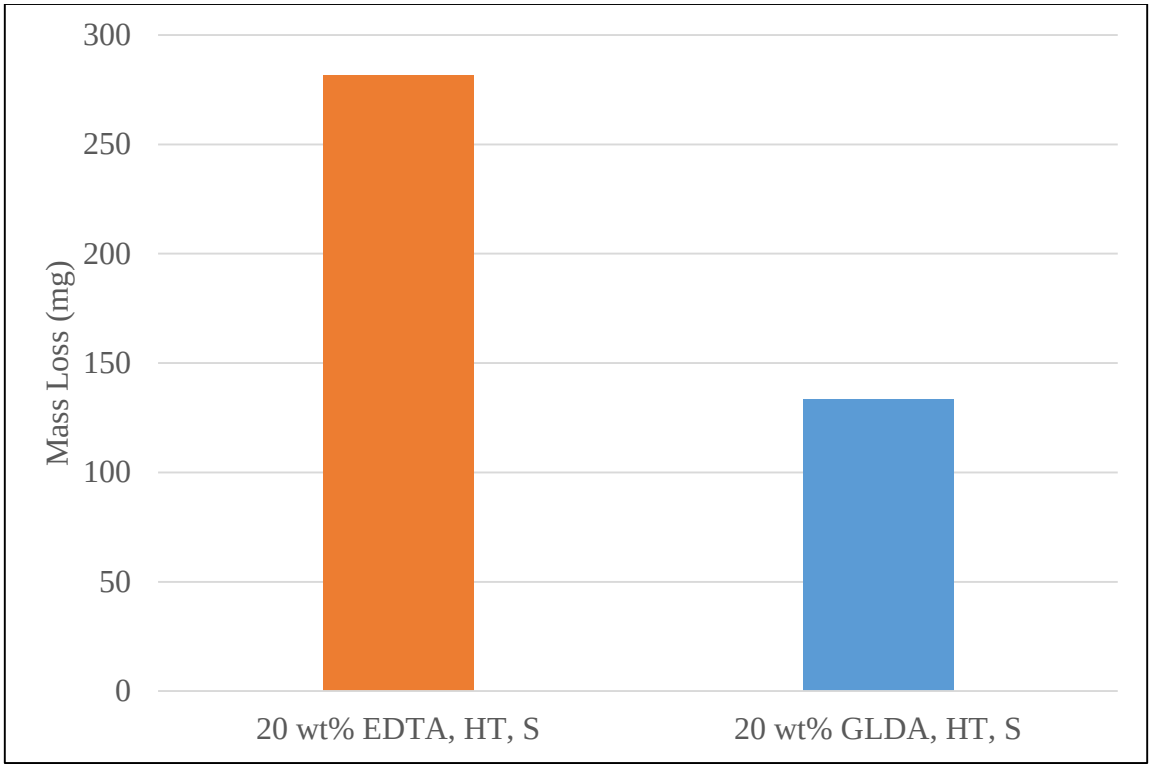

Fig. 44 – ICP-OES results for mass loss for S13Cr-110 test with 20 wt% EDTA (pH = 9) and 20 wt% GLDA (pH = 4). Each test was conducted for 6 hours at >1000 psi at 350°F with 5 wt% NaCl.

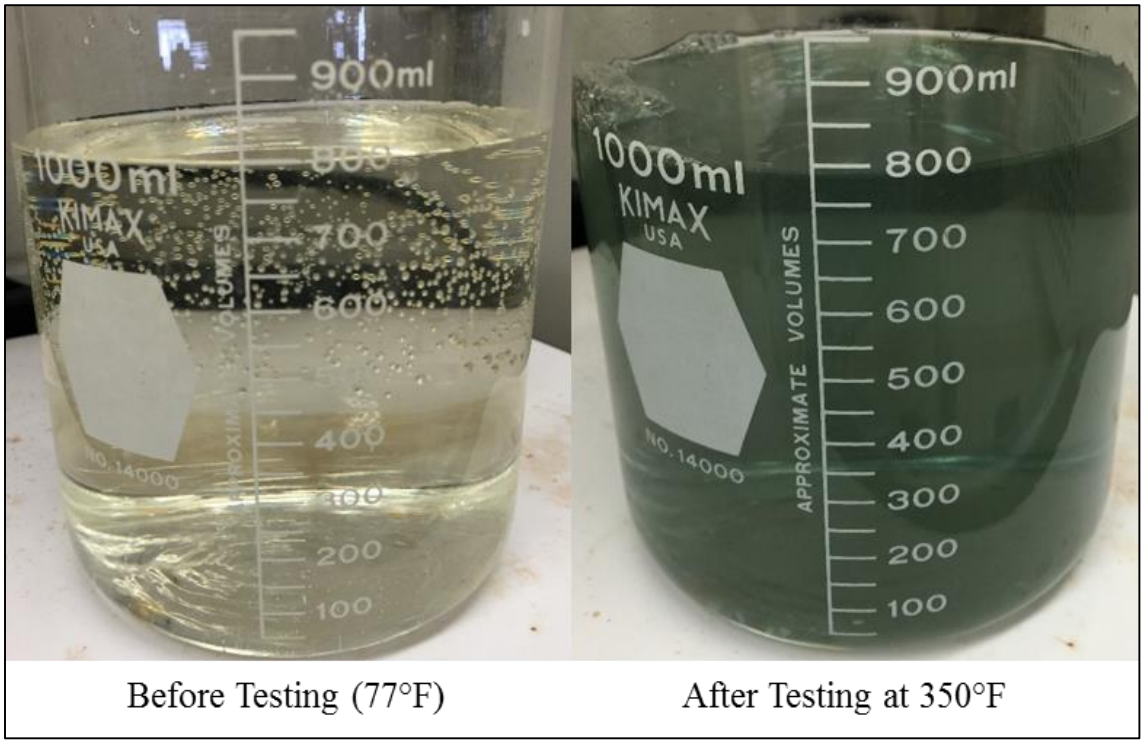

Fig. 45 – Fluid color change for S13Cr-110 test with 20 wt% EDTA (pH = 9). Test was conducted for 6 hours at >1000 psi at 350°F with 5 wt% NaCl.

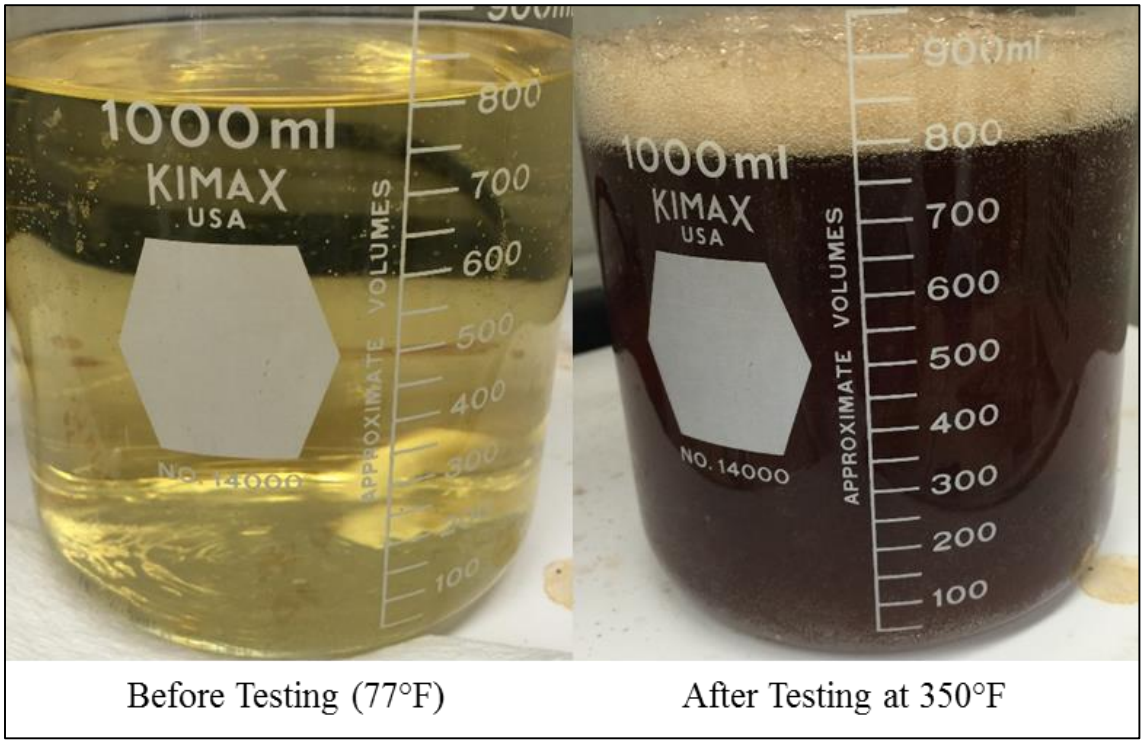

Fig. 46 – Fluid color change for S13Cr-110 test with 20 wt% GLDA (pH = 4). Test was conducted for 6 hours at >1000 psi at 350°F with 5 wt% NaCl.

4. DISCUSSION

4.1 Proof of Concept: L80 and GLDA

The results from the GLDA test on L-80 coupons at 300°F test show a corrosion rate of 0.20 +/-0.01 lb/ft^2 which is above the acceptable industry limit of 0.02-0.05 lb/ft^2 (Kalfayan 2008). When comparing the data to the work of De Wolf et al. (2015), the results are consistent. De Wolf et al. (2015) show a corrosion rate of 0.19 lb/ft^2 up to 0.59 lb/ft^2 depending on the elemental composition of L-80.

The analysis of the results using the 3D surface profiler (ZeGage) are consistent with the high corrosion rate seen in the coupons. Not only is it clear there is corrosion and pitting by viewing the camera photos (Fig. 7 and Fig. 8), significant pitting can be seen when analyzing the ZeGage images (Fig. 10 and Fig. 12). Furthermore, a high level of Fe (>2600 mg) is found in the effluent stream during ICP-OES analysis (Fig. 13). The remainder of the discussion and conclusions will be focused on the work done when corroding S13Cr-110 with EDTA and GLDA.

4.2 S13Cr-110 with EDTA and GLDA

The results of the tests comparing the corrosion rate of S13Cr-110 with EDTA and GLDA have been shown in the previous section. The corrosion rate at 300°F (LT) is an order of magnitude lower than the corrosion rate at 350°F (HT). Therefore, the two datasets have been separated. The corrosion rate data for the LT samples (**Fig. 47**) and HT samples (**Fig. 48**) is summarized by coupon weight loss. The same results are presented in tabular format for LT (**Table 14**) and HT (**Table 15**). Note that the results in Table 14

and Table 15 remove the factor of 10^4 and it is clear that all the corrosion rates are below the industry standard of 0.02-0.05 lb/ft^2 (Kalfayan 2008). A summary of the ICP-OES results are provided in **Fig. 49** (Mn, Cr, Fe) and **Fig. 50** (Mo and Ni) for LT tests. The ICP-OES results of the HT tests are shown in **Fig. 51** (Mn, Cr, Fe) and **Fig. 52** (Mo and Ni). The values are tabulated in **Table 16** for LT tests and in **Table 17** for HT tests. Summing up the results of each cation (Mn, Cr, Fe, Mo, and Ni), an ICP-OES calculated mass loss is shown in **Fig. 53** for LT tests and **Fig. 54** for HT tests. The tabulated values are shown in **Table 18** for LT tests and **Table 19** for HT tests.

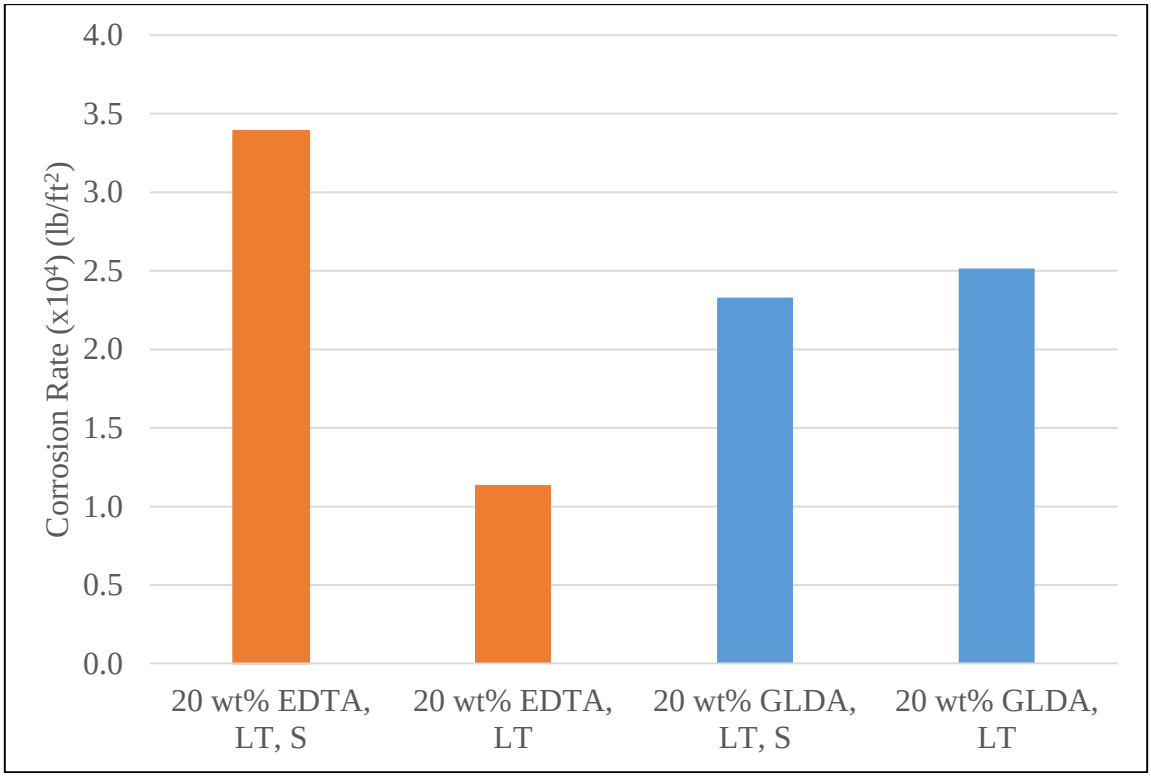

Fig. 47 – Summary of corrosion rate results by weight loss method with S13Cr-110 at 300°F. Tests with salt (S) included 5 wt% NaCl and EDTA with salt was conducted at pH =9. All other tests were conducted at pH =4 with associated fluids. All tests were conducted for 6 hours at >1000 psi.

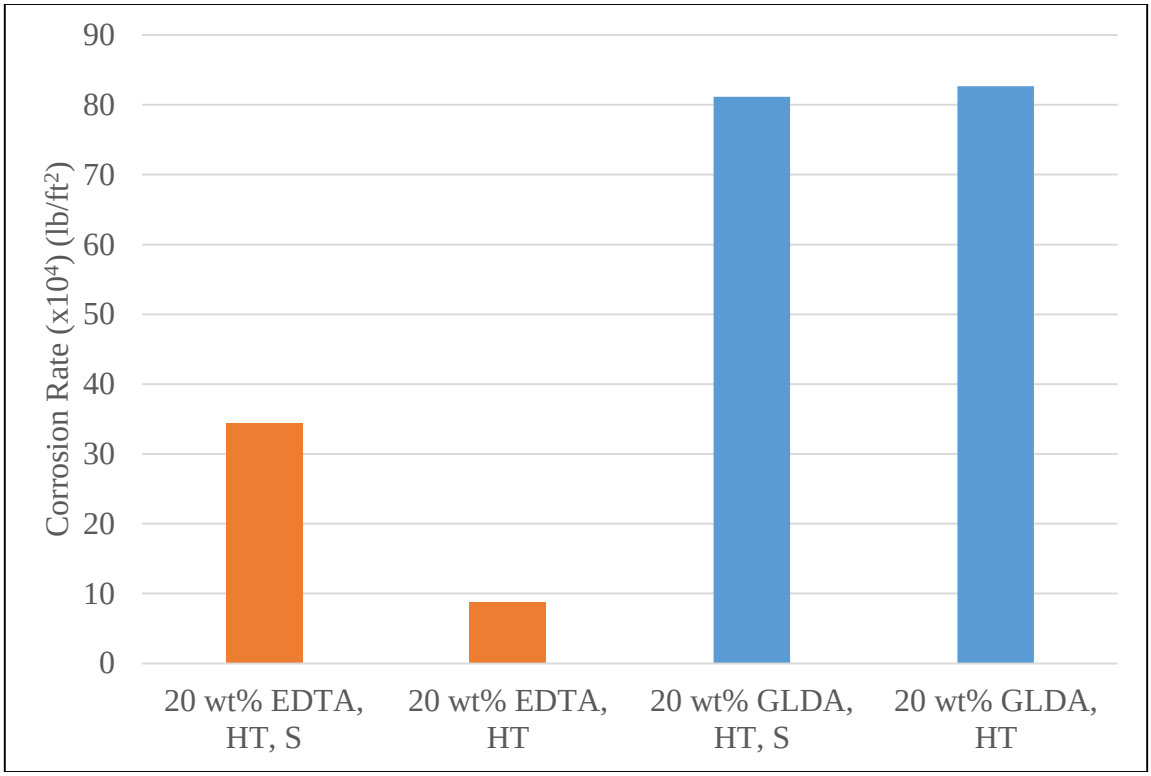

Fig. 48 – Summary of corrosion rate results by weight loss method with S13Cr-110 at 350°F. Tests with salt (S) included 5 wt% NaCl and EDTA with salt was conducted at pH =9. All other tests were conducted at pH =4 with associated fluids. All tests were conducted for 6 hours at >1000 psi.

	Solution pH	Weight Loss Corrosion Rate (lb/ft^2)
20 wt% EDTA, LT, S	9	0.000339
20 wt% EDTA, LT	4	0.000114
20 wt% GLDA, LT, S	4	0.000233
20 wt% GLDA, LT	4	0.000251

Table 14 – Summary of corrosion rate results by weight loss method with S13Cr-110 at 300°F. Tests with salt (S) included 5 wt% NaCl. All tests were conducted for 6 hours at >1000 psi.

	Solution pH	Weight Loss Corrosion Rate (lb/ft^2)
20 wt% EDTA, HT, S	9	0.003450
20 wt% EDTA, HT	4	0.000884
20 wt% GLDA, HT, S	4	0.008115
20 wt% GLDA, HT	4	0.008269

Table 15 – Summary of corrosion rate results by weight loss method with S13Cr-110 at 350°F. Tests with salt (S) included 5 wt% NaCl. All tests were conducted for 6 hours at >1000 psi.

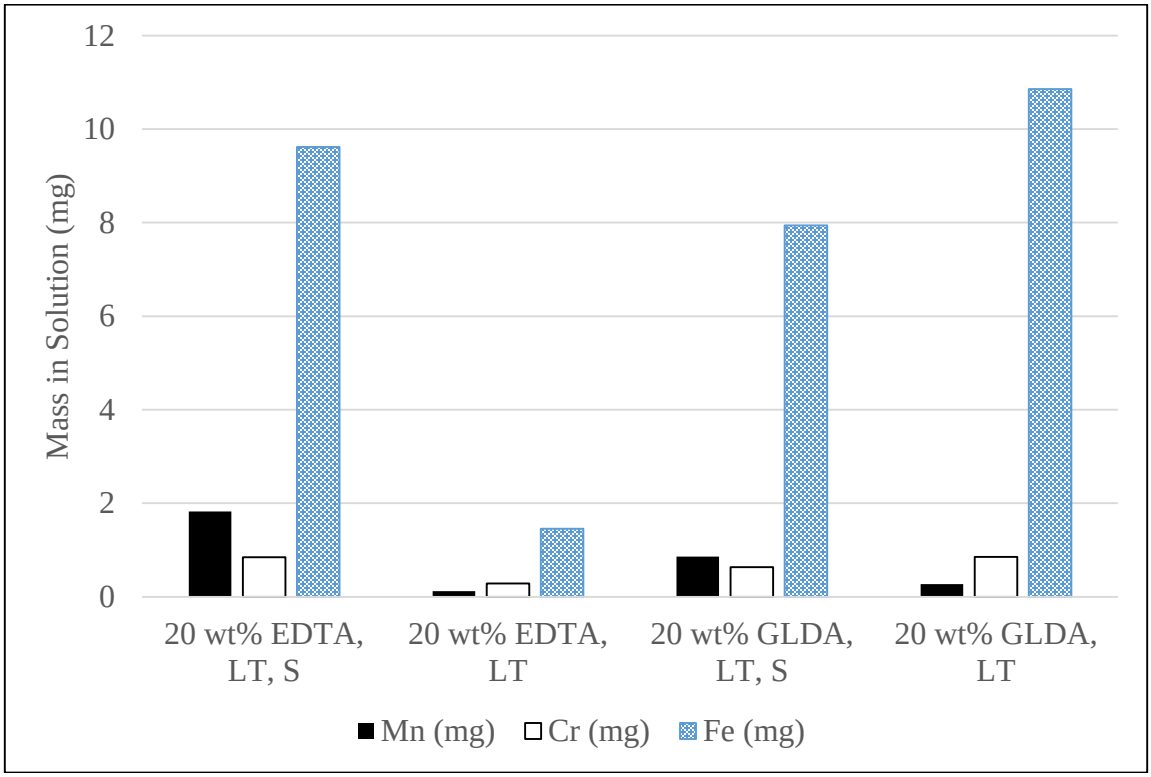

Fig. 49 – Summary of ICP-OES results for Mn, Cr, and Fe with S13Cr-110 at 300°F. Tests with salt (S) included 5 wt% NaCl and EDTA with salt was conducted at pH =9. All other tests were conducted at pH =4 with associated fluids. All tests were conducted for 6 hours at >1000 psi.

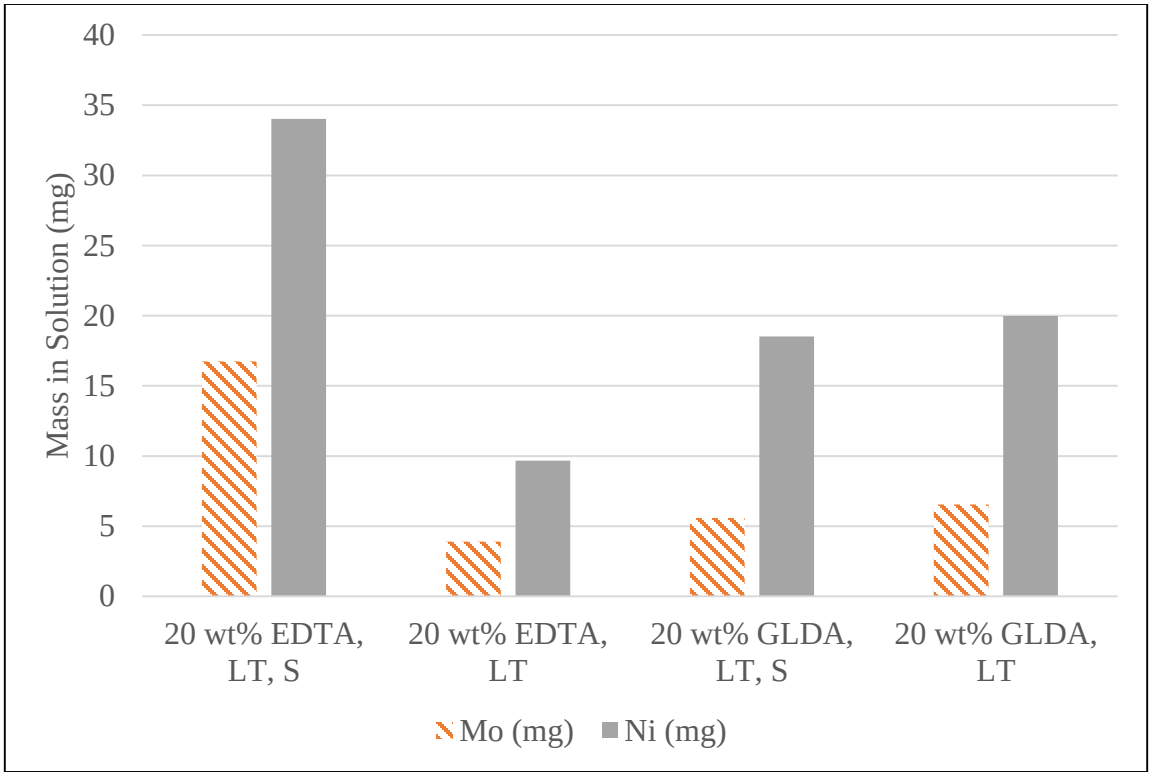

Fig. 50 – Summary of ICP-OES results for Mo and Ni with S13Cr-110 at 300°F. Tests with salt (S) included 5 wt% NaCl and EDTA with salt was conducted at pH =9. All other tests were conducted at pH =4 with associated fluids. All tests were conducted for 6 hours at >1000 psi.

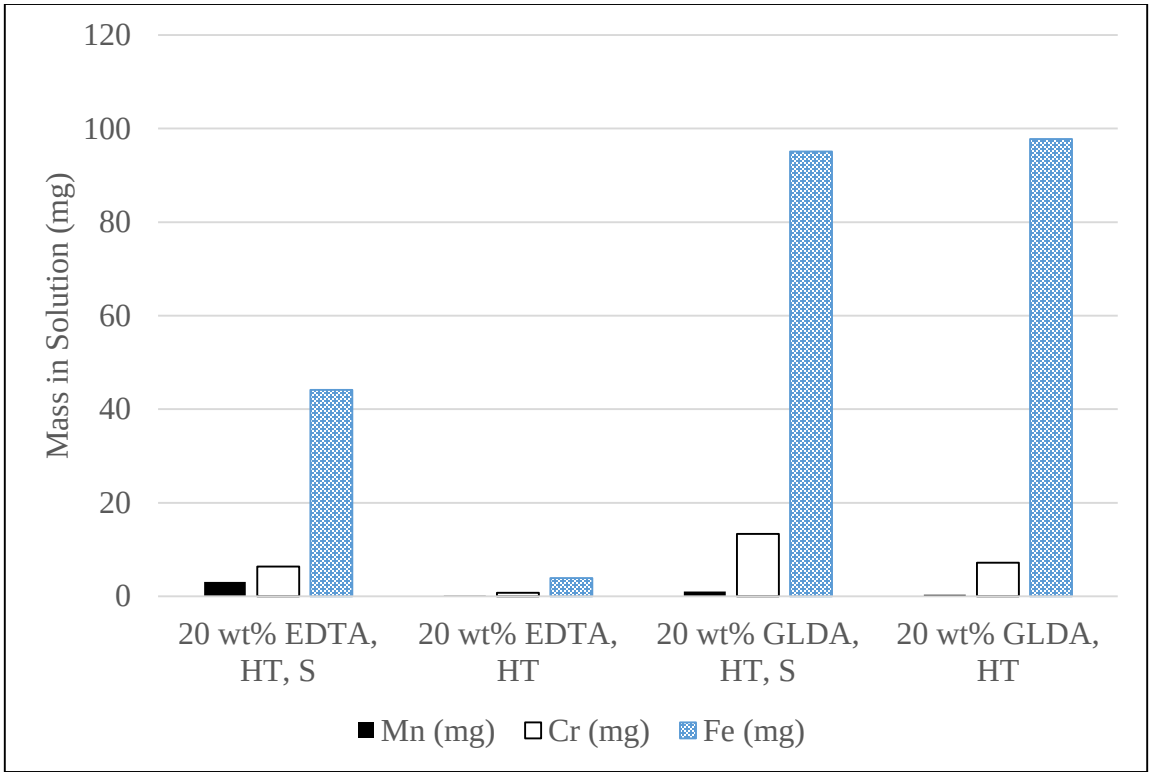

Fig. 51 – Summary of ICP-OES results for Mn, Cr, and Fe with S13Cr-110 at 350°F. Tests with salt (S) included 5 wt% NaCl and EDTA with salt was conducted at pH =9. All other tests were conducted at pH =4 with associated fluids. All tests were conducted for 6 hours at >1000 psi.

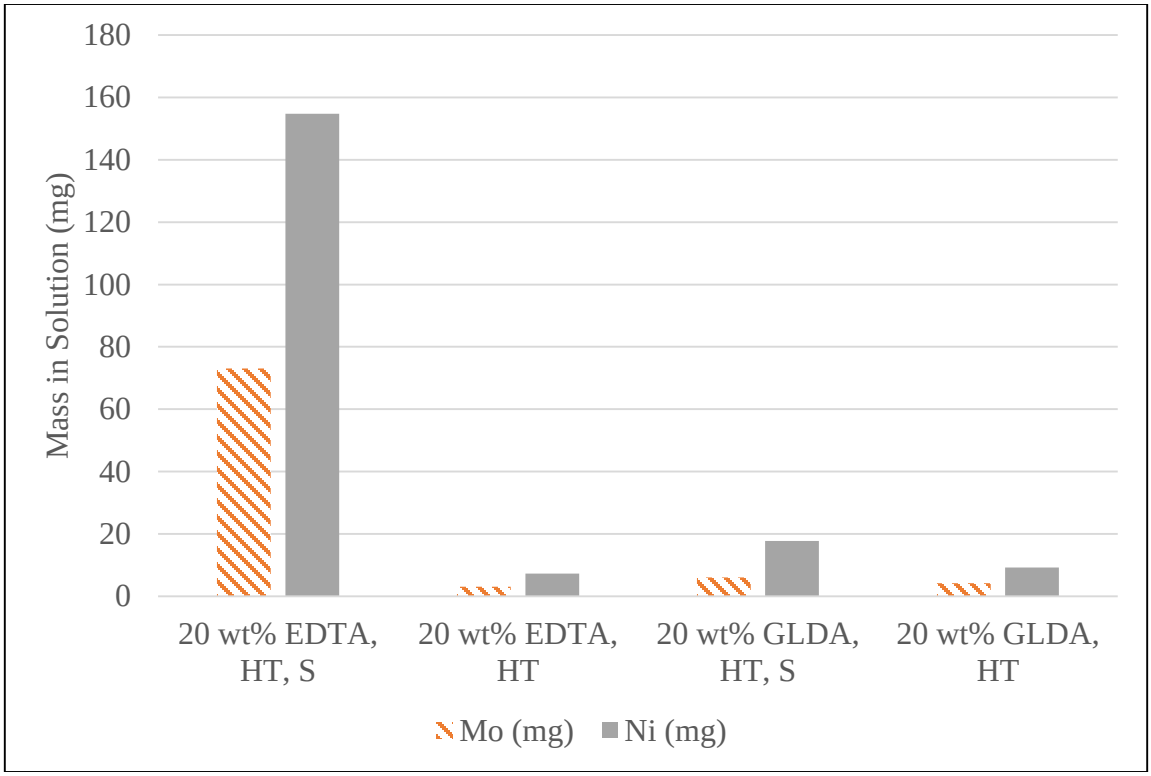

Fig. 52 – Summary of ICP-OES results for Mo and Ni with S13Cr-110 at 350°F. Tests with salt (S) included 5 wt% NaCl and EDTA with salt was conducted at pH =9. All other tests were conducted at pH =4 with associated fluids. All tests were conducted for 6 hours at >1000 psi.

	Solution pH	Mn (mg)	Mo (mg)	Ni (mg)	Cr (mg)	Fe (mg)
20 wt% EDTA, LT, S	9	1.83	16.73	34.03	0.84	9.62
20 wt% EDTA, LT	4	0.12	3.91	9.67	0.29	1.45
20 wt% GLDA, LT, S	4	0.86	5.58	18.52	0.63	7.94
20 wt% GLDA, LT	4	0.27	6.54	19.98	0.85	10.85

Table 16 – Summary of ICP-OES results for key cations with S13Cr-110 at 300°F. Tests with salt (S) included 5 wt% NaCl. All tests were conducted for 6 hours at >1000 psi.

	Solution pH	Mn (mg)	Mo (mg)	Ni (mg)	Cr (mg)	Fe (mg)
20 wt% EDTA, HT, S	9	3.09	73.04	154.77	6.36	44.13
20 wt% EDTA, HT	4	0.11	3.05	7.32	0.74	3.87
20 wt% GLDA, HT, S	4	1.03	6.04	17.78	13.33	95.08
20 wt% GLDA, HT	4	0.32	4.18	9.21	7.18	97.75

Table 17 – Summary of ICP-OES results for key cations with S13Cr-110 at 350°F. Tests with salt (S) included 5 wt% NaCl. All tests were conducted for 6 hours at >1000 psi.

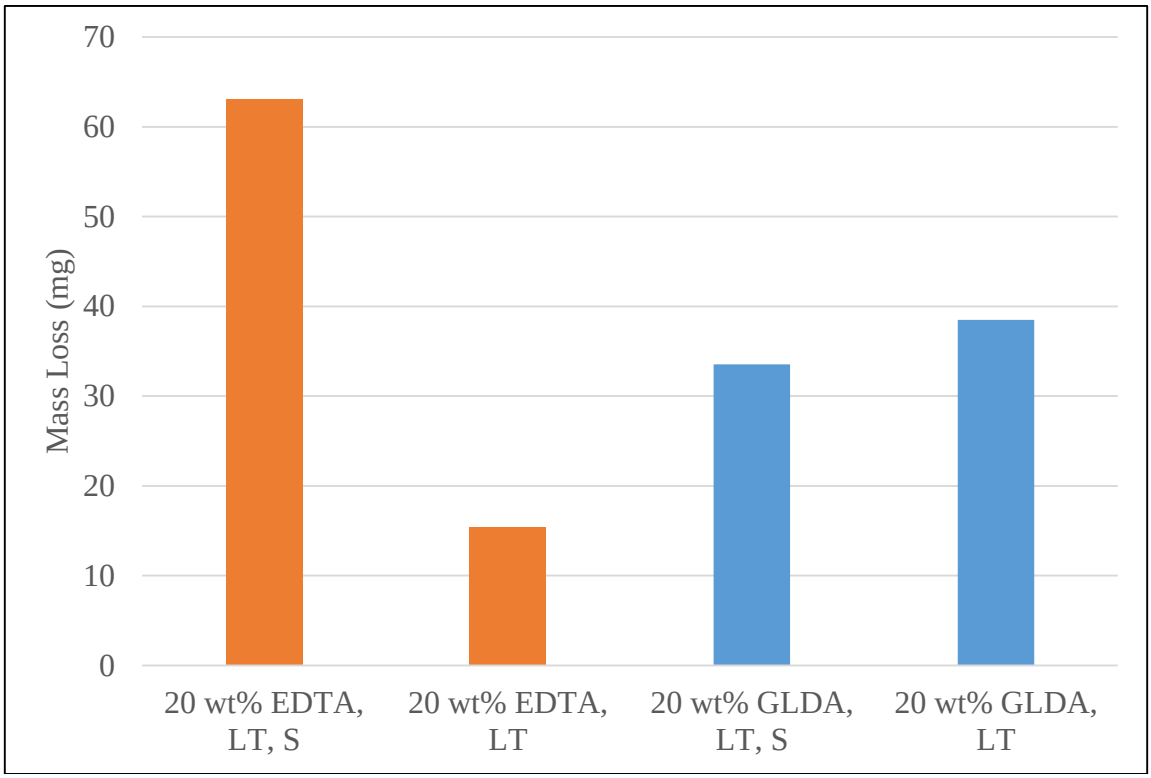

Fig. 53 – Summary of ICP-OES results for mass loss with S13Cr-110 at 300°F. Tests with salt (S) included 5 wt% NaCl and EDTA with salt was conducted at pH =9. All other tests were conducted at pH =4 with associated fluids. All tests were conducted for 6 hours at >1000 psi.

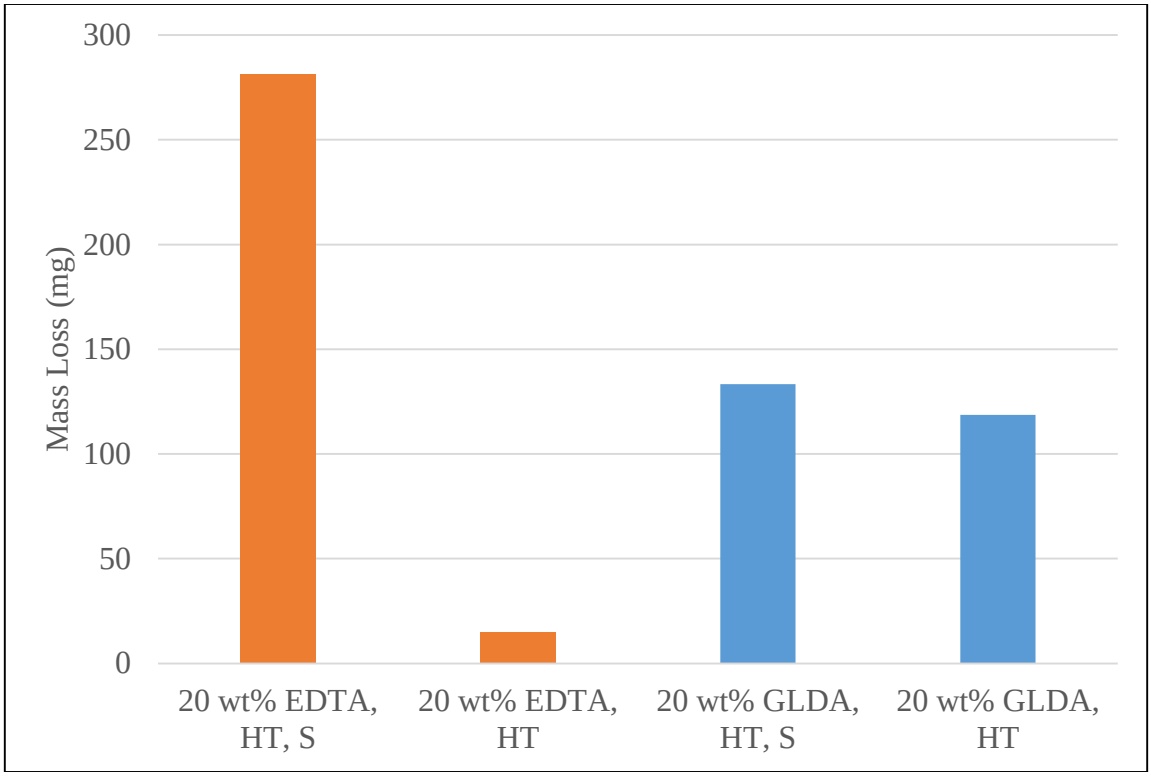

Fig. 54 – Summary of ICP-OES results for mass loss with S13Cr-110 at 350°F. Tests with salt (S) included 5 wt% NaCl and EDTA with salt was conducted at pH =9. All other tests were conducted at pH =4 with associated fluids. All tests were conducted for 6 hours at >1000 psi.

	Solution pH	ICP-OES Mass Loss (mg)
20 wt% EDTA, LT, S	9	63.05
20 wt% EDTA, LT	4	15.44
20 wt% GLDA, LT, S	4	33.53
20 wt% GLDA, LT	4	38.49

Table 18 – Summary of ICP-OES results for mass loss with S13Cr-110 at 300°F. Tests with salt (S) included 5 wt% NaCl. All tests were conducted for 6 hours at >1000 psi.

	Solution pH	ICP-OES Mass Loss (mg)
20 wt% EDTA, HT, S	9	281.38
20 wt% EDTA, HT	4	15.09
20 wt% GLDA, HT, S	4	133.26
20 wt% GLDA, HT	4	118.64

Table 19 – Summary of ICP-OES results for mass loss with S13Cr-110 at 350°F. Tests with salt (S) included 5 wt% NaCl. All tests were conducted for 6 hours at >1000 psi.

The results from the data above provides the following insights:

1. Corrosion rate increases as temperature increases from 300°F to 350°F.
2. In the presence of salt, EDTA pH is lowered to 9 instead of 4 (when no salt is present). When comparing EDTA and GLDA with 5 wt% NaCl at LT, EDTA corrosion rate is consistently higher than GLDA (coupon corrosion rate and ICP-OES mass loss). However, at HT, there is an anomalous result; when analyzing the data by coupon corrosion rate, GLDA at pH 4 is more corrosive than EDTA at pH 9. When analyzing the ICP-OES mass loss data, EDTA at pH 9 is more corrosive than GLDA at pH 4. Furthermore, there is a noticeable color change in the EDTA solution at HT (Fig. 45).
3. GLDA corrodes S13Cr-110 more than EDTA when both fluids are at the same pH (coupon corrosion rate and ICP-OES mass loss method).

4.2.1 Corrosion Rate as a Function of Temperature

Corrosion rate for both EDTA and GLDA increase when the temperature is raised from 300°F to 350°F. As shown in **Fig. 55**, the corrosion rate of EDTA increases from

1.14 x 10^{-4} lb/ft^2 to 8.84 x 10^{-4} lb/ft^2 when the pH is maintained at 4. For GLDA, **Fig. 56** shows the corrosion rate increases from 2.51 x 10^{-4} lb/ft^2 to 82.69 x 10^{-4} lb/ft^2 when the pH is maintained at 4. EDTA corrosion rate increases by a factor of 8 and GLDA corrosion rate increases by a factor of almost 40. The reason for the relative change is due to the conditional stability constants and is explained in the "EDTA corrosion vs. GLDA corrosion" section.

The overall increase in corrosion rate is due to the increase in kinetics and is consistent with literature data on corrosion of S13Cr alloys. This could be explained by the Arrhenius equation which states that surface reaction increases with an increase in temperature (Wikipedia 2016b). Felton and Schofield (1998) state that while 13Cr alloys have significantly lower corrosion than L80, there is a transition from active to partial passivity in the temperature of interest for this study (300°F-400°F). Ueda et al. (1996) shows the corrosion rate of S13Cr alloys to increase from 0.01 mpy to 0.1 mpy in the presence of salt (5 wt% NaCl), CO_2 (3 MPa) and H_2S (0.001 MPa). Though the tests conducted in this study are not in a CO_2 and H_2S environment, it provides insight onto the relative change in corrosion behavior for S13Cr alloys.

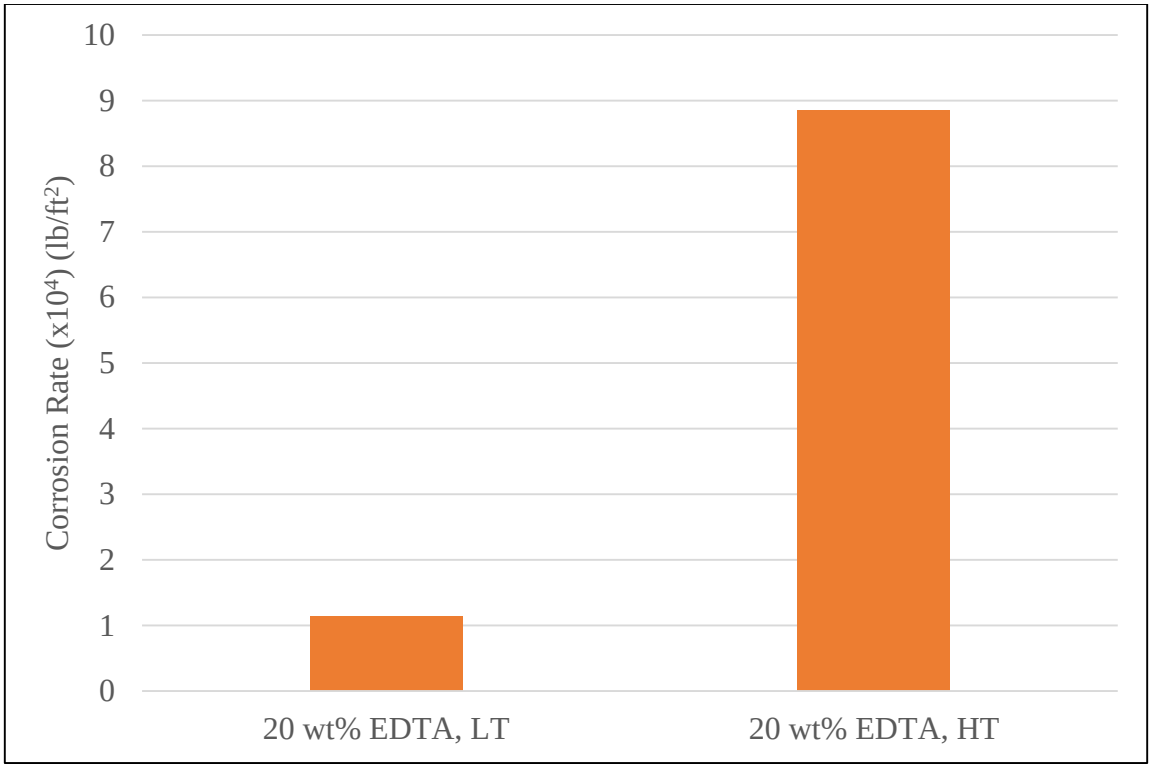

Fig. 55 – Corrosion rate results of S13Cr-110 with 20 wt% EDTA (pH = 4) at 300°F (LT) and 350°F (HT). Each test was conducted for 6 hours at >1000 psi.

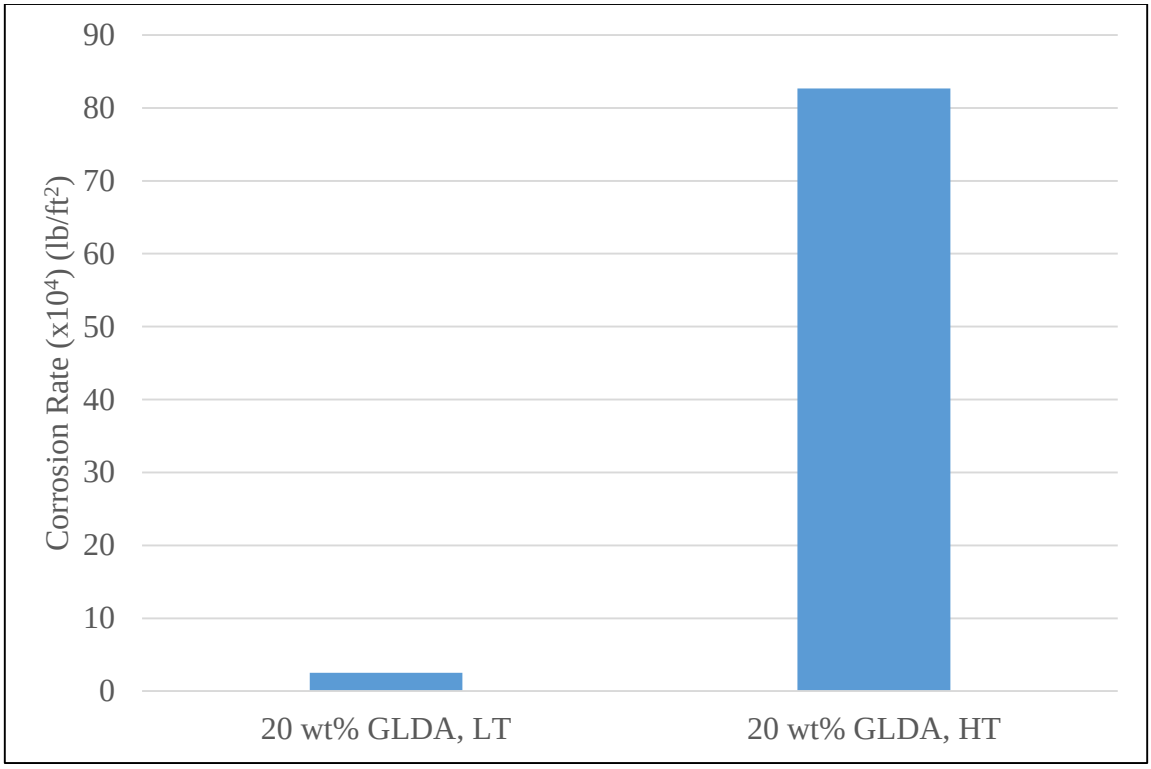

Fig. 56 – Corrosion rate results of S13Cr-110 with 20 wt% GLDA (pH = 4) at 300°F (LT) and 350°F (HT). Each test was conducted for 6 hours at >1000 psi.

4.2.2 Effect of Salt on EDTA and GLDA corrosion

When the pH of EDTA was lowered to 9 instead of 4, two variables where changed; salt was introduced and the fluid was at a higher pH. Sokhanvarian (2012) explains that the addition of NaCl improves thermal stability and can lower reactivity. However, the results for GLDA show a consistent corrosion rate at both LT (Fig. 47 and Fig. 53) and HT (Fig. 48 and Fig. 54). Therefore, to explain the increase in EDTA corrosion rate when salt was added and pH was changed, the pH was determined to be the controlling factor.

4.2.3 Effect of pH on EDTA corrosion

When comparing EDTA at pH 4 vs. pH 9 (5 wt% NaCl), the high pH EDTA is more corrosive at 300°F (LT) when comparing coupon corrosion rates (Fig. 47) and ICP-OES mass loss (Fig. 53). The same is true 350°F (HT) when comparing the coupon corrosion rates (Fig. 48) and ICP-OES mass loss (Fig. 54). As mentioned previously, the NaCl concentration does not seem to affect GLDA, so an increase in pH results in an increase in corrosion rates. The hypothesis being made is that the chelation mechanism of EDTA and GLDA is similar.

The work of Bondietti et al. (1993) discusses chelating agents and metal adsorption and it is further expanded on by Stumm (1997). Their claim is that there are two pathways for a chelating agent to remove metal; either by forming a mononuclear complex or a binuclear complex. Stumm (1997) states that at low pH, binuclear complexes are formed between metal ions and chelating agents, while at high pH, mononuclear complex formation is preferred. Though the exact pathway is not provided, combining the results of Nowack and Sigg (1997), Mercier et al. (2008), and the results of this paper, it is possible to draw conclusions on the proposed pathway. Nowack and Sigg (1997) provide reaction rate data of EDTA complexing with Fe at different pH values. As the pH increases from 5.4 to 8.3, the reaction rate increases doubles from 0.35 s^{-1} to 0.70 s^{-1} while maintaining all other parameters. They also provide a diagram that shows how a Me-EDTA complex can adsorb to a surface with Fe and exchange the Me for Fe-EDTA. Mercier et al. (2008) shows the mechanism of forming the mononuclear complex with Al and Diaminoethane in an aluminum hydroxide environment.

The proposed pathway to form binuclear complexes at low pH and mononuclear complexes at high pH is shown in **Fig. 57** and **Fig. 58**. In both cases, the first step involves an EDTA ligand attacking the metal surface.

In the case of binuclear complex formation (low pH, Fig. 57), the second ligand has three choices; attack a second metal ion, start to form a multi-dentate structure with the first metal ion, or attack the H^+. Based on the speciation diagram, it is unfavorable to form a bond with H^+. It is assumed that MY formation is not as favorable as the M_2Y because in the latter case, a water molecule is released. Therefore, EDTA would form a binuclear complex with the metal cation.

In the case of mononuclear complex formation (high pH, Fig. 58), the second ligand has two choices; attack a second metal ion, or start to form a multi-dentate structure with the first metal ion. Forming a bond with an OH^- is unfavorable because of like charge repulsion. The assumption is that MY (metal to ligand) formation is more favorable than M_2Y because that would result in the release of an OH^- in an already high pH environment. Therefore, EDTA would form a mononuclear complex with the metal cation.

At low pH values, EDTA is bound to 2 metal cations since it forms a binuclear complex. At high pH values, EDTA focuses on 1 metal cation as it forms a mononuclear complex. The attractive forces between EDTA and the metal are stronger in the mononuclear (high pH) scenario since both ligands are bonding to the same cation. Therefore, it is more effective at removing metal ions from the surface. Conversely, it is more energetically unfavorable to remove the metal ions when the chelating agent is in the binuclear complex form (Mercier et al. 2008). This theory is validated by both the weight loss method to determine corrosion rate (Fig. 47 and Fig. 48) and ICP-OES mass loss method (Fig. 53 and Fig. 54).

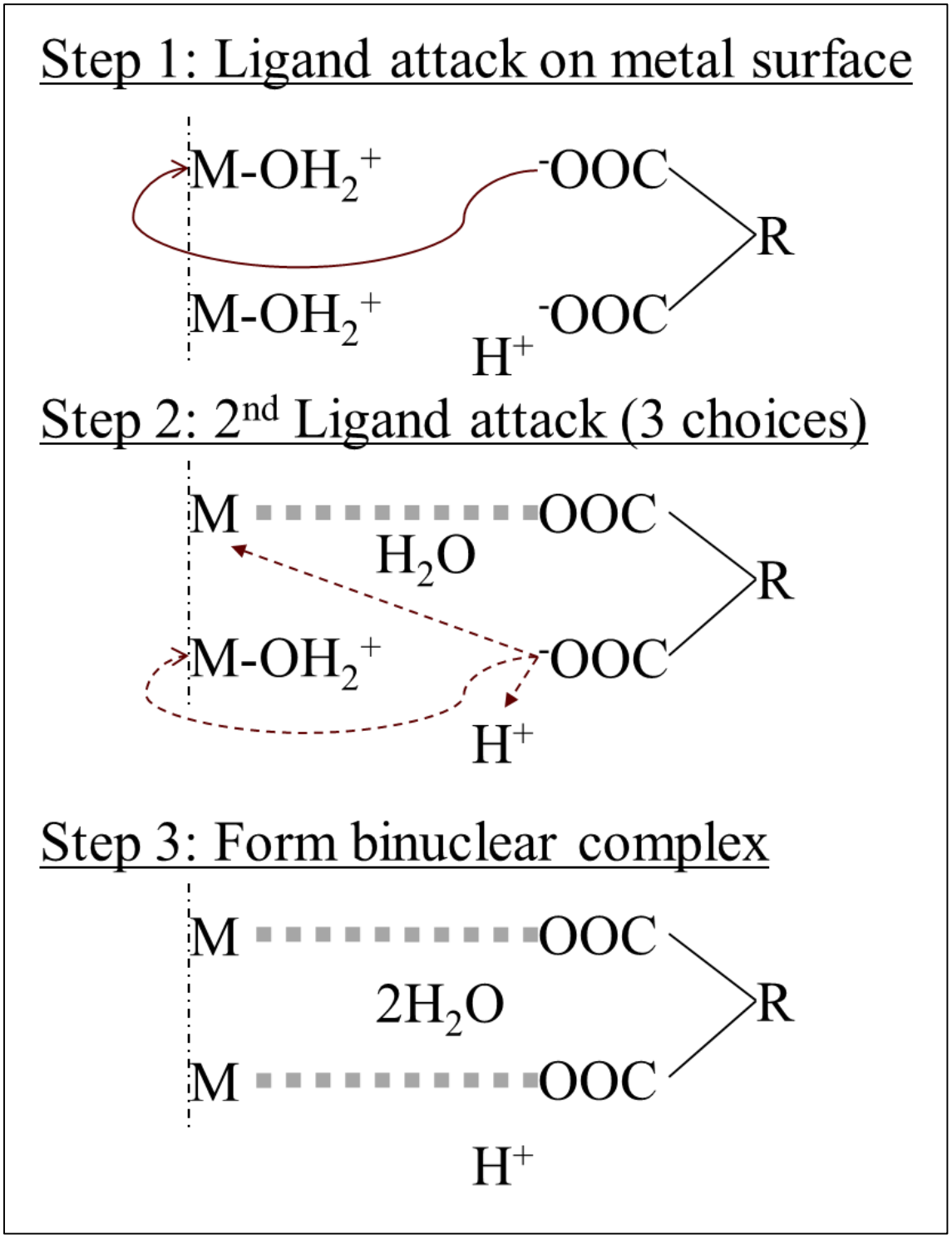

Fig. 57 – Proposed pathway to form binuclear complex between EDTA and metal surface at low pH values. $^{-}$OOC-R-COO^{-} represents EDTA structure and M-OH$_2^+$ represents metal surface.

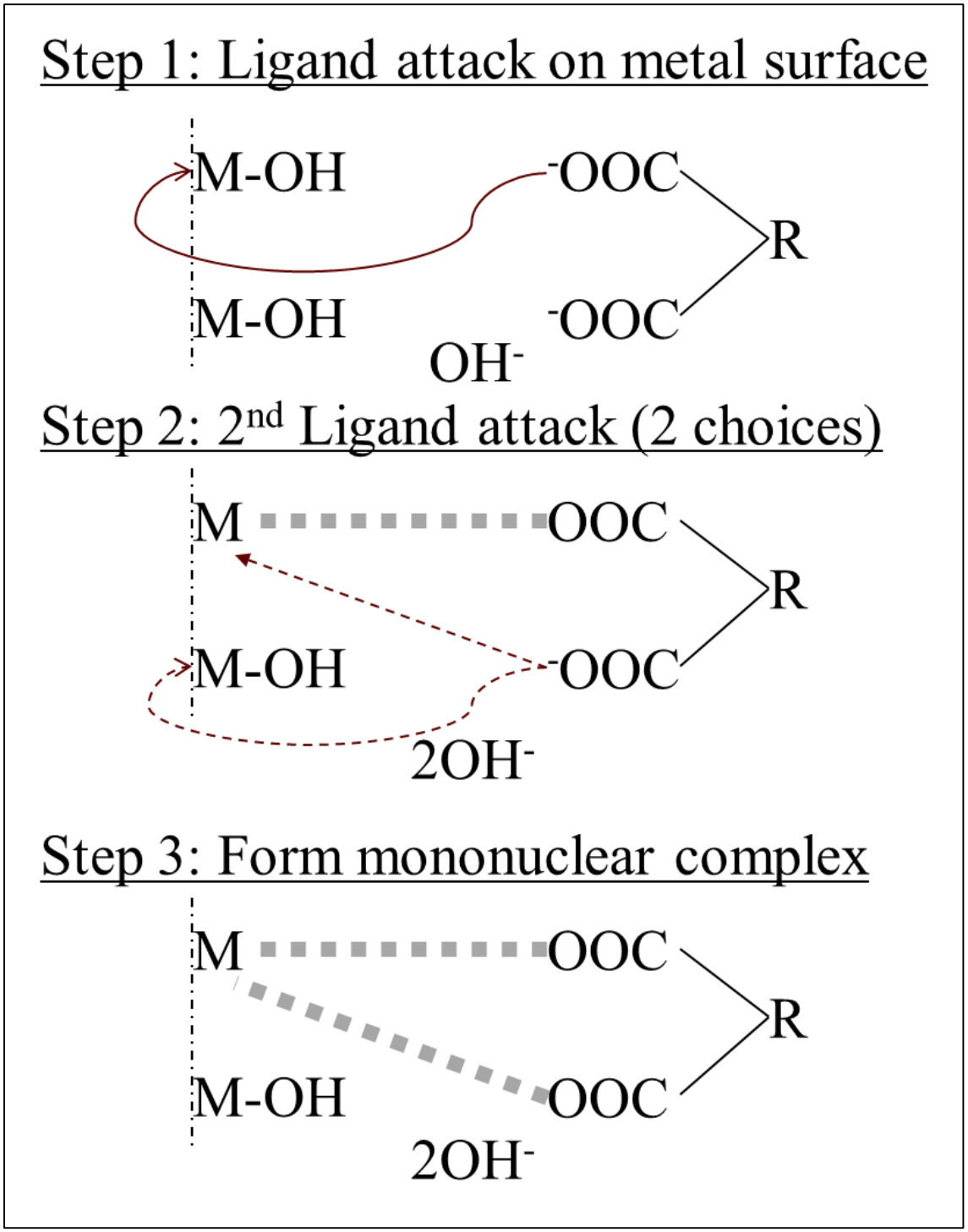

Fig. 58 – Proposed pathway to form mononuclear complex between EDTA and metal surface at high pH. $^{-}$OOC-R-COO^{-} represents EDTA structure and M-OH represents metal surface.

An anomaly in the results was that the EDTA corrosion rate at 350°F did not match the ICP-OES mass loss data. The coupon corrosion rate increased by a factor of 4 from 350°F at pH 4 to 350°F at pH 9 with 5 wt% NaCl (Fig. 48) while the ICP-OES mass loss data showed an increase by a factor of almost 20 (Fig. 54). This suggests that something else was also corroding, and this is supported by the high levels of Mo and Ni (Fig. 52) and the change in color of the solution (Fig. 45). The explanation for the results is that there was some corrosion in the reactor itself, as Hast B-2 does have a high level of both Ni (66 wt%) and Mo (28 wt%) (Haynes 2015). The details of why EDTA at high pH chose to preferentially complex with Mo and Ni instead of Fe and Cr (dominant elements in S13Cr-110 (Table 11)) are currently unknown, but are supported by the work of Chauhan et al. (2015), who shows the % Ni Extraction as a function of reaction time (hr) from spent catalysts at various temperatures. One theory is the relative changes in stability constants of Fe, Ni, and Mo at high pH vs. low pH as discussed in the "EDTA corrosion vs. GLDA corrosion" section based on the work of Begum et al. (2012a; 2012b).

4.2.4 EDTA corrosion vs. GLDA corrosion

When comparing the corrosion rate of EDTA with GLDA at the same conditions, GLDA is consistently more corrosive (Fig. 15 for LT and Fig. 23 for HT). The explanation of these results is based on the differences in the formation constants for the two chelating agents to different metal cations. The formation constant is a measure of the stability of the water soluble complex formed when the chelating agent forms a complex with the metal ion; the higher the stability constant, the more soluble. According to the work of

Begum et al. (2012a; 2012b), the stability constants for EDTA are consistently higher than that for GLDA. Furthermore, EDTA has higher conditional stability constants for divalent (Begum et al. 2012a) and trivalent cations (Begum et al. 2012b) when compared to GLDA. The conditional stability constants consider the formation constant and other interfering reactions (metal hydroxide formation, buffer solutions) and are varied as a function of pH for both divalent and trivalent cations.

The proposed explanation for the results is that GLDA attacks the metal surface in an unchelated form more often than EDTA because of the lower conditional stability constants. Therefore, if there is unchelated solution on the metal surface, it will react, while the complexed solution has a very low re-corrosion rate (Nowack and Sigg 1997).

An explanation for the lower conditional stability constants has to do with the structure of EDTA and GLDA. When EDTA forms a mononuclear structure (**Fig. 59**), the carboxylic groups remove the metal ion from the surface, but it is the nitrogen groups that help stabilize the octahedral structure. Since EDTA has two nitrogen groups and GLDA has only one, this could be an explanation for why EDTA stability constants are consistently higher than GLDA.

This theory explains the results and also provides justification for why the increase corrosion rate for GLDA from 300°F to 350°F is higher than that of EDTA. At higher temperatures, the reaction kinetics are faster, and therefore, this phenomenon is accelerated. Therefore, when temperature is increased, GLDA corrosion rate increases by a factor of almost 40 while EDTA corrosion rate increases by only a factor of 8 at pH 4.

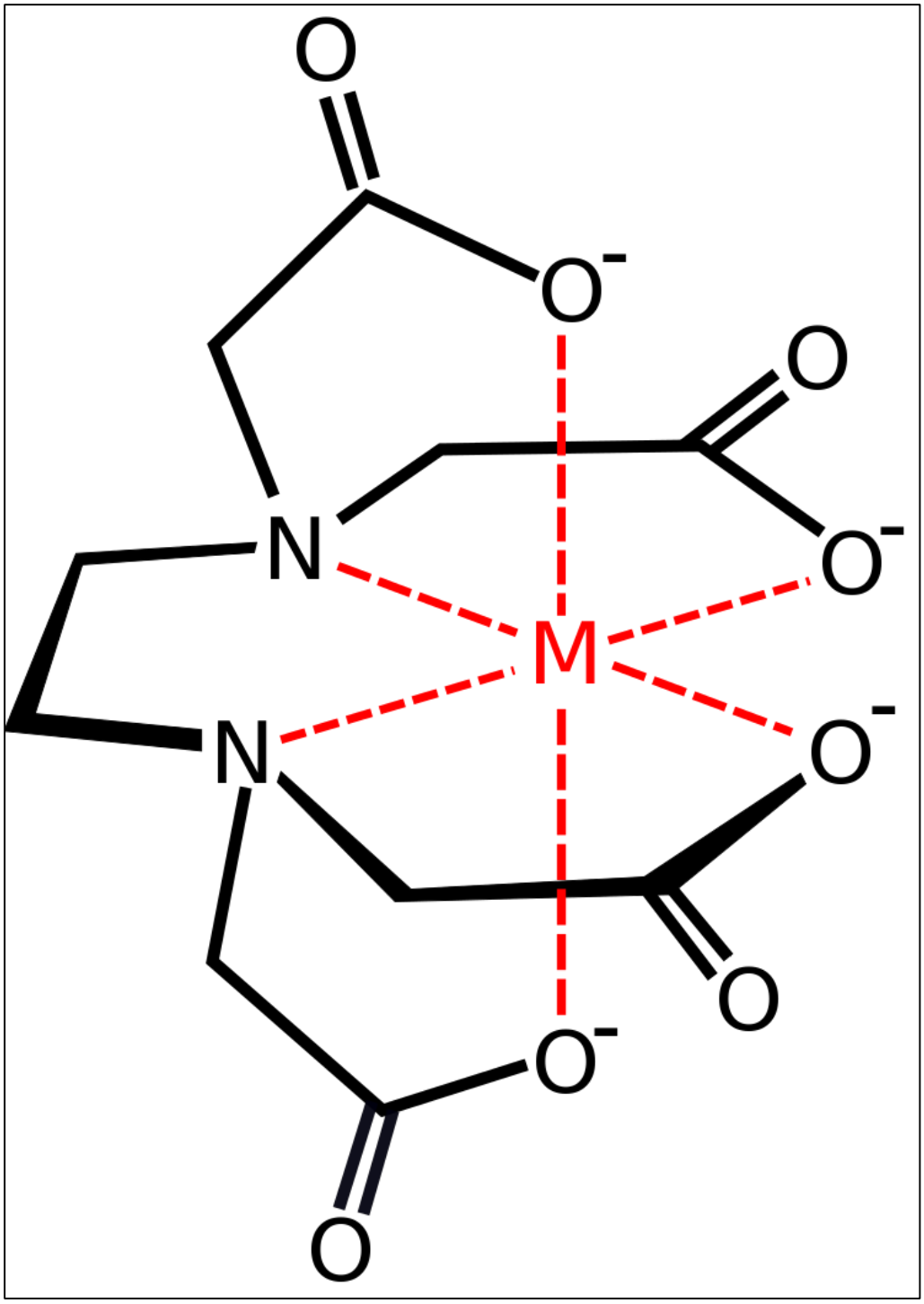

Fig. 59 – Metal complexed mononuclear EDTA.

5. CONCLUSIONS AND RECOMMENDATIONS

5.1 Proof of Concept: L80 and GLDA

In the proof of concept, the workflow to determine corrosion rates was demonstrated. GLDA (20 wt%) was used at 300°F to corrode two L-80 coupons for 4 hours at >1000 psi. The workflow included the procurement of coupons, testing procedures, analysis procedures, and documentation format for ease of knowledge transfer within the research group:

1. Procurement of coupons: Two vendors were chosen to supply the coupons. The proof of concept utilized curved coupons from CPCO. In the S13Cr-110 corrosion study, flat coupons were obtained from ALSPI.
2. Testing procedures: SOP's were developed highlighting the safe operation of using the Parr 4523 bench top reactor. These documents were stored and shared with the research group.
3. Analysis procedures: Corrosion rates were analyzed using weight loss method. In addition, ICP-OES measurements were made for key cations and were converted from a concentration (ppm) to mass (mg). The sum of the mass of cations provided insight into the metal that was removed from the sample. The localized corrosion was quantified using a 3D optical profiler, providing surface roughness parameters.
4. Documentation: A standardized coupon test sheet was created to ensure all required information was noted. A consistent filing system was

implemented to store information and easily transfer the knowledge within the group.

5.2 S13Cr-110 with EDTA and GLDA

The primary work presented in this study highlights the differences in the corrosion rates of S13Cr-110 with two chelating agents; EDTA and GLDA. The corrosion rates were calculated using the weight loss method and ICP-OES mass loss was used as a tool to verify the results. Due to the low corrosion rates, the ZeGage analysis was not used to quantify surface roughness parameters. The variables tested in this work were temperature (300°F and 350°F), fluid type (EDTA and GLDA), the effect of salt (5 wt% NaCl), and the effect of pH (pH 4 vs. pH 9). The conclusions are as follows:

1. For both EDTA and GLDA corrosion on S13Cr-110, the corrosion rate is below 0.02 lb/ft^2, which is the typically accepted industry level. This is true for the tests conducted at both 300°F and 350°F, with and without salt at a pH of 4 (GLDA/EDTA) and pH of 9 (EDTA).
2. Corrosion rates for all fluid were higher at 350°F than 300°F. Therefore, the primary control on corrosion rate is temperature.
3. EDTA at pH 9 was significantly more corrosive than EDTA at pH 4. Therefore, the secondary control on corrosion rate is pH; the higher the pH, the higher the corrosion rate. This is due to the mononuclear complexation of EDTA at high pH and the binuclear complexation of EDTA at low pH.

4. GLDA was more corrosive than EDTA when all the conditions were identical. Therefore, the stability constant is the tertiary control on corrosion rate. This is due to the fact that GLDA stability constants are lower for the 5 cations (Mn, Cr, Fe, Mo, and Ni) tested when compared to EDTA. It is theorized that the lower stability constant leads to increased corrosion because the chelated product is less stable.

5.3 Recommendations

It is recommended to continue work on this topic by extending the scope of study. Some of the extensions could be with other chelating agents, metal alloys (C-95, P-110, L-80), mixing speeds (up to 1700 rpm), and fluid environments (CO_2, different brine compositions). Studying and understanding these effects will help in selection criteria for successful, environmentally friendly stimulations.

REFERENCES

Adenuga, O. O., Nasr-El-Din, H. A., and Sayed, M. A. I. 2013. Reactions of Simple Organic Acids and Chelating Agents with Dolomite. Presented at SPE Production and Operations Symposium, Oklahoma City, Oklahoma, USA, 23-26 March. SPE-164480-MS. http://dx.doi.org/10.2118/164480-MS.

Al-Mutairi, S. H., Nasr-El-Din, H. A., Aldriweesh, S. M., et al. 2005. Corrosion Control during Acid Fracturing of Deep Gas Wells: Lab Studies and Field Cases. Presented at the SPE International Symposium on Oilfield Corrosion, Aberdeen, UK, 13 May. SPE-94639-MS. http://dx.doi.org/10.2118/94639-MS.

American Welding Society. 2016. Classification of Stainless Steel. *American Welding Society*, 2016, https://app.aws.org/wj/1998/11/kotecki/ (accessed 13 February 2016).

ArcelorMittal. 2010. Stainless Steel and Corrosion. *ArcelorMittal*, 10 March 2010, http://www.aperam.com/uploads/stainlesseurope/Brochures/Leaflet%20corrosion_Eng_374Ko.pdf (accessed 13 February 2016).

AZO Materials. 2014. Stainless Steel – Grade 410 (UNS S41000). *AZO Materials*, 25 April 2014, http://www.azom.com/article.aspx?ArticleID=970 (accessed 13 February 2016).

Begum, Z. A., Rahman, I. M., Tate, Y. et al. 2012a. Formation and Stability of Binary Complexes of Divalent Ecotoxic Ions (Ni, Cu, Zn, Cd, Pb) with Biodegradable Aminopolycarboxylate Chelants (DL-2-(2-Carboxymethyl)Nitrilotriacetic Acid, GLDA, and 3-Hydroxy-2,20-Iminodisuccinic Acid, HIDS) in Aqueous Solutions. *J. Chem. Eng. Data* **87**: 1161-1170. http://dx.doi.org/10.1016/j.chemosphere.2012.02.032.

Begum, Z. A., Rahman, I. M., Sawai, H. et al. 2012b. Stability Constants of Fe(III) and Cr(III) Complexes with DL-2-(2-Carboxymethyl) nitrilotriacetic Acid (GLDA) and 3‑Hydroxy-2,2′-iminodisuccinic acid (HIDS) in Aqueous Solution. *J. Chem. Eng. Data* **57**: 2723-2732. http:// dx.doi.org/10.1021/je3005936.

Boellinghaus, T., Hoffmeister, H., Klemme, J., et al. 1999. Hydrogen Permeation in a Low Carbon Martenistic Stainless Steel Exposed to H2S Containing Brines at Free Corrosion. *NACE International*.

Bondietti, G., Sinniger, J., and Stumm, W. 1993. The Reactivity of Fe(III) (hydro)oxides: Effects of Ligands in Inhibiting the Dissolution. *Colloids and Surfaces A: Physiochemical and Engineering Aspects* **79**: 157-167.

Braun, W., De Wolf, C., and Nasr-El-Din, H. A. 2012. Improved Health, Safety and Environmental Profile of a New Field Proven Stimulation Fluid (Russian). Presented at the SPE Russuan Oil and Gas Exploration and Production Technical Conference and Exhibition, Moscow, Russia, 16-18 October. SPE-157467-RU. http://dx.doi.org/10.2118/157467-RU.

Buijse, M., de Boer, P., Breukel, B. et al. 2004. Organic Acids in Carbonate Acidizing. *SPE Prod & Fac* **19** (03): 128-134. http://dx.doi.org/10.2118/82211-PA.

Chauhan, G., Pant K. K., and Nigam, D. P. 2015. Chelation Technology: a Promising Green Approach for Resource Management and Waste Minimization. Environ. Sci.: Processes Impacts **17**: 12-40. http://dx.doi.org/10.1039/c4em00559g.

Cooling, P., Kermani, B., Martin, J. W. et al. 1998. The Application Limits of Alloyed 13%Cr Tubular Steels for Downhole Duties. *NACE International*.

Cunat, P. 2004. Alloying Elements in Stainless Steel and Other Chromium-Containing Alloys. *Euro Inox and International Chromium Development Association* **1**: 1-24.

De Wolf, C. A., Bouwman, A. and Nasr-El-Din, H. A. 2015. "Corrosion Resistance when using Chelating Agents in Carbon-Steel Containing Equipment," U.S. Patent 20150005216 A1.

De Wolf, C. A., Bang, E., Bouwman, A. et al. 2014. Evaluation of Environmentally Friendly Chelating Agents for Applications in the Oil and Gas Industry. Presented at the SPE International Symposium and Exhibition on Formation Damage Control, Lafayette, Louisiana, 26-28 February. SPE-168145-MS. http://dx.doi.org/10.2118/168145-MS.

De Wolf, C. A., Nasr-El-Din, H. A., Bouwman, A. et al. 2012. A New, Low Corrosive Fluid To Stimulate Deep Wells Completed With Cr-based Alloys. Presented at the SPE International Conference and Workshop on Oilfield Corrosion, Aberdeen, UK, 28-29 May. SPE-152716-MS. http://dx.doi.org/10.2118/152716-MS.

Dwyer, F. P. and Mellor, D. P. 1964. *Chelating Agents and Metal Chelates*, first edition. New York, United States: Academic Press Inc.

El-Faramawy, H. S., Ghali, S. N., and Eissa, M. M. 2012. Effect of Titanium Addition on Behavior of Medium Carbon Steel. *Journal of Minerals and Materials Characterization and Engineering* **11**: 1108-1112. http://dx.doi.org/10.4236/jmmce.2012.1111118.

Felton, P. and Schofield, M. J. 1998. Understanding the High Temperature Corrosion Behavior of Modified 13%Cr Martenistic OCTG. *NACE International*.

Finšgar, M. and Jackson, F. 2014. Application of Corrosion Inhibitors for Steels in Acidic media for the Oil and Gas industry: A Review. *Corrosion Science* **86**: 17-41. http://dx.doi.org/10.1016/j.corsci.2014.04.044.

Fredd, C. N. and Fogler, H. S. 1997. Chelating Agents as Effective Matrix Stimulation Fluids for Carbonate Formations. Presented at the International Symposium on Oilfield Chemistry, Houston, 18-21 February. SPE-37212-MS. http://dx.doi.org/10.2118/37212-MS.

Fredd, C. N. and Fogler, H. S. 1996. Alternative Stimulation Fluids and Their Impact on Carbonate Acidizing. Presented at the SPE Formation Damage Control Symposium, Lafayette, Louisiana, 14-15 February. SPE-31704-MS. http://dx.doi.org/10.2118/31074-MS.

Frenier, W. W., Brady, M., Al-Harthy S. et al. 2004. Hot Oil And Gas Wells Can Be Stimulated Without Acids. Presented at the SPE International Symposium and Exhibition on Formation Damage Control, Lafayette, Louisiana, 18-20 February. SPE-86522-MS. http://dx.doi.org/10.2118/86522-MS.

Frenier, W. W., Rainey, M., Wilson, D. et al. 2003. A Biodegradable Chelating Agent is Developed for Stimulation of Oil and Gas Formations. Presented at the SPE/EPA/DOE Exploration and Production Environmental Conference, San Antonio, Texas, 10-12 March. SPE-80597-MS. http://dx.doi.org/10.2118/80597-MS.

Frenier, W. W., Fredd, C. N., and Chang, F. 2001. Hydroxyaminocarboxylic Acids Produce Superior Formulations for Matrix Stimulation of Carbonates at High Temperatures. Presented at the SPE Annual Technical Conference and Exhibition, New Orleans, Louisiana, 30 September-3 October. SPE-71696-MS. http://dx.doi.org/10.2118/71696-MS.

Hashizume, S. and Inohara, Y. 2000. Effects of pH and PH2S on SSC Resistance of Martensitic Stainless Steels. *NACE International*.

Hayes, G. F. 2013. Now is the Time. *World Corrosion Organization*. http://corrosion.org/wco_media/nowisthetime.pdf (accessed 12 February 2016).

Haynes International. 2015. Corrosion-Resistant Alloys. *Haynes International Inc., 2015*. http://www.haynesintl.com/CRAlloys.htm (accessed 18 December 2015).

Kalfayan, L. 2008. *Production Enhancement with Acid Stimulation*, first edition. Tulsa, Oklahoma: PenWell Corporation

Koch, G. H., Brongers, M. P. H., Thompson, N. G. 2001. Corrosive Costs and Preventative Strategies in the United States. *NACE International.* https://www.nace.org/uploadedFiles/Publications/ccsupp.pdf (accessed 12 February 2016).

LePage, J. N., De Wolf, C. Bemelaar, J. et al. 2009. An Environmentally Friendly Stimulation Fluid for High Temperature Applications. Presented at the 2009 SPE International Symposium on Oilfield Chemistry, The Woodlands, Texas, USA, 20–22 April. SPE 121709. http://dx.doi.org/10.2118/121709-MS.

Lopez, C. R. 2004. Keeping Stainless Steels Stainless. *The Tube and Pipe Journal* **568**. http://www.thefabricator.com/article/tubepipeproduction/keeping-stainless-steels-stainless (accessed 13 February 2016).

Mahmoud, M. A., Abdelgawad, K. Z., Akram, A. et al. 2015. Non- Coiled Tubing Stimulation of Water Injectors. Presented at the SPE Middle East Oil and Gas Show and Conference, 8-11 March, Manama, Bahrain. SPE-172572-MS. http://dx.doi.org/10.2118/172572-MS.

Mahmoud, M.A., Nasr-El-Din, H.A., De Wolf, C. et al. 2011. Evaluation of a New Environmentally Friendly Chelating Agent for High-Temperature Applications. *SPE J.* **16** (3): 559-574. SPE-127923-PA. http://dx.doi.org/10.2118/127923-PA.

Masamura, K., Inohara, Y., and Minami, Y. 1998. Effects of C and N on Corrosion Resistance of High Cr alloy in CO2 and H2S Environments. *NACE International*.

Mercier, D., Rouchaud, J. C. and Barthés-Labrousse, M. G. 2008. Interaction of amines with native aluminium oxide layers in non-aqueous environment: Application to the understanding of the formation of epoxy-amine/metal interphases. *Applied Surface Science*, **254** (20): 6495-6503. http://dx.doi.org/10.1016/j.apsusc.2008.04.010.

NACE ASTM G31, Standard Guide for Laboratory Immersion Corrosion Testing of Metals. 2012. Pennsylvania, United States: ASTM.

Nasr-El-Din, H. A., Dana, H., Tomos, V. et al. 2014. Field Treatment to Stimulate an Oil Well in an Offshore Sandstone Reservoir Using a Novel, Low Corrosive, Environmentally Friendly Fluid. Presented at the SPE International Symposium and Exhibition on Formation Damage Control, Lafayette, Louisiana, USA, 26-28 February. SPE-168163-MS. http://dx.doi.org/10.2118/168163-MS.

Nasr-El-Din, H. A., De Wolf, C. A., Stanitzek, T. et al. 2013. Field Treatment to Stimulate a Deep, Sour, Tight-Gas Well Using a New, Low Corrosion and Environmentally Friendly Fluid. *SPE Prod & Oper* **28** (3): 277-285. SPE-163332-PA. http://dx.doi.org/10.2118/163332-PA.

Nowack, B. and Sigg, L. 1997. Dissolution of Fe(III) (hydr) oxides by metal-EDTA complexes. *Geochimica et Cosmochimica Acta* **61** (5): 951-963. http://dx.doi.org/10.1016/S0016-7037(96)00391-2.

Oviedo, C. and Rodriguez, J. 2003. EDTA: The Chelating Agent Under Environmental Scrutiny. *Quimica Nova* **26** (6): 901-905. http://dx.doi.org/10.1590/S0100-40422003000600020.

Pan, T., Cui, Y., Su, H. et al. 2003. Effect of Vanadium on the Strength and Toughness of Wheel Steel at Different Reheat Temperatures. *High-tech Research and Development Program of China*: 161-165.

Parr Instrument Company. 2015. Materials of Construction. *Parr Instrument Company*, 2015, http://www.parrinst.com/products/stirred-reactors/options-accessories/materials-of-construction/ (accessed 18 December 2015).

PerkinElmer. 2010. Optima 7000 DV ICP-OES-OES. *PerkinElmer,* 2010, http://www.perkinelmer.com/CMSResources/Images/46-74713PRD_Optima7000D.pdf (accessed 26 February 2016).

Rabie, A., Mahmoud, M. A., and Nasr-El-Din, H. A. 2011. Reaction of GLDA with Calcite: Reaction Kinetics and Transport Study. Presented at the SPE International Symposium on Oilfield Chemistry, The Woodlands, Texas, USA, 11-13 April. SPE-139816-MS. http://dx.doi.org/10.2118/139816-MS.

Singh, D. D. A. and Dey, A. 1993. Synergistic Effects of Inorganic and Organic Cations on Inhibitive Performance of Propargyl Alcohol on Steel Dissolution in Boiling Hydrochloric Acid Solution, *Corrosion* **49**: 594–600. http://dx.doi.org/10.5006/1.3316090.

Sokhanvarian, K. 2012. *Thermal Stability of Various Chelates that are Used in the Oilfield.* MS thesis, Texas A&M University, College Station, Texas (December 2012).

Stumm, W. 1997. Reactivity at the mineral-water interface - Dissolution and inhibition. *Colloid and Surfaces A: Physiochemical and Engineering Aspects* **120** (1-3): 143-166. http://dx.doi.org/10.1016/S0927-7757(96)03866-6.

Szilagyi, P. A. 2007. *Study of iron-chelates in solid state and aqueous solutions using Mössbauer spectroscopy.* Doctorate thesis, Université Paul Sabatier, Toulose, France (November 2007).

Turnbull, A. and Griffiths, A. 2003. Review: Corrosion and Cracking of Weldable 13 wt-%Cr Martensitic Stainless Steels for Application in the Oil and Gas Industry, *Corrosion Engineering, Science and Technology* **38**:1, 21-50. http://dx.doi.org/10.1179/147842203225001432.

Ueda, M., Amaya, H., Ogawa, K., et al. 1996. Corrosion Resistance of Weldable Super 13Cr Stainless Steel in H2S Containing CO2 Environments. *NACE International*.

Walker, M. L., Dill, W. R., Besler, M. R. et al. 1991. Iron Control in West Texas Sour-Gas Wells Provides Sustained Production Increases. *Society of Petroleum Engineers*. SPE-20122-PA. http://dx.doi.org/10.2118/20122-PA.

Wang, X., Qu, Q., Culter, J. L. et al. 2009. Nonagressive Matrix Stimulation Fluids for Simultaneous Stimulation of Heterogeneous Carbonate Formations. Presented at the SPE International Symposium on Oilfield Chemistry, The Woodlands, Texas, 20-22 April. SPE-121712-MS. http://dx.doi.org/10.2118/121712-MS.

Wikipedia. 2016a. Redox (10 February 2016 revision), https://en.wikipedia.org/wiki/Redox (accessed 13 February 2016).

Wikipedia. 2016b. Arrhenius Equation (27 January 2016 revision), https://en.wikipedia.org/wiki/Arrhenius_equation (accessed 4 March 2016).

Zygo. 2015. ZeGage 3D Optical Surface Profiler. *Zygo, 2015*. http://www.zygo.com/?/met/profilers/zegage/ (accessed 18 December 2015).